# Dynamics of transposable element accumulation in the non-recombining regions of mating-type chromosomes in anther-smut fungi

Marine Duhamel[1,2], Michael E. Hood#[3], Ricardo C. Rodríguez de la Vega#[1], Tatiana Giraud#[1]

# These authors co-supervised the study

[1] Ecologie Systématique Evolution, IDEEV, CNRS, Université Paris-Saclay, AgroParisTech, Bâtiment 680, 12 route RD128, 91190 Gif-sur-Yvette, France.

[2] Evolution der Pflanzen und Pilze, Ruhr-Universität Bochum, Universitätsstraße 150, 44780, Bochum, Germany.

[3] Department of Biology, Amherst College, 01002-5000 Amherst, Massachusetts, United State of America.

*Corresponding author: Marine Duhamel

IDEEV, Bâtiment 680, 12 route RD128, 91190 Gif-sur-Yvette, France

phone: +33 1 69 15 56 69 fax: +33 1 69 15 46 97

marine.c.duhamel@gmail.com

## Abstract

**Background:** Transposable element (TE) activity is generally deleterious to the host fitness, so that genomes often evolve TE control mechanisms, and TE copies are purged by recombination and selection. In the absence of recombination, the number of TE insertions usually increases, but the dynamics of such TE accumulations is unknown.

**Results**: In this study, we investigated the tempo of TE accumulation in the non-recombining genomic regions of 15 *Microbotryum* species, leveraging on a unique dataset of 21 independent evolutionary strata of recombination cessation of different ages in closely related species. We show that TEs have rapidly accumulated following recombination suppression but that the TE content reached a plateau at ca. 50% of occupied base pairs by 1.5 MY following recombination suppression. The same superfamilies repeatedly expanded in independently evolved non-recombining regions, and in particular *Helitrons*, despite being scarce before recombination suppression. TEs from the most abundant elements, *i.e.*, *Copia* and *Ty3/Gypsy* retrotransposon superfamilies, have also expanded independently in the different non-recombining regions. *Copia* and *Ty3* retrotransposons have accumulated through bursts affecting both the non-recombining regions of the mating-type chromosomes and autosomes at the same time, which supports the TE reservoir hypothesis, *i.e.*, that the TEs accumulated in non-recombining regions have a genome-wide impact by transposing to recombining regions.

**Conclusion**: This study sheds light on the genome-wide consequences of the accumulation of TEs in non-recombining regions, thus improving our knowledge on genome evolution.

**Key words:** genomic degeneration, degeneration tempo, recombination suppression, sex chromosomes, centromeres

## Introduction

Transposable elements (TEs) are autonomously replicating DNA sequences ubiquitous in eukaryotic genomes (Hua-Van *et al.*, 2005; Wicker *et al.*, 2007; Bourque *et al.*, 2018). TEs have occasionally been recruited by their host genomes, *e.g.*, as regulatory sequences, for centromere maintenance or other functions (Kaessmann *et al.*, 2009; Martin *et al.*, 2009; Hof *et al.*, 2016; Dallery *et al.*, 2017; Lanciano & Mirouze, 2018). However, TE activity of replication and insertion is generally deleterious to its host genome (Payer & Burns, 2019; Andrenacci *et al.*, 2020; Burns, 2020). Their insertions can indeed disrupt gene coding or regulatory sequences (Hancks & Kazazian, 2016), induce epigenetic changes (Castanera *et al.*, 2016; Choi & Lee, 2020) or promote chromosomal rearrangements via ectopic recombination between non-allelic TE copies (Lim & Simmons, 1994; Han *et al.*, 2008; Ade *et al.*, 2013; Bennetzen & Wang, 2014; Balachandran *et al.*, 2022). TEs can also incur a substantial replication cost as they can represent a large proportion of the genome (Schnable *et al.*, 2009). TE proliferation is therefore often controlled by the host genome, by inactivating TE copies through epigenetic mechanisms such as RNAi silencing (Saito & Siomi, 2010) and DNA methylation (Zemach *et al.*, 2010; Jones, 2012; Bewick *et al.*, 2019; Deniz *et al.*, 2019).

Deleterious TE insertions can also be purged *a posteriori* by recombination between homologous chromosomes carrying different TE insertions. In the absence of recombination, the average number of TE insertions in the population increases with time (Dolgin & Charlesworth, 2008). TEs therefore tend to accumulate in regions with lower recombination rates (Kent *et al.*, 2017; Rifkin *et al.*, 2022), in non-recombining regions, such as in centromeres (Plohl *et al.*, 2014), pericentromeric regions (Wright *et al.*, 2003; Peng & Karpen, 2008; Charlesworth & Campos, 2014), and the non-recombining regions of sex chromosomes in plants and animals (Bachtrog, 2003, 2005; Marais *et al.*, 2008; Ahmed *et al.*, 2014) and of mating-type chromosomes in fungi (Lengeler *et al.*, 2002; Bakkeren *et al.*, 2006; Badouin *et*

*al.*, 2015; Branco *et al.*, 2018). The TE copies accumulating in the non-recombining regions of sex and mating-type chromosomes may form a TE reservoir for the rest of the genome, with TE copies transposing from these regions onto autosomes when epigenetic defenses are insufficient (Hood *et al.*, 2004; Wei *et al.*, 2020).

The accumulation of TEs has been extensively documented, but the pace of their proliferation in non-recombining regions, and whether such accumulation has genome-wide impacts as forming a source of TEs for the rest of the genome, are unknown (Charlesworth, 2021). Comparing TE proportions in non-recombining regions of different ages in closely related species would allow assessing the dynamics of TE accumulation, *i.e.*, the rate at which TEs increase in copy number in the absence of recombination. The cessation of recombination leads to degeneration, which can have non-linear dynamics, as suggested for gene losses on theoretical grounds (Bachtrog, 2013; Charlesworth, 2021) and as shown by genomic data for codon usage (Carpentier *et al.*, 2022). Alternatively, other components of degeneration can have a linear dynamics, as shown for changes in protein sequences (Carpentier *et al.*, 2022). As TEs can be a major degeneration factor, it is important to assess whether TEs accumulate rapidly in young non-recombining regions, whether the accumulation slows down at some point, for example because of the evolution of more efficient control mechanisms, whether the number of TE copies grows exponentially out of control, linearly with time or by occasional bursts. The shape of the curve of TE accumulation could thus inform us about how their proliferation is controlled in the absence of recombination. In addition, comparing the genealogies of TE copies within the genomes using sequence identity and genomic localisation would allow testing whether TE insertion events following recombination suppression are restricted to the non-recombining regions or whether TE copies from non-recombining regions also transpose to the rest of the genome, thus having a genome-wide impact.

Chromosomes carrying the genes for reproductive compatibility are particularly interesting and useful models to address the temporal dynamics of TE accumulation in non-recombining regions. Closely related species can have independently acquired sex chromosomes with non-recombining regions of different sizes and ages, which have often extended in a stepwise manner, providing independent events of recombination suppression within and across species (Lahn & Page, 1999; Bergero & Charlesworth, 2009; Charlesworth, 2017). Such gradual extensions of recombination suppression produce evolutionary strata of different levels of genetic differentiation between sex chromosomes, as first observed on the human sex chromosomes (Lahn & Page, 1999), and later on various sex chromosomes in other animals and plants (Handley *et al.*, 2004; Bergero & Charlesworth, 2009). The accumulation of TEs has even been suggested to play a role in the extension of recombination cessation along sex chromosomes (Li *et al.*, 2016; Kent *et al.*, 2017). TEs can, in particular, promote chromosomal rearrangements by TE-mediated ectopic recombination, including inversions at the margin of non-recombining regions (Ironside, 2010). TE-induced loss-of-function mutations constitute recessive deleterious mutations in the recombining regions adjacent to the non-recombining zone, called pseudo-autosomal regions, which can select for extending the region of recombination suppression that shelters this genetic load (Jay *et al.*, 2022). TE silencing epigenetic modifications, such as DNA methylation and heterochromatin formation, can in themselves block recombination (Maloisel & Rossignol, 1998; Ben-Aroya *et al.*, 2004; Yelina *et al.*, 2012, 2015; Bachtrog, 2013; Li *et al.*, 2016). If TEs accumulate in the margin of non-recombining regions, they may thus drive the extension of recombination suppression (Li *et al.*, 2016; Kent *et al.*, 2017).

Fungal mating-type chromosomes are similarly useful models and share key features with sex chromosomes: they can display large non-recombining regions, with evolutionary strata of different ages as well as footprints of degeneration (Menkis *et al.*, 2008; Whittle *et al.*, 2011;

Fontanillas *et al.*, 2015; Idnurm *et al.*, 2015; Branco *et al.*, 2018; Hartmann *et al.*, 2021; Carpentier *et al.*, 2022). When they occur, the non-recombining regions on fungal mating-type chromosomes are relatively young and some genera display multiple independent events of recombination cessation across closely related species, allowing to study the early stages of genomic degenerescence with independent data points (Carpentier *et al.*, 2022). In addition, fungi generally have small genomes and can be cultivated at the haploid phase, facilitating genomic assemblies and comparisons. The reduced TE load in fungal genomes compared to plants and animals (Amselem *et al.*, 2015) further facilitates assemblies of their chromosomes, including the TE-rich non-recombining regions (Badouin *et al.*, 2015; Branco *et al.*, 2018). Fungal defenses against TE activity include methylation (Castanera *et al.*, 2016; Bewick *et al.*, 2019), as well as a mechanism called repeat-induced point mutation (RIP), targeting specific di- or tri-nucleotides and inducing C to T nucleotide mutations in repeated sequences (Galagan & Selker, 2004; Hood *et al.*, 2005; Amselem *et al.*, 2015).

*Microbotryum* fungi form a complex of closely related plant-castrating species, mostly infecting plants in the Caryophyllaceae, and multiple species have independently evolved non-recombining mating-type chromosomes (Branco *et al.*, 2017, 2018; Carpentier *et al.*, 2019; Duhamel *et al.*, 2022). In *Microbotryum* species, as in most other Basidiomycota fungi, mating only occurs between haploid cells carrying alternative alleles at two mating-type loci: the pheromone-receptor (PR) locus controlling gamete fusion, encompassing genes coding for a pheromone-receptor and pheromones, and the homeodomain (HD) locus controlling dikaryotic hyphal growth, encompassing two homeodomain genes (Kronstad & Staben, 1997). Most *Microbotryum* fungi display only two mating types, called $a_1$ and $a_2$ (Day, 1979), which is due to multiple independent events of recombination suppression having linked the two mating-type loci across the *Microbotryum* genus (Badouin *et al.*, 2015; Branco *et al.*, 2017, 2018; Duhamel *et al.*, 2022; Carpentier *et al.*, 2022) (Figure 1); a few of the studied *Microbotryum*

species still have unliked mating-type loci, but often with linkage of each mating-type locus to its centromere (Carpentier *et al.*, 2019) (Figure 1). These two types of genomic linkage, *i.e.*, of PR and HD mating-type loci to each other or to their centromeres, are beneficial under intra-tetrad mating, as they increase the odds of compatibility among gametes of a single meiosis (Carpentier *et al.*, 2019), the common mating system in *Microbotryum* fungi (Hood & Antonovics, 2000; Giraud *et al.*, 2008). Patterns of decreasing divergence between the alleles on alternative mating-type chromosomes when going farther from the mating-type loci in the ancestral gene order have revealed that recombination extended in a stepwise manner beyond mating-type loci in several *Microbotryum* fungi, forming evolutionary strata of different ages (Branco *et al.*, 2017, 2018; Duhamel *et al.*, 2022; Carpentier *et al.*, 2022) (Figure 1 and Supplementary Table 1). In contrast, the recombining regions of the mating-type chromosomes, called pseudo-autosomal regions, are collinear and highly homozygous in *Microbotryum* fungi (Branco *et al.*, 2017, 2018; Duhamel *et al.*, 2022). The non-recombining regions of the mating-type chromosomes have accumulated TEs compared to the pseudo-autosomal regions and the autosomes (Fontanillas *et al.*, 2015; Branco *et al.*, 2018). However, whether specific TE superfamilies have accumulated and what is the temporal dynamics of TE accumulation across these genomic compartments remain unresolved questions.

At the whole-genome scale, *Microbotryum lychnidis-dioicae* carry long-terminal repeat (LTR) retroelements from the *Copia* and *Ty3* (also known as *Gypsy*, but see Wei *et al.*, 2022) superfamilies (Hood *et al.*, 2005; Amselem *et al.*, 2015) as well as, to a lesser extent, *Helitron* DNA transposons, *i.e.*, rolling-circle replicating TEs (Kapitonov & Jurka, 2001). In the *Microbotryum* species parasitizing *Dianthus carthusianorum*, a burst of *Ty3* retroelements has caused a massive accumulation of this element in a short period of time, in spite of RIP-like activity (Horns *et al.*, 2017). In *Microbotryum* genomes, a RIP-like activity targets TCG

trinucleotides (CGA on the reverse complement strand) rather than di-nucleotides as in ascomycetes (Hood *et al.*, 2005; Johnson *et al.*, 2010; Horns *et al.*, 2012).

In this study, we investigated the tempo of TE accumulation in the non-recombining regions of 15 *Microbotryum* species, leveraging on the existence of 21 independent evolutionary strata of different ages, within and across species (Carpentier *et al.*, 2022) (Figure 1). We show that TEs rapidly accumulate in young non-recombining regions but that their abundance reached a plateau by 1.5 MY following recombination suppression at ca. 50% occupied base pairs. *Helitron* DNA transposons repeatedly expanded in non-recombining regions despite being in short supply in species with recombining mating-type chromosomes. The most abundant TE superfamilies, *i.e.*, *Copia* and *Ty3*, were also over-represented in non-recombining regions and accumulated through multiple bursts that impacted both the non-recombining regions of the mating-type chromosomes and the autosomes at the same time, supporting the TE reservoir hypothesis. TEs however did not preferentially accumulate at the margin of non-recombining regions.

## Material and methods

### Detection and annotation of transposable elements

Transposable elements (TEs) were detected *de novo* in the $a_1$ and $a_2$ haploid genomes of 16 *Microbotryum* species and the red yeast *Rhodothorula babjavae* using LTRharvest (Ellinghaus *et al.*, 2008) from GenomeTools 1.5.10, performing long-terminal repeat (LTR) retrotransposons detection and RepeatModeler 1.0.11 (Smit & Hubley, 2008) combining results from three other programs: RECON (Bao & Eddy, 2002), RepeatScout (Price *et al.*, 2005) and Tandem Repeats Finder (Benson, 1999). The TE detection was enriched by BLASTn 2.6.0+ (Altschul *et al.*, 1990) using the genomes as a database and the previously detected TE

models as queries. To fulfill the repeat criterion, a TE sequence detected by RepeatModeler or LTRHarvest and its BLAST hits were retained only if the query matched at least three sequences in the same species with an identity ≥ 0.8, a sequence length > 100 bp and a coverage ≥ 0.8 (defined as the query alignment length with removed gaps divided by the query length). When these criteria were met, we retained the other query matches for the following parameters: identity ≥ 0.8, sequence length > 100 bp, e-value ≤ 5.3e−33 (75th percentile of e-value distribution) and coverage ≥ 0.8. We performed TE annotation (Wicker *et al.*, 2007) using the fungal Repbase database 23.05 (Bao *et al.*, 2015) based on sequence similarity. We first performed a BLASTn search and a BLASTx search using the fungal Repbase DNA and protein sequence database, respectively, with TE sequences as queries. For each of these similarity-based searches, we set the minimum e-value score at 1e−10 and minimum identity at 0.8. Then, we performed protein domain detection using pfam_scan.pl (ftp://ftp.ebi.ac.uk/pub/databases/Pfam/Tools/) on TE sequences and compared them to protein domain detection in the fungal Repbase database, keeping matches with e-values ≤ 1e−5. We also considered the annotation found by RepeatModeler. In order to determine the best annotation of a TE sequence, we applied a majority rule: we chose the most frequent annotation, and, in case of equality, we kept both annotations, generating a multiple annotation; these multiple annotations can be due to TEs being inserted within other TE copies, generating nested TEs. When we found no annotation, we assigned the TE sequence to an "unclassified" category; we discarded such annotations when overlapping with predicted genes to avoid false positives. We also discarded predicted TE sequences annotated as rRNA or overlapping *Microbotryum* ribosomal sequences (downloaded from https://www.arb-silva.de/ and http://combio.pl/rrna/taxId/5272/) and mitochondrial DNA sequences (NC_020353) with e-value ≤ 1e-10. We used a python script for annotation, and the TE detection and annotation pipeline is available at https://gitlab.com/marine.c.duhamel/microtep.

**Phylogenomic species tree reconstruction**

After removing the genes overlapping with annotated TEs, we inferred a species phylogenomic tree from the coding sequences of the 3,669 single-copy genes present in all *Microbotryum* species and the outgroup *Rhodothorula babjavae*. The protein-gene coding models were previously predicted with EuGene 4.2a (Foissac *et al.*, 2008), trained for *Microbotryum* genomes (Badouin *et al.*, 2015; Branco *et al.*, 2017, 2018; Carpentier *et al.*, 2019, 2022; Duhamel *et al.*, 2022). Orthologous groups were previously defined by Markov clustering (van Dongen, 2000) of high-scoring pairs parsed with orthAgogue (Ekseth *et al.*, 2014) based on all-vs-all BLASTP 2.6.0 (Altschul *et al.*, 1990) on protein sequences (Duhamel *et al.*, 2022). Protein-gene coding sequences of the 3,669 single-copy genes present in all species analysed were aligned independently using MUSCLE (Edgar, 2004) implemented in TranslatorX v1.1 (Abascal *et al.*, 2010). We inferred a maximum likelihood species tree using IQ-TREE 2.0.4 (Minh *et al.*, 2020) under the partition model of substitution chosen according to the Akaike information criterion (AIC) by Model Finder implemented in IQ-TREE (Kalyaanamoorthy *et al.*, 2017). We rooted the phylogenomic tree with the outgroup red yeast species *Rhodothorula babjavae*, and assessed the node robustness with 1000 ultrafast bootstraps (Minh *et al.*, 2013; Hoang *et al.*, 2018) and SH-like approximate likelihood ratio tests (SH-aLRT)(Guindon *et al.*, 2010).

**Evolutionary histories of *Copia* and *Ty3* superfamily retroelements**

We inferred the evolutionary histories of the most abundant elements, *i.e.*, in the *Copia* and *Ty3* retroelement superfamilies, by reconstructing their genealogies based on the sequence of their long terminal repeat (LTR) region at the 5' end of the elements (5'-LTR), the rationale being that, at the time of transposition, the LTR sequences of the new copy are identical to the 5'-LTR sequence of its progenitor (Zhang *et al.*, 2014). We only retained sequences harboring

one or two LTR sequences identified by LTRHarvest (Ellinghaus *et al.*, 2008), thus avoiding nested copies. We distinguished the 5'- from the 3'-LTR based on the orientation of their coding sequences detected using RepeatProteinMask (Smit & Hubley, 2008). Because some retrotransposon sequences were degenerated, their coding sequences could not be identified and thus oriented, so that only a subset of the retrotransposons were used for building the genealogies. We built multi-species genealogies using the TE copies of *Copia* and *Ty3* retrotransposons in all genomes (3,966 and 964 copies, respectively). We built single-species (*i.e.*, within genome) genealogies, only for species with at least 100 copies remaining after filtering for *Copia* retrotransposons and at least 60 copies for *Ty3* retrotransposons (see proportion of TE copies used for the genealogies in Supplementary Figure S1). We then aligned 5'-LTR sequences of *Copia* or *Ty3* elements using MAFFT v7.310 (Katoh *et al.*, 2002). We used IQ-TREE 2.0.4 (Minh *et al.*, 2020) to infer the maximum likelihood tree from the 5'-LTR sequences alignment under the GAMMA + GTR model of substitution. We assessed tree robustness with 1000 replicates for ultrafast bootstrap and SH-aLRT. Trees were plotted using phytools (Revell, 2012) and ggtree (Yu *et al.*, 2017) rooted using midpoint rooting (*midpoint.root*, phytools, Revell, 2012). Pairwise sequence divergence values in trees were obtained using *cophenetic.phylo* from ape 5.0 (Paradis & Schliep, 2019).

**Detection of centromeres and telomeres in the autosomes of *Microbotryum* genomes**

We identified centromeres (Supplementary Table 2) as in Duhamel *et al.* (2022) by blasting (BLASTN 2.6.0, Altschul *et al.*, 1990) the centromeric repeats previously described in *Microbotryum* fungi (Badouin *et al.*, 2015) on autosomal contigs larger than 20 kb; the largest stretch of centromeric repeats on a given contig was annotated as its predicted centromere. We delimited the predicted centromere by recursively extending the focal region by 1 kb intervals as long as gene density remained lower than 0.25 in the focal window. We detected telomeres

(Supplementary Table 3) within 100 bp regions at the end of contigs carrying at least five times the telomere-specific TTAGGG motif (CCCTAA on reverse complementary strand), as done previously (Badouin *et al.*, 2015). Subtelomeric regions were defined as the 20 kb regions adjacent to the telomeres, plus the 100 bp telomeres.

**RIP-like index**

We computed values for a RIP-like index in non-overlapping 1 kb genomic regions along the mating-type chromosomes and autosomal contigs as previously described (Beckerson *et al.*, 2019). The RIP-like index was calculated as the ratio *t/n*, *t* being the ratio of the RIP-affected sites (TTG + CAA trinucleotides, forward and reverse; Hood et al., 2005) over the non RIP-affected sites (TCG + CGA, minus overlapping tetra-nucleotides TGCA) for the RIP target sites, and *n* being the same ratio for non-RIP target sites ([A,C,G]TG + CA[C,G,T] over [A,C,G]CG + CG[C,G,T] - [A,C,G]CG[C,G,T]), to control for sequence composition. The RIP index was normalized as *t/n - 1*, so that a normalized RIP index greater than 0 was indicative of an excess of RIP-like mutations compared to random expectations. We used the *SlidingWindow* function of the *evobiR* package (mean values, 10 kb steps - Blackmon & Adams, 2015) and *ggplot2* (Wickham, 2009) to plot the distribution of RIP along the mating-type chromosomes and autosomal contigs and identify the RIP-affected regions. We used the parameters to plot the density of genes and TEs in the same non-overlapping 1 kb windows. In order to test the relationship between the abundance of RIP footprint in TEs in non-recombining regions and the age of evolutionary strata, we calculated the average of the RIP index of the TEs in each stratum and performed a two-sided Pearson's correlation test.

**Estimates of TE content in non-recombining regions**

The distinct evolutionary strata within non-recombining regions have been previously distinguished based on the following criteria: i) the distribution of recombination suppression across the phylogenetic tree to assess when recombination suppression evolved and thereby identifying distinct evolutionary strata, *i.e.*, genomic regions that stopped recombining at different times, and ii) the level of trans-specific polymorphism (*i.e.*, alleles clustering by mating type rather than by species), which is also a strong indicator of the time of recombination suppression (Branco *et al.*, 2017, 2018; Carpentier *et al.*, 2019, 2022; Duhamel *et al.*, 2022) (Supplementary Table 3). Young non-recombining regions, formed after the linkage of the PR and HD loci (*i.e.*, the white and pink strata in *M. v. paradoxa* and the light blue stratum in *M. v. caroliniana*; Figure 1) were not rearranged with other strata, so that it was straightforward to compute their percentages of base pairs occupied by TEs. In contrast, the ancient blue and purple strata (Figure 1), having evolved at the base of the *Microbotryum* clade, were too much rearranged and intermingled with other strata for their specific TEs to be identified in species with large non-recombining regions, but they were very small (*i.e.*, encompassing on average only 12 genes). We therefore pooled the ancient blue and purple strata with the larger strata with which they were intermingled. For the multiple independent evolutionary strata corresponding to the linkage of the HD locus with the PR locus in a single step (black strata; Figure 1), it was straightforward to compute their percentage of base pairs occupied by TEs. In *M. v. viscidula*, *M. v. melanantha*, *M. v. gracilicaulis* and *M. v paradoxa*, recombination suppression extended gradually to link the HD and PR loci and then underwent multiple rearrangements that intermingled their genes and TEs. In order to avoid misassignment of TEs to these intermingled strata, we only considered regions spanning at least 80 kb (corresponding to the size of the smallest stratum from the dataset, the pink stratum in *M. v. paradoxa*) and with only genes from a single stratum. We defined the limit between

two strata as the middle point between two genes from two distinct rearranged strata. The resulting blocks assigned to strata overall represented 66.52 to 90.26% of the total non-recombining regions formed by intermingled strata (Supplementary Figure S2), which should thus give a good estimate of the stratum TE contents. We used circos (Krzywinski *et al.*, 2009) to visualize the blocks assigned to strata. For the non-recombining regions linking the HD or PR loci and their respective centromere (blue-to-centromere and purple-to-centromere respectively, in *M. lagerheimii* and *M. saponariae*), the percentage of base pairs occupied by TEs was calculated in the region between the end of the centromere and the mating-type locus. For each stratum, we took the mean percentage of TEs across $a_1$ and $a_2$ haploid genomes, and for the strata shared across several species, the mean of the $a_1$ and $a_2$ values across all the species sharing the same recombination suppression event. The ancestral size of the non-recombining regions were estimated by calculating the average size of the corresponding genomic region in the $a_1$ and $a_2$ haploid genomes of *M. intermedium*, *i.e.*, the *Microbotryum* species most distant from the other species in our dataset, with unlinked mating-type loci and with little recombination suppression (Duhamel *et al.*, 2022).

To test whether TEs also preferentially accumulate at the margin of the non-recombining regions, we compared the average number of base pairs occupied by TEs within the 100 kb of the pseudo-autosomal regions flanking the non-recombining regions to the distribution of TE load in 100 kb non-overlapping windows in fully recombining autosomes (100 kb away from the centromeres and after removal of 10 kb corresponding to subtelomeric regions). We only considered the species with a length of the pseudo-autosomal region at least equal to 100 kb (thus excluding *M. v. paradoxa*) and with at least 30 non-overlapping windows of 100 kb on their autosomes (thus excluding *M. scabiosae* and *M. v. parryi*, for which the genome assemblies were too much fragmented). We set the window length at

100 kb because this is the DNA fragment size at which linkage disequilibrium decreases below $r^2 = 0.2$ in *Microbotryum* populations (Badouin *et al.*, 2017).

We estimated the fraction of intact *Copia*, *Ty3* and *Helitron* copies in each stratum based on their length. For each stratum, we calculated the ratio of putative intact TE copies (5-7.5 kb for *Copia* and *Ty3* and 5-11 kb for *Helitron*) over the total number of *Copia* and *Ty3* copies or *Helitron* copies. For each stratum, we also calculated the mean fraction of intact TE copies across $a_1$ and $a_2$ haploid genomes and for the strata shared by several species, the mean across species deriving from the same recombination suppression event.

**Estimates of non-recombining region ages**

In *Microbotryum* fungi, sexual reproduction occurs before the infection of a new plant, which will produce spores in its flowers at the next flowering seasons, so that one year corresponds to one generation for these fungi. We used the dates of recombination suppression estimated in previous studies (Duhamel *et al.*, 2022; Carpentier *et al.*, 2022), for 21 genomic regions corresponding to independent events of recombination suppression distributed across 15 *Microbotryum* species. The *M. scabiosae* non-recombining regions used in a previous study (Carpentier *et al.*, 2022) was not considered here due to the large confidence interval on its estimated age. To this dataset of 15 *Microbotryum* species, we added the TE content in the autosomes of *M. intermedium* as the zero time point; indeed, the autosomes are recombining and there is little potential for a reservoir effect in *M. intermedium* as the non-recombining regions are very small, being restricted to close proximity around the separate mating-type loci (Duhamel *et al.*, 2022); we set the age since recombination suppression at 0.00000003 MY for

*M. intermedium* autosomes, corresponding to one day since the recombination suppression event, to avoid the zero value for logarithm computation in tempo analyses.

**Statistical analyses**

We tested whether the genomic percentage of base pairs occupied by TEs was different between the $a_1$ and $a_2$ mating-type haploid genomes using a paired two-sided Wicoxon's rank test. To compare the percentages of base pairs occupied by TEs in the autosomes, the pseudo-autosomal regions and the non-recombining regions of the mating-type chromosomes, we performed a variance analysis (ANOVA) after testing the normality of the TE percentage distributions (Kolmogorov-Smirnov test). We then performed post-hoc Tukey's range tests to identify the pairs of genomic compartments which displayed significantly different TE loads, using the *TukeyHSD* R function providing adjusted p-values for multiple comparisons. We assessed the correlation between TE loads in autosomes and non-recombining regions using the two-sided Pearson's test.

In order to assess the shape of the functions for accumulation of TEs in the non-recombining regions of the *Microbotryum* mating-type chromosomes, we performed regressions using generalized additive models (*gam* function of R, Wood, 2011) and non-linear regression models (*drm* function of the drc package, Ritz *et al.*, 2019). Based on the Akaike information criterion (AIC), we evaluated the model fits for predicting the percentage of base pairs occupied by TEs in the non-recombining regions as a function of the time since recombination suppression, with the ancestral size of the non-recombining region as a covariable, and assuming either a linear or a logarithmic relationship with the time since recombination suppression, with or without smoothing spline, or a negative exponential model.

In order to assess the relationship between the fraction of intact *Copia*, *Ty3* and *Helitron* copies and time since recombination suppression, we performed a local regression using the *loess.as* function from the fANCOVA package, using the Akaike Information Criterion for automated parameter selection (Hurvich *et al.*, 1998; Wang & Ji, 2020).

## Results

### Transposable element content and superfamilies in *Microbotryum* genomes

We identified transposable elements (TEs) in the $a_1$ and $a_2$ haploid genomes deriving from a single diploid individual of each of 15 *Microbotryum* species and of a genome of the red yeast *Rhodothorula babjavae*, an outgroup with the ancestral condition of the PR and HD mating-type loci on separate chromosomes. We detected no significant difference in TE content between the two haploid genomes within species (Wilcoxon paired test, V=5284, *p-value*=0.2079, Supplementary Figure S3). In the following analyses, we therefore calculated the mean from the $a_1$ and $a_2$ genomes for each species. *Microbotryum* genomes, with an average of 18.3% base pairs occupied by TEs, contained more TEs than *R. babjavae* (Supplementary Figure S3). *Microbotryum intermedium*, with fully recombining mating-type chromosomes, had the lowest TE content (6.57%), closely followed by *M. v. lateriflora* (7.02%) with a very young non-recombining region (0.304 My), while *M. violaceum paradoxa* with the largest and among the oldest non-recombining regions had the highest TE load (30.33%) (Figure 2a and Supplementary Figure S4 and Supplementary Table 4; detailed comparison below).

All *Microbotryum* genomes contained a substantial fraction of long-terminal repeat (LTR) retrotransposons from the *Copia* and *Ty3* superfamilies (6.04% and 4.97% of occupied base

pairs on average for *Copia* and *Ty3* retroelements, respectively, Supplementary Table 4). These retroelements were particularly abundant in the *Microbotryum* genomes with non-recombining mating-type chromosomes, *Copia* TEs being for example nine times as abundant in *M. coronariae* (10.27% of occupied base pairs) as in *M. intermedium* (1.08% of occupied base pairs). Taken together, *Copia* and *Ty3* superfamilies represented 76.93 to 94.01% of the centromeric TEs across species (Figure 2B). The trimodal distributions of *Copia* and *Ty3* retroelement length (Figure 2C and Supplementary Figure S5a) show that, while most copies are shorter than 1 kb and are likely degenerated and fragmented, a high proportion of these retroelements, being 5 kb and 7 kb length on average, are likely intact TE copies (González & Deyholos, 2012). TE copies with a length greater than 10 kb likely represent nested TE copies, and were particularly abundant in the young, white stratum of *M. v. paradoxa* (Supplementary Figure S5a).

DNA transposons were mostly represented by *Helitrons* and terminal inverted repeats (TIR) elements in most *Microbotryum* genomes (1.44 and 0.42% of occupied base pairs on average, respectively), while these were nearly absent in *M. intermedium* (0.04% of base pairs occupied by *Helitrons* and no TIR elements) and in *M. scabiosae* (Figure 2a). The proportion of TEs annotated as "*unclassified*" was generally low (0.83 to 3.25% of occupied base pairs), being highest in genomes with high TE content, such as *M. v. paradoxa* and *M. v. gacilicaulis* (7.4 and 10.18% of occupied base pairs, respectively). The low average size of "*unclassified*" TE copies (263.13 bp, Supplementary Figure S5b) suggests that they represent highly fragmented TE relics. Such "*unclassified*" elements were predominant in subtelomeric regions (Figure 2B).

**Higher content of transposable element and of RIP-like footprints in non-recombining regions**

TEs represented significantly higher proportions of base pairs in non-recombining regions compared to pseudo-autosomal regions and autosomes (ANOVA post-hoc Tukey test, adj. *p-value* < 0.01), being on average 41.68% and 40.31% higher in the non-recombining regions compared to pseudo-autosomal regions and autosomes, respectively (Supplementary Table 6, Supplementary Figure S6). No significant difference was observed between pseudo-autosomal regions and autosomes (ANOVA post-hoc Tukey test, adj. *p-value* = 0.9215, Supplementary Table 6), despite tendencies in some species for lower content of some elements in pseudo-autosomal regions (Figure 2C and Supplementary Figure S6). The centromeres of all species displayed a high density of TEs (73% of base pairs occupied by TEs on average, Supplementary Table 7). Plotting the density of TEs along mating-type chromosomes further illustrated that it was higher in the non-recombining regions than in the pseudo-autosomal regions, and that the TE-rich regions corresponded to gene-poor regions (see Figure 3 for *M. lychnidis-dioicae* and Supplementary Figure S7A to S7O for the other *Microbotryum* species).

TE density was generally higher in older evolutionary strata such as the purple stratum (Supplementary Figure S7H, S7J and S7O) and lower in young strata such as the young pink and white strata of *M. v. paradoxa* (Supplementary Figure S7G). In part because of this variation in TE content, the size of the mating-type chromosomes varied greatly across *Microbotryum* species (Figure 1B), from 1,177,022 bp in *M. scabiosae* to 10,060,889 bp in *M. v. paradoxa* (3,076,521 bp on average); the size of the mating-type chromosomes also varies because different chromosomal rearrangements were at the origin of HD-PR locus linkage (Duhamel *et al.*, 2022). For the same reasons, the size of the non-recombining regions was variable, ranging from 630,774 bp in *M. scabiosae* to 9,461,162 bp in *M. v. paradoxa*, thus

spanning almost the full length of the mating-type chromosome in this later species (Figure 1B), and being absent in *M. intermedium*.

We found no particular accumulation of TEs in the proximal flanking region of the non-recombining regions when comparing the number of base pairs occupied by TEs within the 100 kb of the pseudo-autosomal regions flanking the non-recombining regions to the distribution of the TE proportions in regions of the same size in fully recombining autosomes (Supplementary Figure S8). We compared the TE content in the flanking region of the non-recombining region to that in autosomes because the pseudo-autosomal regions were too small for building a distribution.

The non-recombining regions had more RIP-like signatures than autosomes and pseudo-autosomal regions in most species (Figure 3 and Supplementary Figure S7). The youngest strata, such as the pink and white strata of *M. v. paradoxa* and the young light blue stratum in *M. v. caroliniana,* were in contrast less affected by RIP than the older non-recombining regions (Supplementary Figure S7G and S7L, respectively).

**Particular TE family expansions in non-recombining regions**

Some TE families appeared to have particularly expanded in non-recombining regions. *Copia* and *Ty3* elements displayed higher proportions in the non-recombining regions compared to autosomes and pseudo-autosomal regions in almost all species (ANOVA post-hoc Tukey test, adj. *p-value* < 0.01, see Supplementary Table 6 and Figure 2C). *Helitron* elements have also expanded in non-recombining regions, while they are relatively rare in the recombining mating-type chromosomes of *M. intermedium* and in autosomes in all species (ANOVA post-hoc Tukey test, adj. *p-value* < 0.01, see Supplementary Table 6 and

Figure 2B and 2C). The proportion of *TIR* DNA transposons was higher in the non-recombining regions compared to pseudo-autosomal regions but not compared to autosomes (ANOVA post-hoc Tukey test, adj. *p-value* < 0.01, Supplementary Table 6 and Figure 2C).

**Genome-wide bursts of transposable elements following recombination suppression**

We found a significant and strong correlation between TE proportions on autosomes and non-recombining regions (r = 0.67; *p-value* = 0.006171; Supplementary Figure S9), which supports the reservoir hypothesis, *i.e.*, that the TE copies accumulating in non-recombining regions have a genome-wide impact by transposing to autosomes.

We inferred TE genealogies of the *Copia* and *Ty3* superfamilies independently, using the alignment of their 5'-LTR sequences. Because the genealogies rely on the identification of the 5'-LTR sequences of the retrotransposons, only a subset of the *Copia* and *Ty3* retroelements were used to reconstruct the genealogies (on average 17.88 and 6.41% of the annotated *Copia* and *Ty3* superfamily retroelements, respectively, Supplementary Figure S1) and genealogies were built for the species having sufficiently large sets of retained *Copia* and *Ty3* sequences.

The *Copia* and *Ty3* genealogies revealed the existence of many copies clustering within clades with very low divergence, suggesting recent bursts of transposition of these retroelements that impacted all genomic compartments and all species (Figure 4 and Supplementary Figures S10 and S11), including the species with old non-recombining regions (Figure 4B and Supplementary Figures S10I-K and S11G). This shows that *Copia* and *Ty3* retrotransposons are active in *Microbotryum* genomes. In several species, the

centromeric TE copies tended to cluster together (Figure 4 and Supplementary figure S10 and S11). In a few species, such as *M. v. paradoxa* (Figure 4B), we identified *Copia* TE bursts specific to non-recombining regions. The clustering of copies from autosomes and non-recombining regions in the same TE clades with low divergence however indicates that TEs transpose from one compartment to the other. We found similar distributions of divergence between TE copies in autosomes and in the non-recombining regions of the mating-type chromosomes (Supplementary Figure S12). This indicates that bursts occurred at the same time in the two genomic compartments, thus suggesting that non-recombining regions serves as a reservoir from which TEs can transpose in autosomes. This was the case in all species except in *M. saponariae*, which carries its two mating-type loci on different chromosomes and has very young non-recombining regions linking the mating-type loci to their respective centromeres. In this species, the burst in autosomes appeared to be slightly delayed compared to the peak on the mating-type chromosomes (Supplementary Figure S12).

In order to assess whether these TE bursts occurred following recombination suppression, we inferred TE genealogies for *Copia* and *Ty3* retroelements with the sequences of all species. The TE copies resulting from the recent TE bursts often clustered by species and by group of species deriving from the same recombination suppression event, supporting the inference that TE accumulation has followed recombination suppression (Figures 5 and Supplementary Figure S13). The bursts of retrotransposon accumulation occurred at different times across lineages, as shown by the different phylogenetic distances of the clades with short branches to the root (Supplementary Figure S14A and S14B). The only exception was the occurrence of three *Copia* bursts at the same time, in the three species of

the *M. v. gracilicaulis* clade, as the three bursts appeared equidistant to the root (Supplementary Figure S14A, pointed by arrows and aligned on the green circle).

**Tempo of TE accumulation in non-recombining regions on mating-type chromosomes**

The multiple independent events of recombination suppression across the *Microbotryum* phylogeny, with a range of ages, provides a unique opportunity to investigate the tempo of TE accumulation. The large non-recombining regions of different ages formed by the stepwise recombination suppression between the HD and PR loci were highly rearranged in *M. v. viscidula*, *M. v. melanantha*, *M. v. gracilicaulis* and *M. v paradoxa*, rendering difficult the assignment of some TE copies to a given age of recombination suppression. In order to be conservative, we therefore only considered TE copies that could be assigned to a stratum with high confidence, by taking into account only blocks of at least 80 kb (size of the pink stratum, the smallest stratum of the dataset) and encompassing at least two genes of a given stratum. The resulting blocks represented 66.52 to 90.52% of the total non-recombining region sizes (Supplementary Figure S2), thus likely yielding good estimates of their TE content. We excluded from analyses the orange stratum (Figure 1) shared by all or most of the species (Branco *et al.*, 2017, 2018; Carpentier *et al.*, 2019, 2022; Duhamel *et al.*, 2022), as it is small and might not represent independent events of recombination suppression. We also excluded from analyses the small strata that were too much fragmented (for example the red stratum in *M. lychnidis-dioicae* and *M. silenes-dioicae;* Figure 1; Branco *et al.*, 2018). To avoid pseudoreplication, we considered the mean of the percentages of base pairs occupied by TEs in the $a_1$ and $a_2$ genomes for each species. Similarly, for the strata shared by multiple species, we took the mean values across the species derived from the same recombination suppression event. We used the TE content in the autosomes of *M. intermedium* as the point at time zero,

*i.e.*, before recombination suppression, as its mating-type chromosomes still recombine, thereby precluding any potential TE reservoir effect.

We tested whether the percentage of base pairs occupied by TEs in the non-recombining regions could be explained by the time since recombination suppression and the ancestral size of the non-recombining region. We compared generalized additive models assuming linear or logarithmic relationships with the time since recombination suppression, with or without smoothing splines (*i.e.*, phases), as well as a non-linear negative exponential model. The percentage of base pairs occupied by TEs in the non-recombining regions was best explained by the negative exponential model with the age of the stratum as an explanatory variable of the percentage of TEs in this stratum (Figure 6 and Supplementary Table 8). We found that TEs rapidly accumulated until 1.5 million years following recombination suppression and then reached relatively abruptly a plateau at around 50% of TEs. A similar curve was obtained when fitting the tempo of TE accumulation with the average synonymous divergence ($d_S$) between $a_1$ and $a_2$ associated alleles of the genes within strata, as expected considered the quasi-linear relationship between $d_S$ and stratum age (Supplementary Figure S15). The ancestral size of the non-recombining region did not significantly impact TE content in the retained negative exponential model.

We found that the relative abundance of RIP-like footprints was highly variable in the young strata and remained constant with time since recombination suppression, with values greater than zero, suggesting that a process similar to RIP efficiently mutates TE copies in young and old non-recombining regions (Supplementary Figure S16). There was indeed no significant correlation between the age since recombination suppression and the abundance of RIP-like footprints in the TEs of the strata (two-sided Pearson's correlation test, *p-value* = 0.9003).

The fraction of detected intact *Helitron* copies decreased with time since recombination suppression and even reached zero after 4 MY (Supplementary Figure S17). The proportion of

intact copies of *Copia* and *Ty3* retroelements decreased rapidly following recombination suppression, from 20% down to 10%, and then stayed stable at around 10% (Supplementary Figure S17).

## Discussion

We found a large degree of variation among *Microbotryum* species in their TE load, and the key to understanding this variation seems to be the evolution of the recombination landscape associated with regions determining reproductive compatibility. Moreover, there appears to be a significant feedback of the TE accumulation on non-recombining mating-type chromosomes where the buildup is rapid, and the rest of the genome is then burdened with greater repetitive element insertions. Leveraging on a unique dataset with 21 regions having independently evolved recombination suppression, we found that TEs accumulated rapidly following recombination cessation but then reached a plateau at ca. 50% of occupied base pairs, after 1.5 MY.

We indeed found variable genomic TE loads in closely related *Microbotryum* genomes, ranging from 6.5 to 30% base pairs occupied by TEs, with an intermediate TE content in the most studied species *M. lychnidis-dioicae* (19.4%). We were able to annotate a large proportion of the detected TE copies, e.g. 89% in *M. lychnidis-dioicae*. In comparison, a previous study using Illumina paired-end sequencing estimated the genomic TE content of *M. lychnidis-dioicae* at 14.1% and only 60% of the TE copies were annotated (Amselem *et al.*, 2015). Compared to other fungi, *Microbotryum* genomes carry intermediate TE contents, generally lower than their close relatives in the Pucciniomycotina (Raffaele & Kamoun, 2012). We found that LTR

retrotransposons, especially from the *Copia* and *Ty3* superfamilies, represented the majority of the base pairs occupied by TEs in *Microbotryum* genomes. These LTR retrotransposons summed up to 87% of the base pairs occupied by TEs in *M. intermedium* and 70% in *M. lychnidis-dioicae*, which was much higher than previously estimated and among the highest retrotransposon content, relative to other TE categories, in fungi (Amselem *et al.*, 2015). Compared to plant genomes, the proportions of *Copia* and *Ty3* in terms of annotated base pairs were higher and lower, respectively, than in the genome of *Arabidopsis thaliana* (Quesneville, 2020), were similar to the flax genome (González & Deyholos, 2012) and lower than in the *Silene latifolia* genome (Puterova *et al.*, 2018).

We found higher TE loads in non-recombining regions of mating-type chromosomes compared to recombining autosomal or pseudo-autosomal regions, indicating that the lack of recombination has allowed the accumulation of TEs by a lower efficacy of selection against deleterious insertions. The accumulation of TEs has been widespread in non-recombining regions of sex chromosomes of plants and animals (Erlandsson *et al.*, 2000; Bachtrog, 2003, 2005; Marais *et al.*, 2008; Ahmed *et al.*, 2014; Śliwińska *et al.*, 2016; Mawaribuchi *et al.*, 2017). In the absence of recombination, the average number of TE copies can only increase with time in the population, because chromosomes devoid of new TE copies cannot be generated by recombination and the chromosomes carrying fewer TE copies can be randomly lost, a phenomenon known as Muller's ratchet (Muller, 1918; Charlesworth & Charlesworth, 2000; Bachtrog, 2003; Dolgin & Charlesworth, 2008). In *Drosophila miranda*, TEs played an early and important role in the degeneration of the neo-Y chromosome (Bachtrog, 2005). We detected RIP-like footprints in *Microbotryum* genomes, but this genome defense mechanism was not sufficient to control TE proliferation without recombination, as previously noted in some *Microbotryum* species (Johnson *et al.*, 2010; Horns *et al.*, 2017).

Transposable elements from the *Copia*, *Ty3* and *Helitron* superfamilies were particularly involved in the repeat accumulation in non-recombining regions. *Copia* and *Ty3* retrotransposons proliferated independently and repeatedly following the multiple independent events of recombination suppression across *Microbotryum* lineages. *Copia* and *Ty3* superfamilies are predominant in *M. intermedium* and in autosomes of all species, suggesting that they were already abundant before recombination suppression, and then proliferated due to transposition and Muller's ratchet. *Helitron* elements were in contrast rare in *M. intermedium* and in autosomes of all species, and yet have also accumulated in the multiple non-recombining regions, as observed in the non-recombining regions of the sex chromosomes of *Drosophila pseudoobscura* and *D. affinis* (Nguyen *et al.*, 2022). *Helitrons* transpose by a mechanism similar to rolling-circle replication via a single-stranded DNA intermediate and have been suggested to preferentially insert in AT-rich regions; RIP and RIP-related mechanisms increase the percentage in AT and are more abundant in non-recombining regions, which could have facilitated the accumulation of *Helitrons* (Grabundzija *et al.*, 2016). It is striking that the same superfamilies preferentially expanded repeatedly in multiple non-recombining regions of *Microbotryum* fungi. Their particular mechanisms of transpositions may be particularly efficient in regions where recombination is suppressed, perhaps due to the chromatin landscape (Quadrana *et al.*, 2019); LTR elements for example preferentially target heterochromatin (Marsano & Dimitri, 2022).

We inferred TE copy genealogies of the most abundant superfamilies in non-recombining regions (*Copia* and *Ty3* superfamilies) to investigate the dynamics of their accumulation in the different genomic compartments and the impact of recombination suppression events. We found recent accumulation of TE copies through bursts occurring in all genomic compartments, *i.e.*, the non-recombining regions, the autosomes and the centromeres, many of them being

shared by species deriving from a same recombination suppression event. This suggests that TE accumulation in *Microbotryum* genomes followed recombination suppression, not only in the non-recombining regions, but also in the rest of the genome and therefore having genome-wide impact. The genealogies were based on a fraction of the *Copia* and *Ty3* retrotransposon copies, due to the necessity to identify the 5'-LTR sequences, on which the genealogies are based. However, the 5'-LTR sequences were sometimes lost in degraded TE copies or could not be distinguished from the 3'-LTR sequence when the coding sequences were degenerated and could not be oriented. Nevertheless, considering the very low divergence between the TE copies within the genealogies, the burst patterns should not be affected by the sub-sampling of TE copies. Moreover, we found TE bursts involving copies from divergent *Microbotryum* species, indicating that the sampling of the TE copies used for the genealogies was good enough to capture accumulation events older than species divergence. This analysis thus informs on the TE dynamics in genomes of species with a large range of ages of recombination suppression. Further supporting the TE reservoir hypothesis (Hood *et al.*, 2004; Wei *et al.*, 2020), we found a similar pattern of copy divergence between the non-recombining regions and the autosomes of the *Copia* and *Ty3* retroelements and a strong significant positive correlation between TE load in the non-recombining regions and the autosomes. These bursts of accumulation likely result from relaxed purifying selection following recombination suppression rather than from increased intrinsic TE activity, as shown also following polyploidization (Baduel *et al.*, 2019).

We found similar TE content in pseudo-autosomal regions compared to autosomes, without preferential accumulation of TE copies at the margin of the non-recombining regions. TEs nevertheless accumulate everywhere in genomes following the formation of a non-recombining region acting as a TE reservoir. The copies thereby accumulating at the margin of the non-recombining regions may impact their evolution (Maloisel & Rossignol, 1998; Ben-Aroya *et*

*al.*, 2004; Yelina *et al.*, 2012; Kent *et al.*, 2017). TEs can trigger chromosomal rearrangements (Balachandran *et al.*, 2022), and they carry silencing marks, such as DNA methylation and heterochromatin formation, that can suppress recombination (Maloisel & Rossignol, 1998; Ben-Aroya *et al.*, 2004; Yelina *et al.*, 2012, 2015; Bachtrog, 2013; Li *et al.*, 2016; Kent *et al.*, 2017). TEs can also induce deleterious mutations, which can select for recombination suppression for sheltering them (Jay *et al.*, 2022). A DNA fragment evolving recombination cessation capturing fewer deleterious mutations than the population average should be selected for, but will express its load at the homozygous state when it rises in frequency, unless it also captures a permanently heterozygous allele such as a mating-type allele (Jay *et al.*, 2022). The more deleterious mutations segregate in genomes, the more this effect can act: a given fragment evolving recombination cessation and capturing a permanently heterozygous allele will have a higher chance to have a higher fitness differential with the average if the distribution of the number of deleterious mutations in this fragment is wider in the population, so that selection will be stronger (Jay *et al.*, 2022).

We found that TEs have rapidly accumulated in mating-type chromosomes following recombination suppression, but TE content reached a plateau relatively abruptly at about 50% of occupied base pairs after 1.5 MY. The rapid initial accumulation of TEs is expected: under the lack of recombination, new TE insertions cannot be purged, and each new copy can further make new copies (Quadrana *et al.*, 2019; Legrand *et al.*, 2019). The slowdown of TE accumulation after 1.5 MY can be due to several, non-exclusive phenomena: i) selection against new insertions or for a more efficient control may be stronger when the load becomes higher if its costs increase with copy number, or if TE insertions are more deleterious with time because genes become hemizygous. Indeed, TE insertions in genes would be sheltered in a heterozygous state early after recombination suppression but not anymore following hemizygous gene losses,

as often occurs in sex chromosomes and in particular in *Microbotryum* fungi (Bachtrog, 2013; Badouin *et al.*, 2015); ii) extant control mechanisms against TE proliferation can become more efficient with time by a cumulative effect, e.g. if methylation accumulates with generations (Teixeira & Colot, 2010), or could even evolve to become more efficient; iii) new TE insertions nested in more ancient copies can further contribute to inactivate TEs, as suggested by the decreased proportion of *Helitrons* intact copies with time since recombination suppression in non-recombining regions; *Helitrons* in particular often display high proportions of non-autonomous copies (Sweredoski *et al.*, 2008); iv) the chromatin landscape of non-recombining regions may become less favorable to new insertions, as for example histone can induce a preferential integration of C*opia* retrotransposons (Quadrana *et al.*, 2019).

The rate of degeneration for non-recombining regions in *Microbotryum* fungi has been previously analysed in terms of non-synonymous substitutions and frequency of optimal codons (Carpentier *et al.*, 2022). Purifying selection on non-synonymous substitutions was lower in non-recombining regions than in autosomes and remained nearly constant through time (Carpentier *et al.*, 2022). The frequency of optimal codons decreased rapidly following recombination suppression and then reached an asymptote at a level above random codon usage. It is not unexpected to find different shapes of degeneration tempo for DNA substitutions and TE insertions, as they correspond to very different mechanisms of evolution.

## Conclusion

In conclusion, this study leverages on a unique dataset of 21 independent evolutionary strata of different ages in closely related species to assess the dynamics of TE accumulation with time following recombination suppression. We show that TEs have rapidly accumulated following recombination cessation and that the TE accumulation slowed down abruptly around 50% of

occupied base pairs after 1.5 MY. We further show that some superfamilies repeatedly expanded in independent non-recombining regions, and in particular *Helitrons* that were yet not abundant before recombination suppression. *Copia* and *Ty3* superfamilies were also over-represented in non-recombining regions and have accumulated through bursts, both in the non-recombining regions of the mating-type chromosomes and in the autosomes of *Microbotryum* species at the same time; this finding supports the TE reservoir hypothesis, i.e., that the TEs accumulated in non-recombining regions have a genome-wide impact by transposing to recombining regions. This study thus sheds light on important processes to improve our knowledge on genome evolution and in particular on the consequences of recombination suppression.

## Additional files and pipelines

All supplementary tables (Supplementary Tables 1 - 8) are included as xlsx files. The TE detection pipeline is available at https://gitlab.com/marine.c.duhamel/microtep.

## Competing interests

The authors declare that they have no competing interests.

## Funding

This work was supported by the National Institute of Health (NIH) grant R15GM119092 to M. E. H., the Louis D. Foundation award and the EvolSexChrom ERC advanced grant #832352 to T. G., and an IDEX Paris-Saclay Bochum University PhD grant to M.D.

## Author contributions

M.D., T.G., R.C.R.d.l.V. and M.E.H designed the study. T.G., R.C.R.d.l.V. and M.E.H supervised the study. M.D. performed the genomic and statistical analyses and produced the figures. R.C.R.d.l.V. validated the analyses. T.G. and M.D. wrote the original draft. All authors contributed to the manuscript.

## Acknowledgements

We thank Dominik Begerow, Sebastian Klenner, Lena Steins and Frederick Witfeld for providing useful comments on the manuscript. We thank Gilles Fisher, Paul Jay and Jacqui Shykoff for useful discussions.

## References

**Abascal F, Zardoya R, Telford MJ**. **2010**. TranslatorX: multiple alignment of nucleotide sequences guided by amino acid translations. *Nucleic Acids Research* **38**: W7-13.

**Ade C, Roy-Engel AM, Deininger PL**. **2013**. Alu elements: An intrinsic source of human genome instability. *Current opinion in virology* **3**: 639–645.

**Ahmed S, Cock JM, Pessia E, Luthringer R, Cormier A, Robuchon M, Sterck L, Peters AF, Dittami SM, Corre E, *et al.*2014**. A haploid system of sex determination in the brown alga Ectocarpus sp. *Current biology: CB* **24**: 1945–1957.

**Altschul SF, Gish W, Miller W, Myers EW, Lipman DJ**. **1990**. Basic local alignment search tool. *Journal of Molecular Biology* **215**: 403–410.

**Amselem J, Lebrun M-H, Quesneville H**. **2015**. Whole genome comparative analysis of transposable elements provides new insight into mechanisms of their inactivation in fungal genomes. *BMC genomics* **16**: 141.

**Andrenacci D, Cavaliere V, Lattanzi G**. **2020**. The role of transposable elements activity in aging and their possible involvement in laminopathic diseases. *Ageing Research Reviews* **57**: 100995.

**Bachtrog D**. **2003**. Accumulation of Spock and Worf, two novel non-LTR retrotransposons, on the neo-Y chromosome of Drosophila miranda. *Molecular Biology and Evolution* **20**: 173–181.

**Bachtrog D**. **2005**. Sex chromosome evolution: Molecular aspects of Y-chromosome degeneration in Drosophila. *Genome Research* **15**: 1393–1401.

**Bachtrog D**. **2013**. Y chromosome evolution: emerging insights into processes of Y chromosome degeneration. *Nature reviews. Genetics* **14**: 113–124.

**Badouin H, Gladieux P, Gouzy J, Siguenza S, Aguileta G, Snirc A, Prieur SL, Jeziorski C, Branca A, Giraud T**. **2017**. Widespread selective sweeps throughout the genome of model plant pathogenic fungi and identification of effector candidates. *Molecular Ecology* **26**: 2041–2062.

**Badouin H, Hood ME, Gouzy J, Aguileta G, Siguenza S, Perlin MH, Cuomo CA, Fairhead C, Branca A, Giraud T**. **2015**. Chaos of rearrangements in the mating-type chromosomes of the anther-smut fungus *Microbotryum lychnidis-dioicae*. *Genetics* **200**: 1275–1284.

**Baduel P, Quadrana L, Hunter B, Bomblies K, Colot V**. **2019**. Relaxed purifying selection in autopolyploids drives transposable element over-accumulation which provides variants for local adaptation. *Nature Communications* **10**: 5818.

**Bakkeren G, Jiang G, Warren RL, Butterfield Y, Shin H, Chiu R, Linning R, Schein J, Lee N, Hu G, *et al.*2006**. Mating factor linkage and genome evolution in basidiomycetous pathogens of cereals. *Fungal genetics and biology: FG & B* **43**: 655–666.

**Balachandran P, Walawalkar IA, Flores JI, Dayton JN, Audano PA, Beck CR**. **2022**. Transposable element-mediated rearrangements are prevalent in human genomes. : 2022.06.16.496479.

**Bao Z, Eddy SR**. **2002**. Automated de novo identification of repeat sequence families in sequenced genomes. *Genome Research* **12**: 1269–1276.

**Bao W, Kojima KK, Kohany O**. **2015**. Repbase Update, a database of repetitive elements in eukaryotic genomes. *Mobile DNA* **6**: 11.

**Beckerson WC, Rodríguez de la Vega RC, Hartmann FE, Duhamel M, Giraud T, Perlin MH**. **2019**. Cause and effectors: whole-genome comparisons reveal shared but rapidly evolving effector sets among host-specific plant-castrating fungi. *mBio* **10**: e02391-19.

**Ben-Aroya S, Mieczkowski PA, Petes TD, Kupiec M**. **2004**. The compact chromatin structure of a Ty repeated sequence suppresses recombination hotspot activity in Saccharomyces cerevisiae. *Molecular Cell* **15**: 221–231.

**Bennetzen JL, Wang H**. **2014**. The contributions of transposable elements to the structure, function, and evolution of plant genomes. *Annual Review of Plant Biology* **65**: 505–530.

**Benson G**. **1999**. Tandem repeats finder: a program to analyze DNA sequences. *Nucleic Acids Research* **27**: 573–580.

**Bergero R, Charlesworth D**. **2009**. The evolution of restricted recombination in sex chromosomes. *Trends in Ecology & Evolution* **24**: 94–102.

**Bewick AJ, Hofmeister BT, Powers RA, Mondo SJ, Grigoriev IV, James TY, Stajich JE, Schmitz RJ**. **2019**. Diversity of cytosine methylation across the fungal tree of life. *Nature Ecology & Evolution* **3**: 479–490.

**Blackmon H, Adams RH**. **2015**. EvobiR: Tools for comparative analyses and teaching evolutionary biology.

**Bourque G, Burns KH, Gehring M, Gorbunova V, Seluanov A, Hammell M, Imbeault M, Izsvák Z, Levin HL, Macfarlan TS, *et al.*2018**. Ten things you should know about transposable elements. *Genome Biology* **19**: 199.

**Branco S, Badouin H, Rodríguez de la Vega RC, Gouzy J, Carpentier F, Aguileta G, Siguenza S, Brandenburg J-T, Coelho MA, Hood ME, *et al.*2017**. Evolutionary strata on young mating-type chromosomes despite the lack of sexual antagonism. *Proceedings of the National Academy of Sciences of the United States of America* **114**: 7067–7072.

**Branco S, Carpentier F, Rodríguez de la Vega RC, Badouin H, Snirc A, Le Prieur S, Coelho MA, de Vienne DM, Hartmann FE, Begerow D, *et al.*2018**. Multiple convergent supergene evolution events in mating-type chromosomes. *Nature Communications* **9**.

**Burns KH**. **2020**. Our Conflict with Transposable Elements and Its Implications for Human Disease. *Annual Review of Pathology* **15**: 51–70.

**Carpentier F, Rodríguez de la Vega RC, Branco S, Snirc A, Coelho MA, Hood ME, Giraud T**. **2019**. Convergent recombination cessation between mating-type genes and centromeres in selfing anther-smut fungi. *Genome Research* **29**: 944–953.

**Carpentier F, Rodríguez de la Vega RC, Jay P, Duhamel M, Shykoff JA, Perlin MH, Wallen RM, Hood ME, Giraud T**. **2022**. Tempo of degeneration across independently evolved non-recombining regions. *Molecular Biology and Evolution*: msac060.

**Castanera R, López-Varas L, Borgognone A, LaButti K, Lapidus A, Schmutz J, Grimwood J, Pérez G, Pisabarro AG, Grigoriev IV, *et al.*2016**. Transposable elements

versus the fungal genome: Impact on whole-genome architecture and transcriptional profiles. *PLOS Genetics* **12**: e1006108.
**Charlesworth D**. **2017**. Evolution of recombination rates between sex chromosomes. *Philosophical Transactions of the Royal Society B: Biological Sciences* **372**: 20160456.
**Charlesworth D**. **2021**. The timing of genetic degeneration of sex chromosomes. *Philosophical Transactions of the Royal Society B: Biological Sciences* **376**: 20200093.
**Charlesworth B, Campos JL**. **2014**. The relations between recombination rate and patterns of molecular variation and evolution in *Drosophila*. *Annual Review of Genetics* **48**: 383–403.
**Charlesworth B, Charlesworth D**. **2000**. The degeneration of Y chromosomes. *Philosophical Transactions of the Royal Society of London. Series B, Biological Sciences* **355**: 1563–1572.
**Choi JY, Lee YCG**. **2020**. Double-edged sword: The evolutionary consequences of the epigenetic silencing of transposable elements. *PLoS Genetics* **16**: e1008872.
**Dallery J-F, Lapalu N, Zampounis A, Pigné S, Luyten I, Amselem J, Wittenberg AHJ, Zhou S, de Queiroz MV, Robin GP, *et al.*2017**. Gapless genome assembly of Colletotrichum higginsianum reveals chromosome structure and association of transposable elements with secondary metabolite gene clusters. *BMC Genomics* **18**: 667.
**Day AW**. **1979**. Mating type and morphogenesis in Ustilago violacea. *Botanical Gazette* **140**: 94–101.
**Deniz Ö, Frost JM, Branco MR**. **2019**. Regulation of transposable elements by DNA modifications. *Nature Reviews. Genetics* **20**: 417–431.
**Dolgin ES, Charlesworth B**. **2008**. The Effects of Recombination Rate on the Distribution and Abundance of Transposable Elements. *Genetics* **178**: 2169–2177.
**van Dongen S**. **2000**. Graph clustering by flow simulation. *PhD thesis, Center for Math and Computer Science (CWI)*.
**Duhamel M, Carpentier F, Begerow D, Hood ME, Rodríguez de la Vega RC, Giraud T**. **2022**. Onset and stepwise extensions of recombination suppression are common in mating-type chromosomes of Microbotryum anther-smut fungi. *Journal of Evolutionary Biology* **n/a**.
**Edgar RC**. **2004**. MUSCLE: a multiple sequence alignment method with reduced time and space complexity. *BMC Bioinformatics* **5**: 113.
**Ekseth OK, Kuiper M, Mironov V**. **2014**. orthAgogue: an agile tool for the rapid prediction of orthology relations. *Bioinformatics (Oxford, England)* **30**: 734–736.
**Ellinghaus D, Kurtz S, Willhoeft U**. **2008**. LTRharvest, an efficient and flexible software for de novo detection of LTR retrotransposons. *BMC bioinformatics* **9**: 18.
**Erlandsson R, Wilson JF, Pääbo S**. **2000**. Sex chromosomal transposable element accumulation and male-driven substitutional evolution in humans. *Molecular Biology and Evolution* **17**: 804–812.
**Foissac S, Gouzy J, Rombauts S, Mathe C, Amselem J, Sterck L, de Peer Y, Rouze P, Schiex T**. **2008**. Genome annotation in plants and fungi: EuGene as a model platform. *Current Bioinformatics* **3**: 87–97.
**Fontanillas E, Hood ME, Badouin H, Petit E, Barbe V, Gouzy J, de Vienne DM, Aguileta G, Poulain J, Wincker P, *et al.*2015**. Degeneration of the non-recombining regions in the mating-type chromosomes of the anther-smut fungi. *Molecular Biology and Evolution* **32**: 928–943.
**Galagan JE, Selker EU**. **2004**. RIP: the evolutionary cost of genome defense. *Trends in Genetics* **20**: 417–423.
**Giraud T, Yockteng R, López-Villavicencio M, Refrégier G, Hood ME**. **2008**. Mating system of the anther smut fungus Microbotryum violaceum: selfing under heterothallism. *Eukaryotic Cell* **7**: 765–775.
**González LG, Deyholos MK**. **2012**. Identification, characterization and distribution of transposable elements in the flax (Linum usitatissimum L.) genome. *BMC Genomics* **13**: 644.
**Grabundzija I, Messing SA, Thomas J, Cosby RL, Bilic I, Miskey C, Gogol-Döring A, Kapitonov V, Diem T, Dalda A, *et al.*2016**. A Helitron transposon reconstructed from bats

reveals a novel mechanism of genome shuffling in eukaryotes. *Nature Communications* **7**: 10716.
**Guindon S, Dufayard J-F, Lefort V, Anisimova M, Hordijk W, Gascuel O**. **2010**. New algorithms and methods to estimate maximum-likelihood phylogenies: assessing the performance of PhyML 3.0. *Systematic Biology* **59**: 307–321.
**Han K, Lee J, Meyer TJ, Remedios P, Goodwin L, Batzer MA**. **2008**. L1 recombination-associated deletions generate human genomic variation. *Proceedings of the National Academy of Sciences of the United States of America* **105**: 19366–19371.
**Hancks DC, Kazazian HH**. **2016**. Roles for retrotransposon insertions in human disease. *Mobile DNA* **7**: 9.
**Handley L-JL, Ceplitis H, Ellegren H**. **2004**. Evolutionary strata on the chicken Z chromosome: implications for sex chromosome evolution. *Genetics* **167**: 367–376.
**Hartmann FE, Duhamel M, Carpentier F, Hood ME, Foulongne-Oriol M, Silar P, Malagnac F, Grognet P, Giraud T**. **2021**. Recombination suppression and evolutionary strata around mating-type loci in fungi: documenting patterns and understanding evolutionary and mechanistic causes. *The New Phytologist* **229**: 2470–2491.
**Hoang DT, Chernomor O, von Haeseler A, Minh BQ, Vinh LS**. **2018**. UFBoot2: Improving the ultrafast bootstrap approximation. *Molecular Biology and Evolution* **35**: 518–522.
**Hof AE van't, Campagne P, Rigden DJ, Yung CJ, Lingley J, Quail MA, Hall N, Darby AC, Saccheri IJ**. **2016**. The industrial melanism mutation in British peppered moths is a transposable element. *Nature* **534**: 102–105.
**Hood ME, Antonovics J**. **2000**. Intratetrad mating, heterozygosity, and the maintenance of deleterious alleles in Microbotryum violaceum (=Ustilago violacea). *Heredity* **85 Pt 3**: 231–241.
**Hood ME, Antonovics J, Koskella B**. **2004**. Shared forces of sex chromosome evolution in haploid-mating and diploid-mating organisms. *Genetics* **168**: 141–146.
**Hood ME, Katawczik M, Giraud T**. **2005**. Repeat-induced point mutation and the population structure of transposable elements in Microbotryum violaceum. *Genetics* **170**: 1081–1089.
**Horns F, Petit E, Hood ME**. **2017**. Massive expansion of gypsy-like retrotransposons in Microbotryum fungi. *Genome Biology and Evolution* **9**: 363–371.
**Horns F, Petit E, Yockteng R, Hood ME**. **2012**. Patterns of repeat-induced point mutation in transposable elements of basidiomycete fungi. *Genome Biology and Evolution* **4**: 240–247.
**Hua-Van A, Le Rouzic A, Maisonhaute C, Capy P**. **2005**. Abundance, distribution and dynamics of retrotransposable elements and transposons: similarities and differences. *Cytogenetic and Genome Research* **110**: 426–440.
**Hurvich CM, Simonoff JS, Tsai C-L**. **1998**. Smoothing parameter selection in nonparametric regression using an improved Akaike information criterion. *Journal of the Royal Statistical Society: Series B (Statistical Methodology)* **60**: 271–293.
**Idnurm A, Hood ME, Johannesson H, Giraud T**. **2015**. Contrasted patterns in mating-type chromosomes in fungi: hotspots versus coldspots of recombination. *Fungal Biology Reviews* **29**: 220–229.
**Ironside JE**. **2010**. No amicable divorce? Challenging the notion that sexual antagonism drives sex chromosome evolution. *BioEssays* **32**: 718–726.
**Jay P, Tezenas E, Véber A, Giraud T**. **2022**. Sheltering of deleterious mutations explains the stepwise extension of recombination suppression on sex chromosomes and other supergenes. *PLOS Biology* **20**: e3001698.
**Johnson LJ, Giraud T, Anderson R, Hood ME**. **2010**. The impact of genome defense on mobile elements in Microbotryum. *Genetica* **138**: 313–319.
**Jones PA**. **2012**. Functions of DNA methylation: islands, start sites, gene bodies and beyond. *Nature Reviews Genetics* **13**: 484–492.
**Kaessmann H, Vinckenbosch N, Long M**. **2009**. RNA-based gene duplication: mechanistic and evolutionary insights. *Nature Reviews Genetics* **10**: 19–31.
**Kalyaanamoorthy S, Minh BQ, Wong TKF, von Haeseler A, Jermiin LS**. **2017**.

ModelFinder: fast model selection for accurate phylogenetic estimates. *Nature Methods* **14**: 587–589.
**Kapitonov VV, Jurka J**. **2001**. Rolling-circle transposons in eukaryotes. *Proceedings of the National Academy of Sciences of the United States of America* **98**: 8714–8719.
**Katoh K, Misawa K, Kuma K, Miyata T**. **2002**. MAFFT: a novel method for rapid multiple sequence alignment based on fast Fourier transform. *Nucleic Acids Research* **30**: 3059–3066.
**Kent TV, Uzunović J, Wright SI**. **2017**. Coevolution between transposable elements and recombination. *Philosophical Transactions of the Royal Society B: Biological Sciences* **372**: 20160458.
**Kronstad JW, Staben C**. **1997**. Mating type in filamentous fungi. *Annual Review of Genetics* **31**: 245–276.
**Krzywinski M, Schein J, Birol I, Connors J, Gascoyne R, Horsman D, Jones SJ, Marra MA**. **2009**. Circos: an information aesthetic for comparative genomics. *Genome Research* **19**: 1639–1645.
**Lahn BT, Page DC**. **1999**. Four evolutionary strata on the human X chromosome. *Science (New York, N.Y.)* **286**: 964–967.
**Lanciano S, Mirouze M**. **2018**. Transposable elements: all mobile, all different, some stress responsive, some adaptive? *Current Opinion in Genetics & Development* **49**: 106–114.
**Legrand S, Caron T, Maumus F, Schvartzman S, Quadrana L, Durand E, Gallina S, Pauwels M, Mazoyer C, Huyghe L, *et al.*2019**. Differential retention of transposable element-derived sequences in outcrossing Arabidopsis genomes. *Mobile DNA* **10**: 30.
**Lengeler KB, Fox DS, Fraser JA, Allen A, Forrester K, Dietrich FS, Heitman J**. **2002**. Mating-type locus of Cryptococcus neoformans: a step in the evolution of sex chromosomes. *Eukaryotic Cell* **1**: 704–718.
**Li S-F, Zhang G-J, Yuan J-H, Deng C-L, Gao W-J**. **2016**. Repetitive sequences and epigenetic modification: inseparable partners play important roles in the evolution of plant sex chromosomes. *Planta* **243**: 1083–1095.
**Lim JK, Simmons MJ**. **1994**. Gross chromosome rearrangements mediated by transposable elements in Drosophila melanogaster. *BioEssays: News and Reviews in Molecular, Cellular and Developmental Biology* **16**: 269–275.
**Maloisel L, Rossignol JL**. **1998**. Suppression of crossing-over by DNA methylation in Ascobolus. *Genes & Development* **12**: 1381–1389.
**Marais G, Nicolas M, Bergero R, Chambrier P, Kejnovsky E, Monéger F, Hobza R, Widmer A, Charlesworth D**. **2008**. Evidence for degeneration of the Y chromosome in the dioecious plant Silene latifolia. *Current biology : CB* **18**: 545–9.
**Marsano RM, Dimitri P**. **2022**. Constitutive heterochromatin in eukaryotic genomes: A mine of transposable elements. *Cells* **11**: 761.
**Martin A, Troadec C, Boualem A, Rajab M, Fernandez R, Morin H, Pitrat M, Dogimont C, Bendahmane A**. **2009**. A transposon-induced epigenetic change leads to sex determination in melon. *Nature* **461**: 1135–1138.
**Mawaribuchi S, Takahashi S, Wada M, Uno Y, Matsuda Y, Kondo M, Fukui A, Takamatsu N, Taira M, Ito M**. **2017**. Sex chromosome differentiation and the W- and Z-specific loci in Xenopus laevis. *Developmental Biology* **426**: 393–400.
**Menkis A, Jacobson DJ, Gustafsson T, Johannesson H**. **2008**. The mating-type chromosome in the filamentous Ascomycete Neurospora tetrasperma represents a model for early evolution of sex chromosomes. *PLoS Genetics* **4**.
**Minh BQ, Nguyen MAT, von Haeseler A**. **2013**. Ultrafast approximation for phylogenetic bootstrap. *Molecular Biology and Evolution* **30**: 1188–1195.
**Minh BQ, Schmidt HA, Chernomor O, Schrempf D, Woodhams MD, von Haeseler A, Lanfear R**. **2020**. IQ-TREE 2: New models and efficient methods for phylogenetic inference in the genomic era. *Molecular Biology and Evolution* **37**: 1530–1534.
**Muller HJ**. **1918**. Genetic variability, twin hybrids and constant hybrids, in a case of balanced lethal factors. *Genetics* **3**: 422–499.

**Nguyen A, Wang W, Chong E, Chatla K, Bachtrog D**. **2022**. Transposable element accumulation drives size differences among polymorphic Y Chromosomes in Drosophila. *Genome Research*: gr.275996.121.
**Paradis E, Schliep K**. **2019**. ape 5.0: an environment for modern phylogenetics and evolutionary analyses in R. *Bioinformatics (Oxford, England)* **35**: 526–528.
**Payer LM, Burns KH**. **2019**. Transposable elements in human genetic disease. *Nature Reviews. Genetics* **20**: 760–772.
**Peng JC, Karpen GH**. **2008**. Epigenetic regulation of heterochromatic DNA stability. *Current opinion in genetics & development* **18**: 204.
**Plohl M, Meštrović N, Mravinac B**. **2014**. Centromere identity from the DNA point of view. *Chromosoma* **123**: 313–325.
**Price AL, Jones NC, Pevzner PA**. **2005**. De novo identification of repeat families in large genomes. *Bioinformatics (Oxford, England)* **21 Suppl 1**: i351-358.
**Puterova J, Kubat Z, Kejnovsky E, Jesionek W, Cizkova J, Vyskot B, Hobza R**. **2018**. The slowdown of Y chromosome expansion in dioecious Silene latifolia due to DNA loss and male-specific silencing of retrotransposons. *BMC Genomics* **19**: 153.
**Quadrana L, Etcheverry M, Gilly A, Caillieux E, Madoui M-A, Guy J, Bortolini Silveira A, Engelen S, Baillet V, Wincker P, *et al.*2019**. Transposition favors the generation of large effect mutations that may facilitate rapid adaption. *Nature Communications* **10**: 3421.
**Quesneville H**. **2020**. Twenty years of transposable element analysis in the Arabidopsis thaliana genome. *Mobile DNA* **11**: 28.
**Raffaele S, Kamoun S**. **2012**. Genome evolution in filamentous plant pathogens: why bigger can be better. *Nature Reviews Microbiology* **10**: 417–430.
**Revell LJ**. **2012**. phytools: an R package for phylogenetic comparative biology (and other things): *phytools: R package*. *Methods in Ecology and Evolution* **3**: 217–223.
**Rifkin JL, Hnatovska S, Yuan M, Sacchi BM, Choudhury BI, Gong Y, Rastas P, Barrett SCH, Wright SI**. **2022**. Recombination landscape dimorphism and sex chromosome evolution in the dioecious plant Rumex hastatulus. *Philosophical Transactions of the Royal Society B*.
**Ritz C, Jensen SM, Gerhard D, Streibig JC**. **2019**. *Dose-Response Analysis Using R*. New York.
**Saito K, Siomi MC**. **2010**. Small RNA-mediated quiescence of transposable elements in animals. *Developmental Cell* **19**: 687–697.
**Schnable PS, Ware D, Fulton RS, Stein JC, Wei F, Pasternak S, Liang C, Zhang J, Fulton L, Graves TA, *et al.*2009**. The B73 maize genome: complexity, diversity, and dynamics. *Science (New York, N.Y.)* **326**: 1112–1115.
**Śliwińska EB, Martyka R, Tryjanowski P**. **2016**. Evolutionary interaction between W/Y chromosome and transposable elements. *Genetica* **144**: 267–278.
**Smit AFA, Hubley R**. **2008**. RepeatModeler Open-1.0.
**Sweredoski M, DeRose-Wilson L, Gaut BS**. **2008**. A comparative computational analysis of nonautonomous Helitron elements between maize and rice. *BMC Genomics* **9**: 467.
**Teixeira FK, Colot V**. **2010**. Repeat elements and the Arabidopsis DNA methylation landscape. *Heredity* **105**: 14–23.
**Wang X, Ji X**. **2020**. fANCOVA: Nonparametric Analysis of Covariance.
**Wei K, Aldaimalani R, Mai D, Zinshteyn D, Prv S, Blumenstiel JP, Kelleher ES, Brooks E**. **2022**. Rethinking the “gypsy” retrotransposon: A roadmap for community-driven reconsideration of problematic gene names.
**Wei KH-C, Gibilisco L, Bachtrog D**. **2020**. Epigenetic conflict on a degenerating Y chromosome increases mutational burden in Drosophila males. *Nature Communications* **11**: 5537.
**Whittle CA, Sun Y, Johannesson H**. **2011**. Degeneration in codon usage within the region of suppressed recombination in the mating-type chromosomes of Neurospora tetrasperma. *Eukaryotic Cell* **10**: 594–603.
**Wicker T, Sabot F, Hua-Van A, Bennetzen JL, Capy P, Chalhoub B, Flavell A, Leroy P,**

**Morgante M, Panaud O, *et al.*2007**. A unified classification system for eukaryotic transposable elements. *Nature Reviews Genetics* **8**: 973–982.
**Wickham H**. **2009**. *ggplot2: Elegant graphics for data analysis*. New York: Springer-Verlag.
**Wood SN**. **2011**. Fast stable restricted maximum likelihood and marginal likelihood estimation of semiparametric generalized linear models. *Journal of the Royal Statistical Society: Series B (Statistical Methodology)* **73**: 3–36.
**Wright SI, Agrawal N, Bureau TE**. **2003**. Effects of recombination rate and gene density on transposable element distributions in Arabidopsis thaliana. *Genome Research* **13**: 1897–1903.
**Yelina NE, Choi K, Chelysheva L, Macaulay M, de Snoo B, Wijnker E, Miller N, Drouaud J, Grelon M, Copenhaver GP, *et al.*2012**. Epigenetic remodeling of meiotic crossover frequency in Arabidopsis thaliana DNA methyltransferase mutants. *PLoS Genetics* **8**: e1002844.
**Yelina NE, Lambing C, Hardcastle TJ, Zhao X, Santos B, Henderson IR**. **2015**. DNA methylation epigenetically silences crossover hot spots and controls chromosomal domains of meiotic recombination in Arabidopsis. *Genes & Development* **29**: 2183–2202.
**Yu G, Smith DK, Zhu H, Guan Y, Lam TT-Y**. **2017**. ggtree: an r package for visualization and annotation of phylogenetic trees with their covariates and other associated data. *Methods in Ecology and Evolution* **8**: 28–36.
**Zemach A, McDaniel IE, Silva P, Zilberman D**. **2010**. Genome-wide evolutionary analysis of eukaryotic DNA methylation. *Science (New York, N.Y.)* **328**: 916–919.
**Zhang L, Yan L, Jiang J, Wang Y, Jiang Y, Yan T, Cao Y**. **2014**. The structure and retrotransposition mechanism of LTR-retrotransposons in the asexual yeast Candida albicans. *Virulence* **5**: 655–664.

## Figures

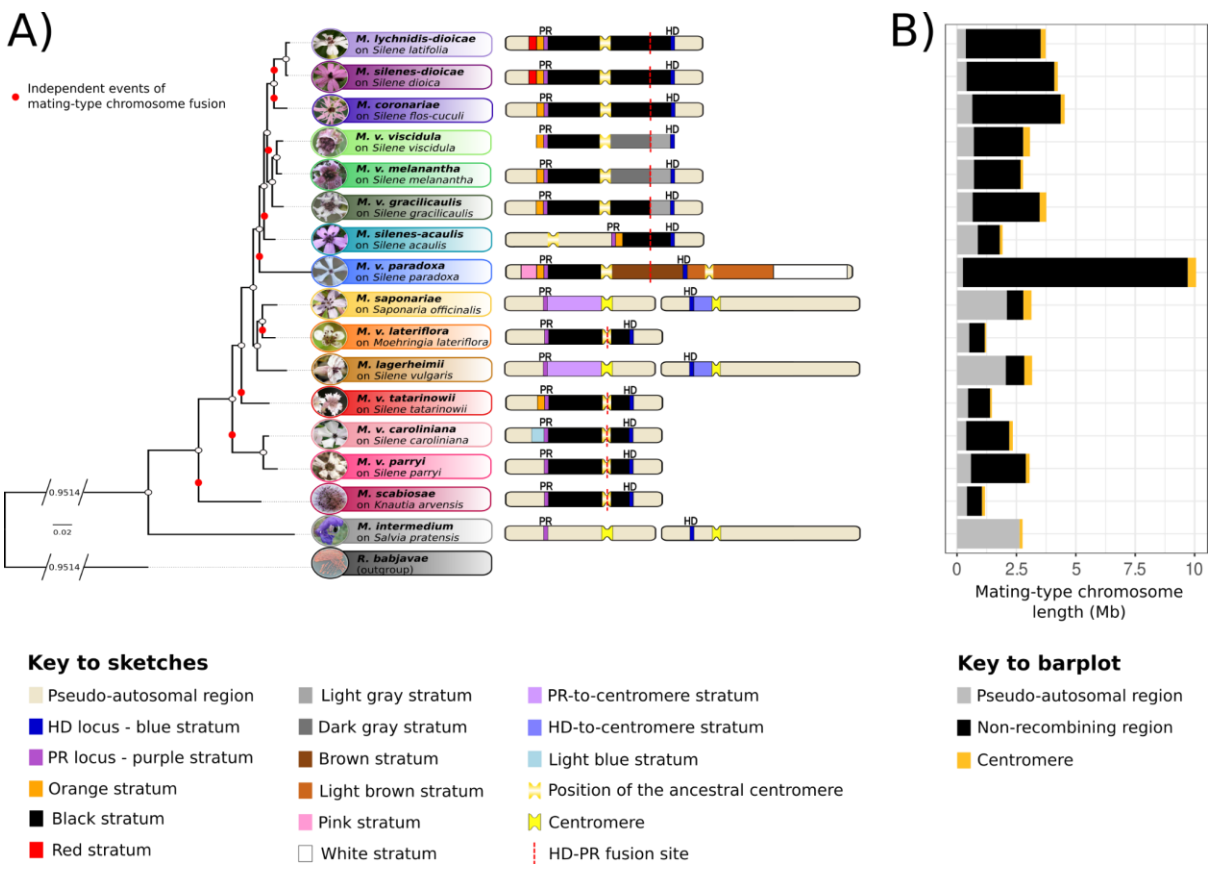


**Figure 1: Multiple evolutionary strata formed by independent events of mating-type locus linkage and stepwise extension of recombination suppression in *Microbotryum* fungi. A)** The mating-type chromosomes of *Microbotryum* species with linked mating-type loci have had many rearrangements but are depicted here according to the gene order at the moment of the fusion between the homeodomain (HD) and pheromone-receptor (PR) chromosomes, the fusion site being indicated by a dashed red line. The ancestral gene order was inferred from *Microbotryum lagerheimii* and *M. intermedium* which have unlinked mating-type loci and collinear mating-type chromosomes. The old blue and purple strata have evolved before diversification of the *Microbotryum* clade. In *M. saponariae* and *M. lagerheimii*, recombination cessation linked each mating-type locus to their respective centromeres, forming the HD- and

PR-to-centromere strata. The black strata correspond to the events of recombination suppression having linked the two mating-type loci, which occurred independently at least nine times in *Microbotryum*, indicated by red dots on the phylogeny. In some species (*M. violaceum viscidula*, *M. v. melanantha*, *M. v. gracilicaulis)*, recombination between the mating-type loci was gradually suppressed following the chromosomal fusion event, and formed several strata called black, light gray and dark gray strata. In *M. v. paradoxa*, recombination was partially restored by introgression before being suppressed again, forming the brown stratum. In many species, recombination cessation further extended beyond the mating-type loci, capturing different sets of genes and forming strata that were named as indicated in the figure key. **B)** Average ($a_1$-$a_2$) size of the mating-type chromosomes in *Microbotryum* fungi. The average ($a_1$-$a_2$) size of the pseudo-autosomal region, non-recombining region and centromere is represented in gray, black and yellow, respectively.

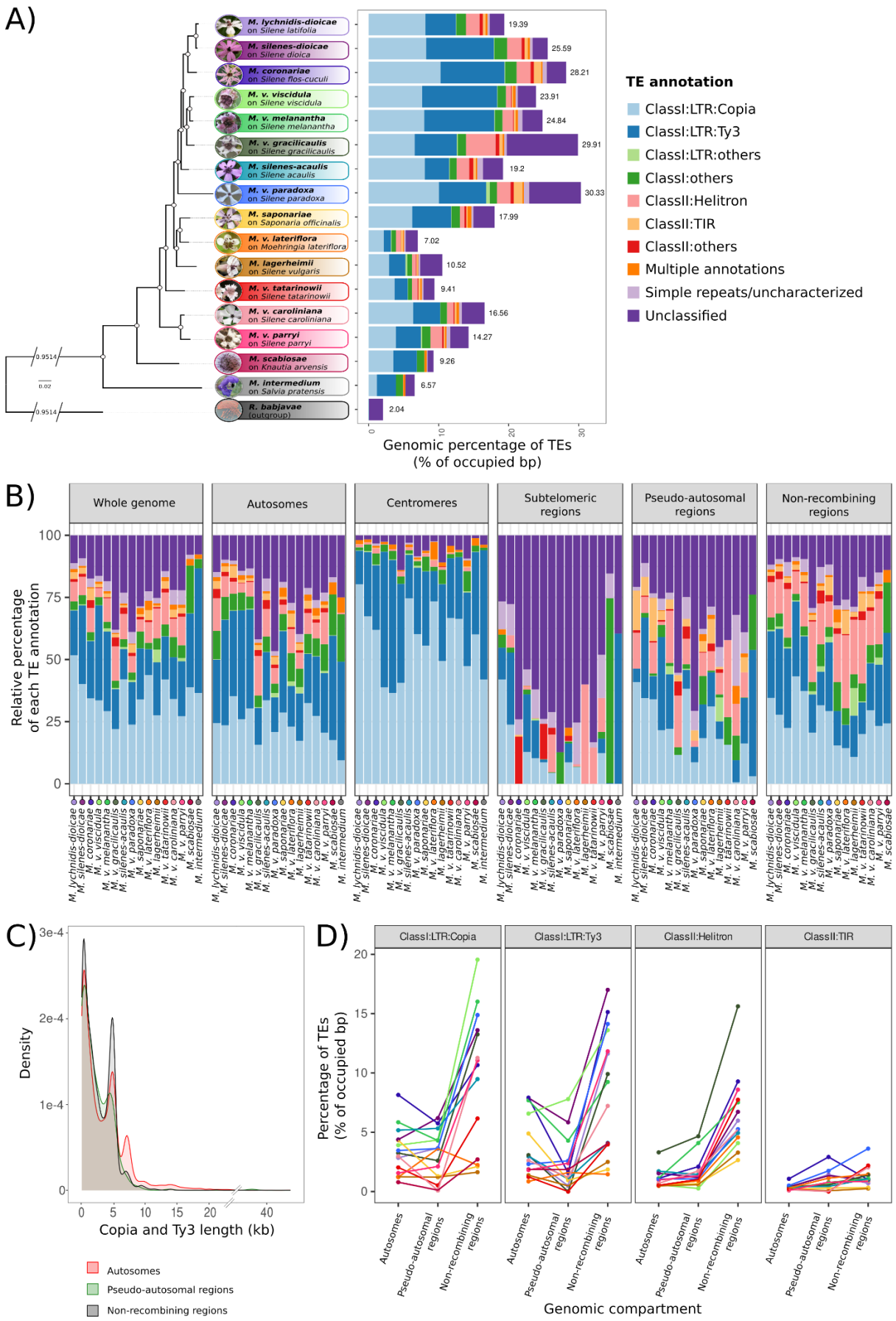
A)
M. lychnidis-dioicae on Silene latifolia
M. silenes-dioicae on Silene dioica
M. coronariae on Silene flos-cuculi
M. v. viscidula on Silene viscidula
M. v. melanantha on Silene melanantha
M. v. gracilicaulis on Silene gracilicaulis
M. silenes-acaulis on Silene acaulis
M. v. paradoxa on Silene paradoxa
M. saponariae on Saponaria officinalis
M. v. lateriflora on Moehringia lateriflora
M. lagerheimii on Silene vulgaris
M. v. tatarinowii on Silene tatarinowii
M. v. caroliniana on Silene caroliniana
M. v. parryi on Silene parryi
M. scabiosae on Knautia arvensis
M. intermedium on Salvia pratensis
R. babjavae (outgroup)
19.39
25.59
28.21
23.91
24.84
29.91
19.2
30.33
17.99
7.02
10.52
9.41
16.56
14.27
9.26
6.57
2.04
0.9514
0.02
0.9514
0
10
20
30
Genomic percentage of TEs
(% of occupied bp)
TE annotation
ClassI:LTR:Copia
ClassI:LTR:Ty3
ClassI:LTR:others
ClassI:others
ClassII:Helitron
ClassII:TIR
ClassII:others
Multiple annotations
Simple repeats/uncharacterized
Unclassified
B)
Whole genome
Autosomes
Centromeres
Subtelomeric regions
Pseudo-autosomal regions
Non-recombining regions
Relative percentage of each TE annotation
100
75
50
25
0
M. lychnidis-dioicae
M. silenes-dioicae
M. coronariae
M. v. viscidula
M. v. melanantha
M. v. gracilicaulis
M. silenes-acaulis
M. saponariae
M. v. lateriflora
M. lagerheimii
M. v. tatarinowii
M. v. caroliniana
M. v. parryi
M. scabiosae
M. intermedium
C)
Density
3e-4
2e-4
1e-4
0
0
5
10
15
20
40
Copia and Ty3 length (kb)
Autosomes
Pseudo-autosomal regions
Non-recombining regions
D)
ClassI:LTR:Copia
ClassI:LTR:Ty3
ClassII:Helitron
ClassII:TIR
Percentage of TEs
(% of occupied bp)
20
15
10
5
0
Autosomes
Pseudo-autosomal regions
Non-recombining regions
Genomic compartment

**Figure 2: Transposable element (TE) composition of *Microbotryum* genomes. A)** Whole-genome TE load (as percentage of occupied base pairs) across the *Microbotryum* phylogeny, each color representing a TE category. Numeric values correspond to the $a_1$-$a_2$ average. **B)** Relative proportions of the various TE categories in the different genomic compartments of *Microbotryum* genomes. Each color represents a TE category, as in A). **C)** Distribution of the length of *Copia* and *Ty3* retroelements in the autosomes, the pseudo-autosomal regions and the non-recombining regions of *Microbotryum* fungi, in red, green and black, respectively. **D)** TE load per genomic compartment, *i.e.*, autosomes (without the non-recombining centromeres), pseudo-autosomal regions and non-recombining regions for the main TE categories (*Copia*, *Ty3*, *Helitron*, terminal inverted repeats - TIR). The lines connect the values in the same species, to facilitate comparisons. Each color represents a *Microbotryum* species.

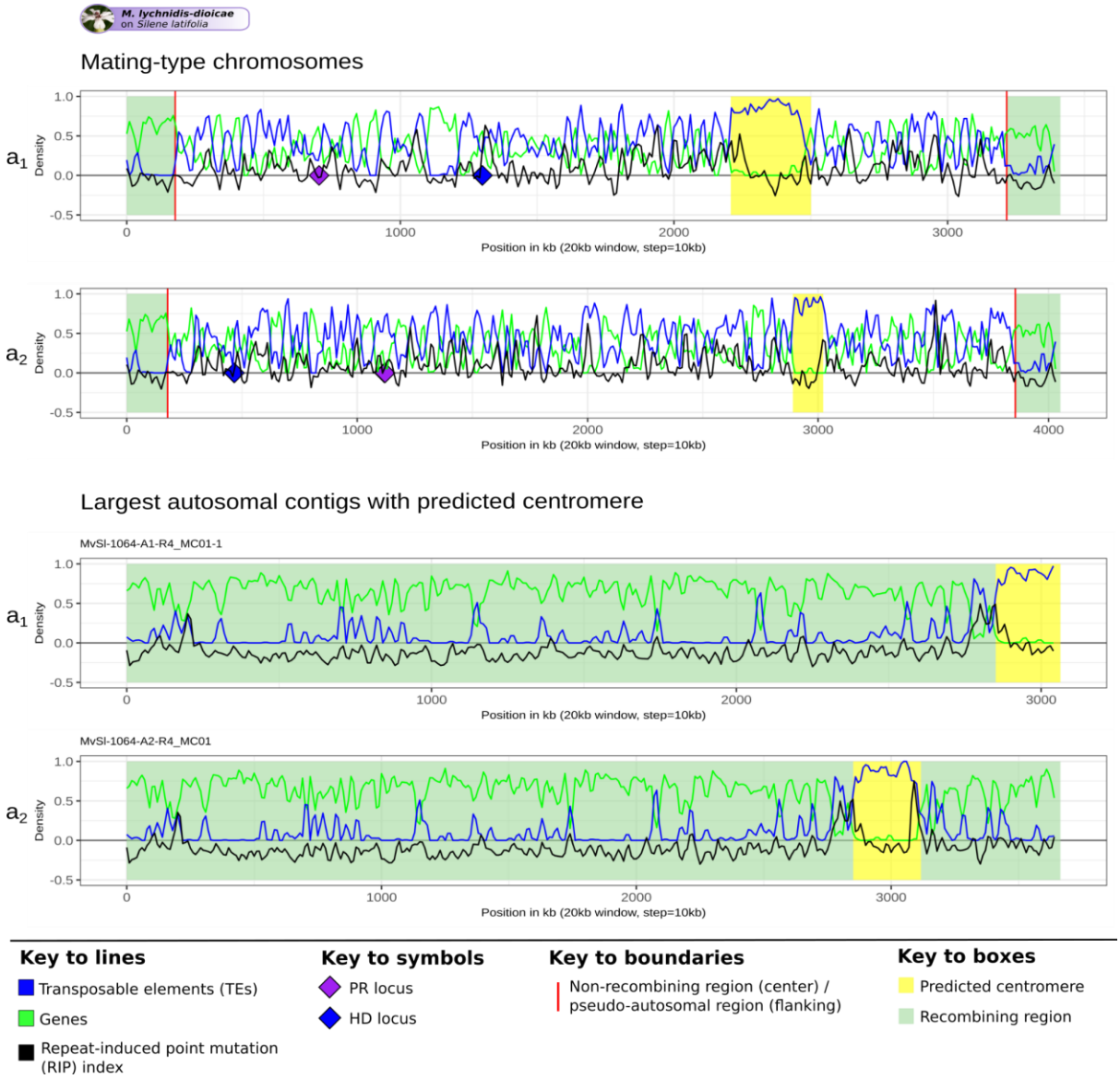


**Figure 3: Density of transposable elements (TEs), genes and repeat-induced point mutations (RIP) along the mating-type chromosome and the autosomes of *Microbotryum lychnidis-dioicae*.** Density of TEs, genes and RIP-like index were calculated in 20 kb non-overlapping windows. A RIP-like index greater than zero indicates that the region is affected by a mechanism leading to C to T transitions resembling RIP. Predicted centromeres are indicated in yellow. Recombining regions of the mating-type chromosomes (pseudo-autosomal regions) and an autosome (the largest autosomal contig in the genome harboring a predicted centromere) are highlighted in pale green. The non-recombining region is delimited by red

1135 lines. Pheromone-receptor (PR) and homeodomain (HD) loci are indicated by purple and blue diamonds, respectively. The plots for the other species are shown in Figure S6.

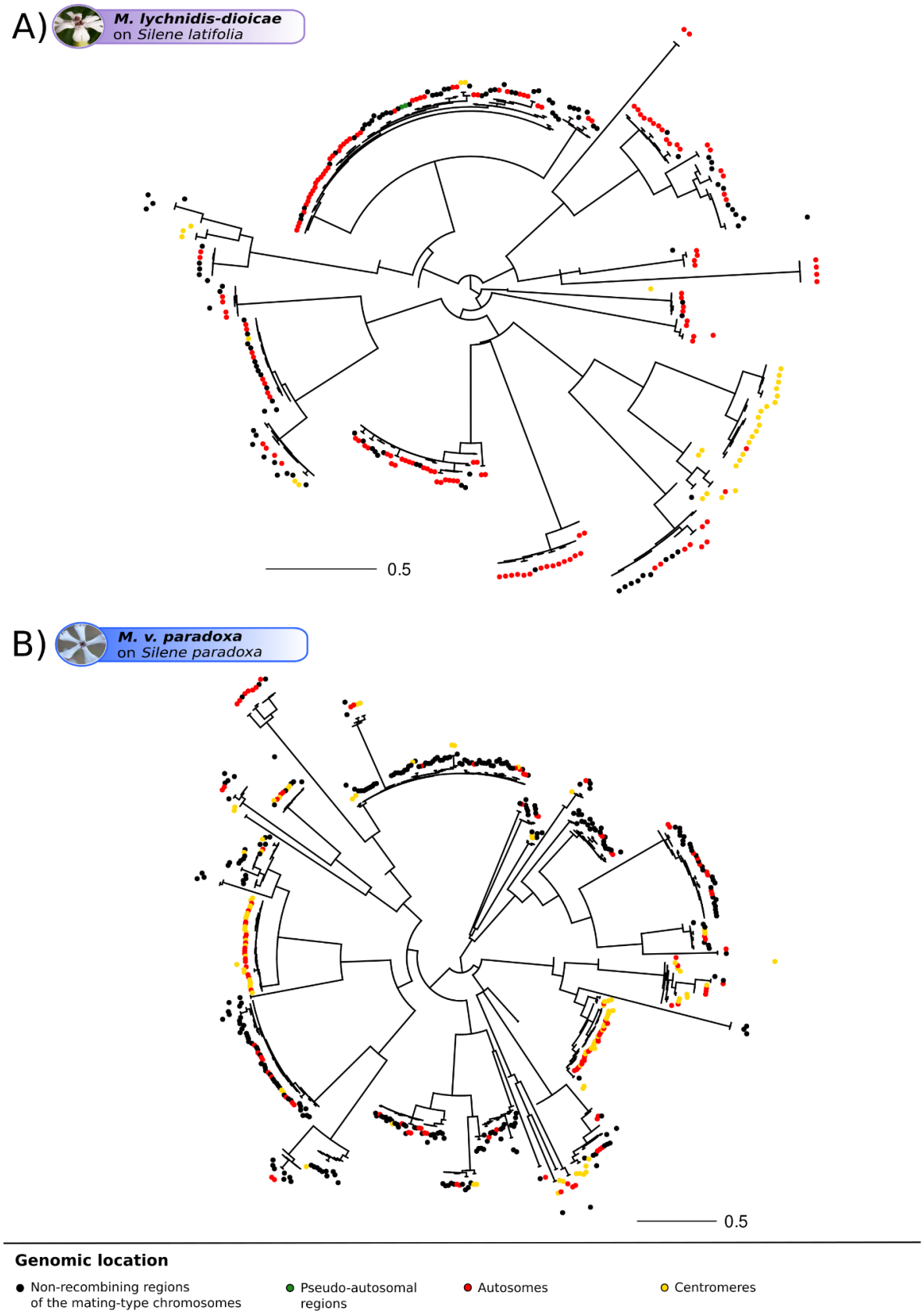


**Figure 4: Single-species genealogies of *Copia* retroelement copies in *Microbotryum***

**genomes.** Single-species genealogies of *Copia* copies in *Microbotryum lychnidis-dioicae* **(A)** and *Microbotryum violaceum paradoxa* **(B)**. The color of the dots at the tip of the branches corresponds to the genomic location of the transposable element (TE) copies. Other single-species *Copia* and *Ty3* genealogies are shown in Supplementary Figures S11 and S12, respectively.

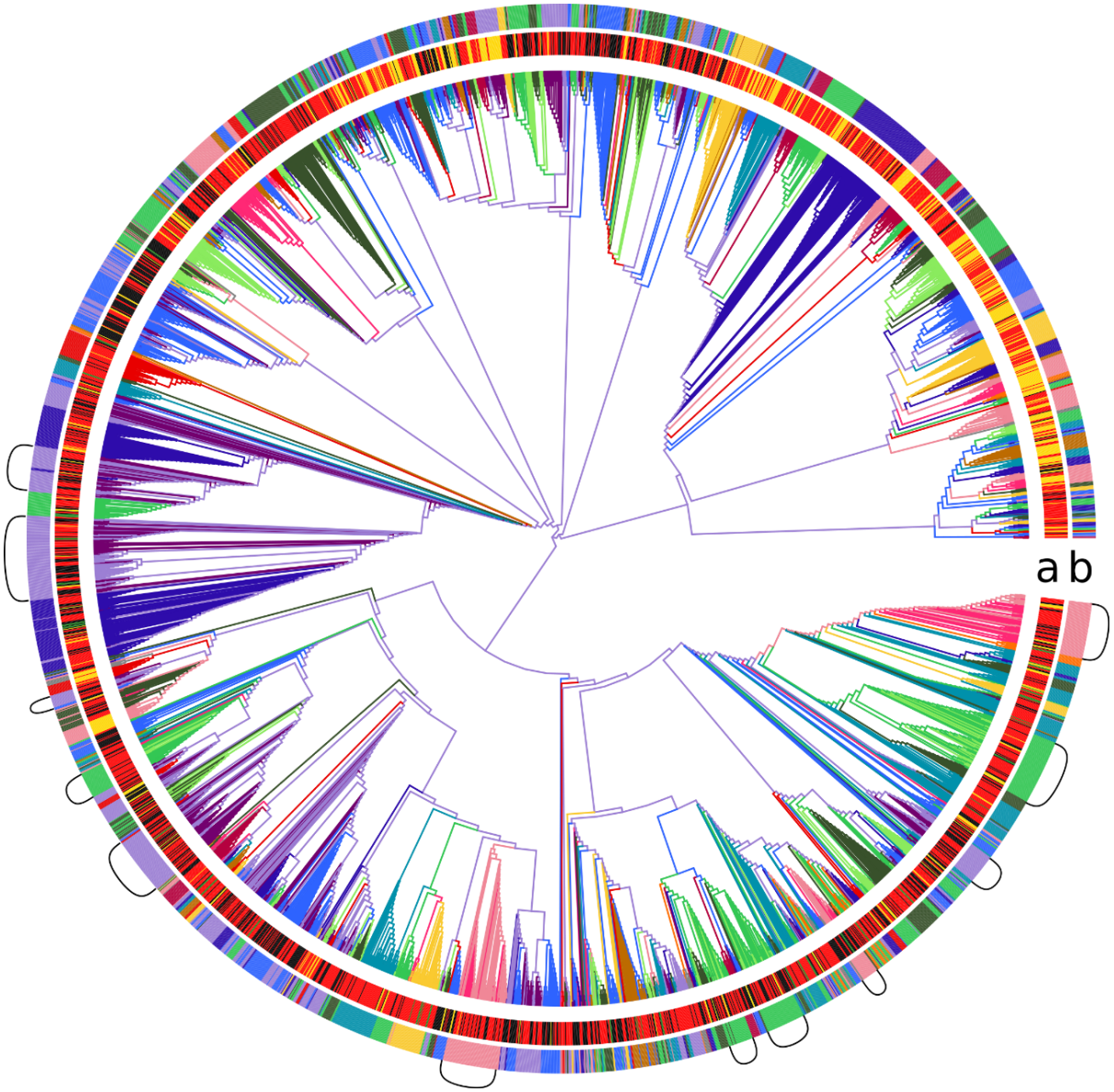


**Genomic location (a)**

- Non-recombining regions of the mating-type chromosomes
- Pseudo-autosomal regions)
- Centromeres
- Autosomes

**Species (branch color)**

**Recombination suppression event group (b)**

- *M. lychnidis-dioicae* on *Silene latifolia*
- *M. silenes-dioicae* on *Silene dioica*
- *M. coronariae* on *Silene flos-cuculi*
- *M. v. viscidula* on *Silene viscidula*
- *M. v. melanantha* on *Silene melanantha*
- *M. v. gracilicaulis* on *Silene gracilicaulis*
- *M. silenes-acaulis* on *Silene acaulis*
- *M. v. paradoxa* on *Silene paradoxa*
- *M. saponariae* on *Saponaria officinalis*
- *M. v. lateriflora* on *Moehringia lateriflora*
- *M. lagerheimii* on *Silene vulgaris*
- *M. v. tatarinowii* on *Silene tatarinowii*
- *M. v. caroliniana* on *Silene caroliniana*
- *M. v. parryi* on *Silene parryi*
- *M. scabiosae* on *Knautia arvensis*
- *M. intermedium* on *Salvia pratensis*

**Figure 5: Multi-species genealogies of *Copia* retroelement copies in *Microbotryum* genomes.** Multi-species *Copia* tree of all *Microbotryum* species of this study. The branch color corresponds to the species, the first inner track (a) corresponds to the genomic location of the TE copies, the second outer track (b) corresponds to the linkage event group of the species carrying the TE copy. Brackets highlight bursts of TEs. Multi-species *Ty3* tree of all *Microbotryum* species is shown in Supplementary Figure S14. Multi-species *Copia* and *Ty3* genealogies with branch lengths are shown in Supplementary Figure S15.

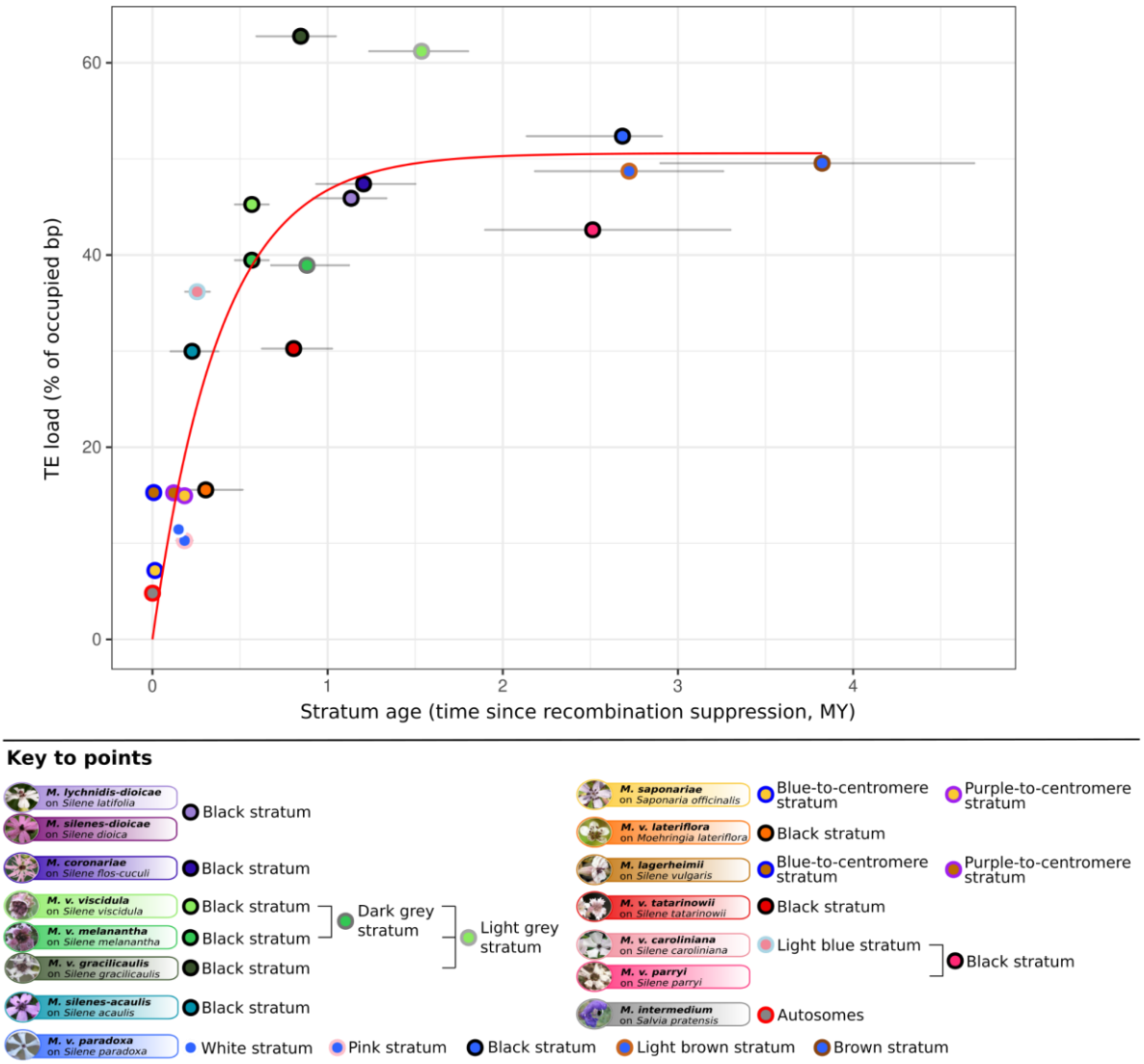


**Figure 6: Tempo of transposable element (TE) accumulation in the non-recombining regions of the *Microbotryum* mating-type chromosomes.** Percentage of base pairs occupied by TEs in non-recombining regions (means in $a_1$ and $a_2$ genomes and means across species sharing the same strata) as a function of their age in million years (MY) with confidence intervals. The red curve shows the prediction of the best model corresponding to a negative exponential model. Each dot corresponds to an independent evolutionary stratum.

**Supplementary Figure S1: Relative percentage and number of transposable element (TE) sequences per genomic compartment used for the genealogies based on their 5'-LTR sequences, for *Copia* (A) and *Ty3* (B) elements.** The total number of 5'-LTR sequences available per species is indicated in brackets under the species name. Single-species genealogies were only built for species with grey filled rectangles around their names.

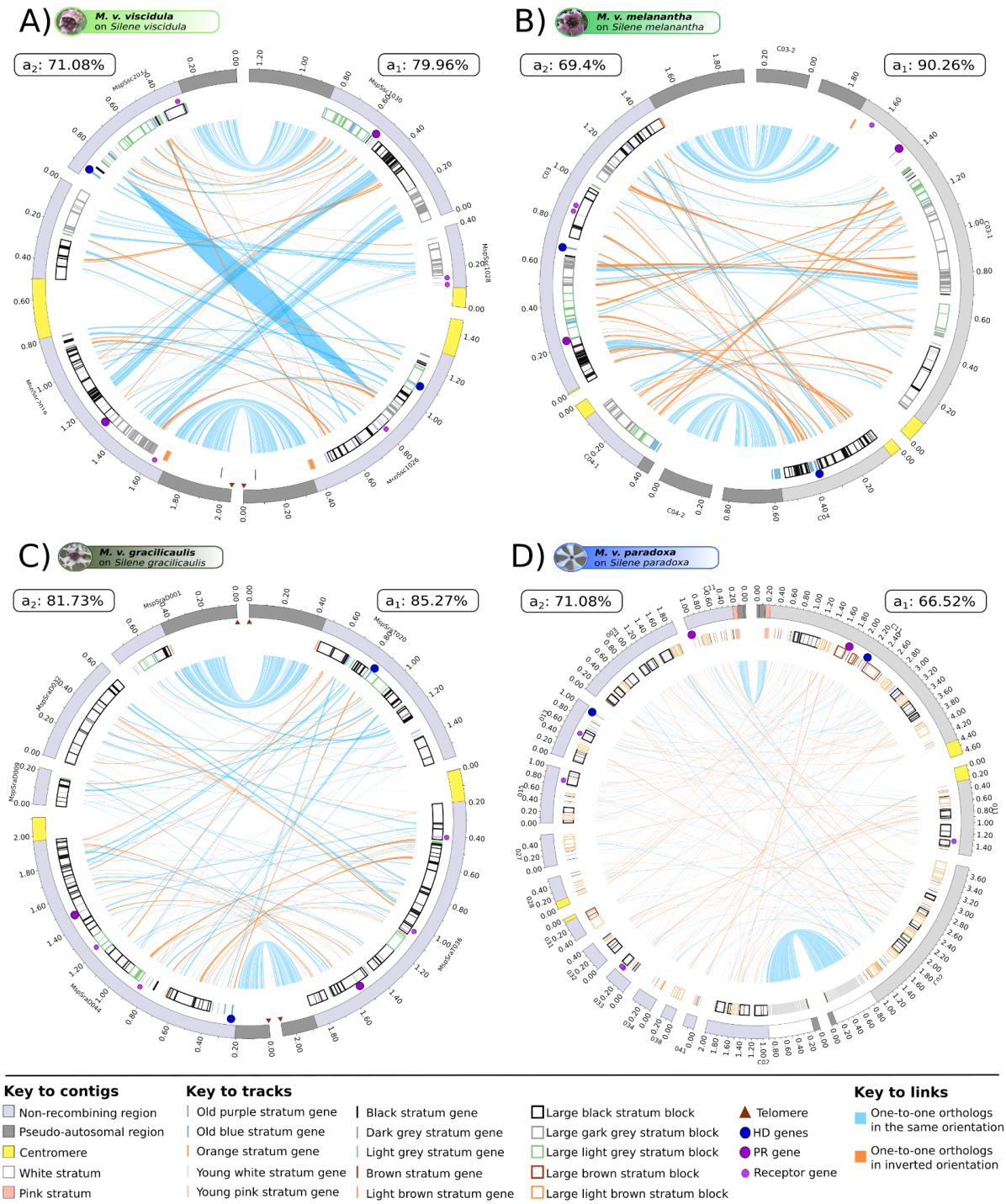


**Supplementary Figure S2: Delimitation of blocks for the rearranged evolutionary strata in mating-type chromosomes.** The PR, HD and pheromone genes are represented by purple, blue and small light purple circles, respectively. The outer track represents contigs, with length ticks every 200 kb and centromeres indicated in yellow. Non-recombining regions are

displayed in dark grey and pseudo-autosomal regions in light gray. The young, non-rearranged white and pink strata of *M. v. paradoxa* are highlighted on the outer track. Genes from the different strata are displayed by bars on the inner track (see Figure 1 for the stratum formation history). Large blocks (greater than 80 kb) of genes from a single stratum are indicated on the inner track by rectangles. The light grey stratum is displayed in green to facilitate visualization. The percentage of non-recombining regions retained in the blocks of strata are indicated next to the mating type, on each side of the circos plots. Blue and orange lines link alleles, the latter corresponding to inversions. The link width is proportional to the corresponding gene length.

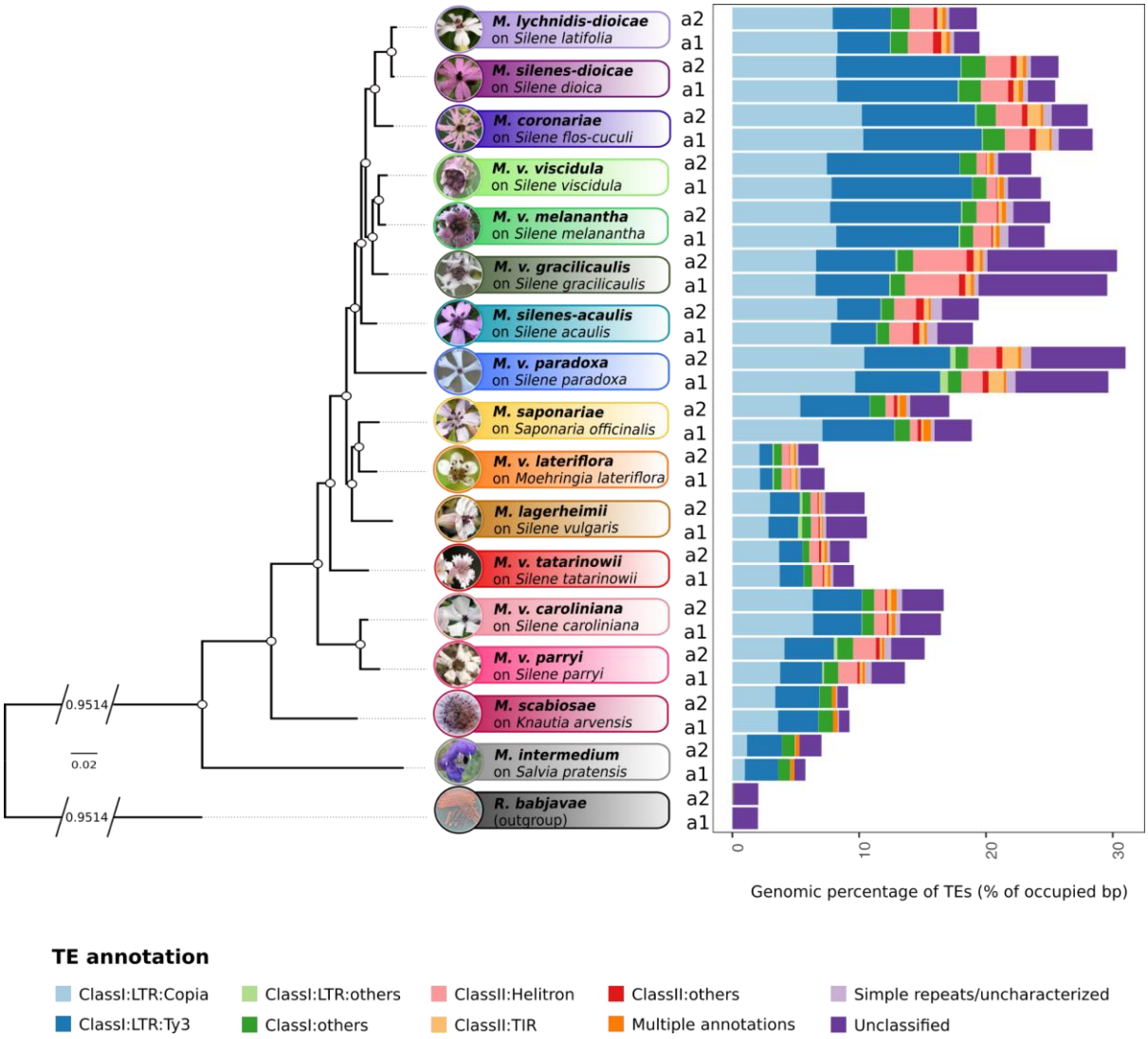


**Supplementary figure S3: Percentage of base pairs occupied by transposable elements (TEs) in *Microbotryum* genomes, both for $a_1$ and $a_2$ mating-type chromosomes.** Whole-genome TE content across the *Microbotryum* phylogeny, for each mating-type genome, each color representing a TE category.

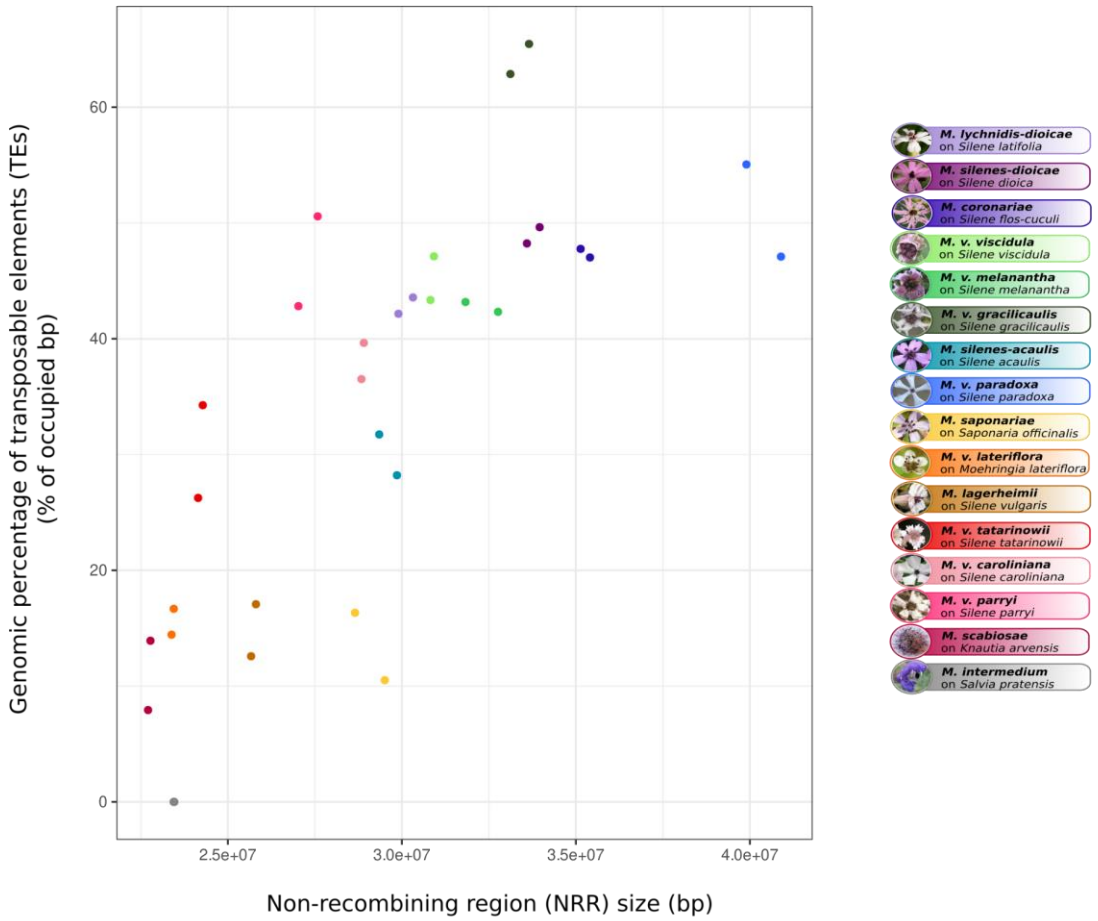


**Supplementary figure S4: Relationship between the percentage of base pairs occupied by TEs and the total size of non-recombining regions.** Each color represents one species,, one point per mating type.

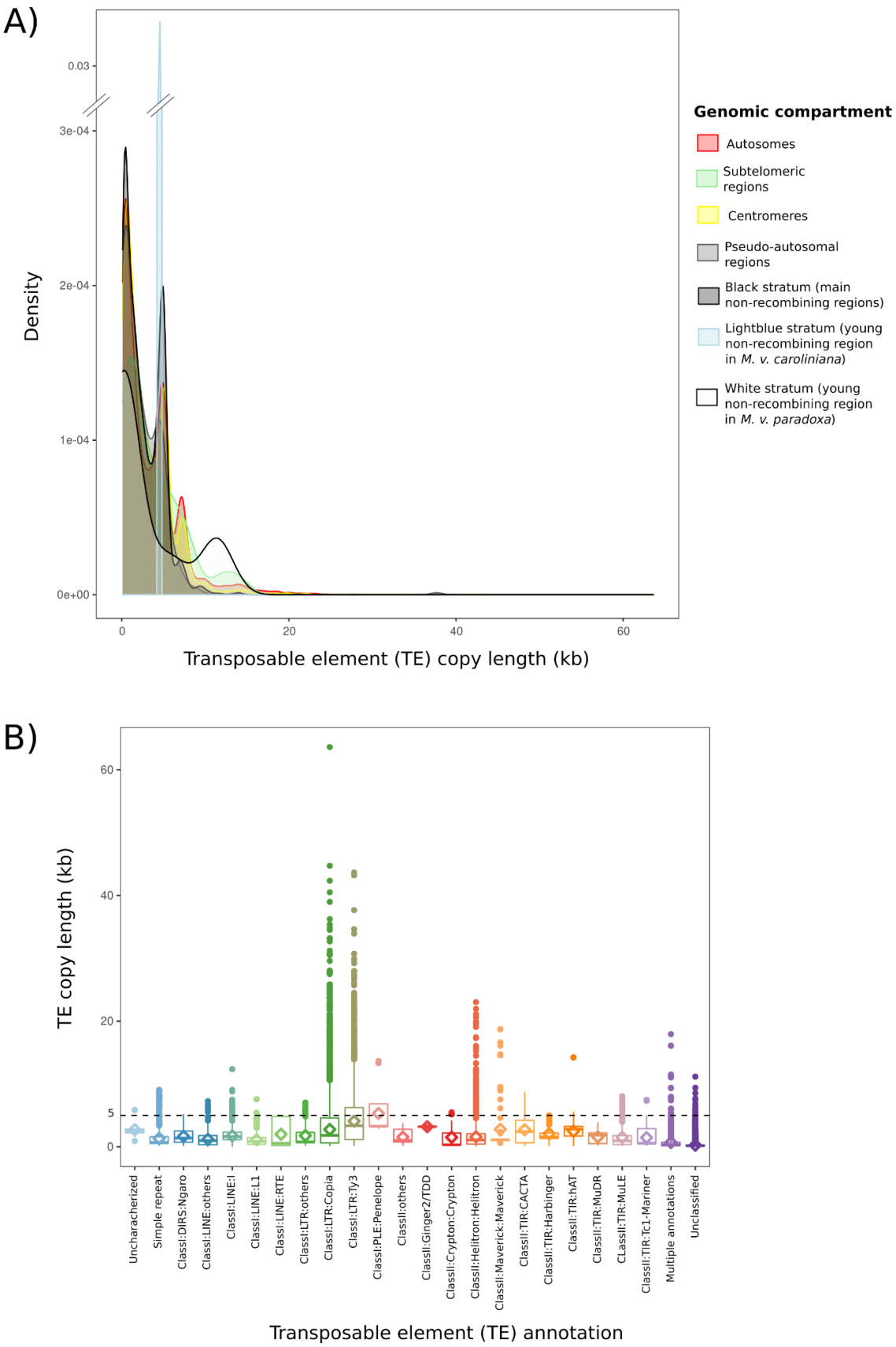


1205

**Supplementary figure S5: Distribution of transposable element (TE) copy length in**

***Microbotryum* genomes. A)** Distribution of the *Copia* and *Ty3* retrotransposon copy length in the different genomic compartments in various *Microbotryum* species. Note that the Y axis is interrupted by parallel bars. **B)** Distribution of the length of individual TE copies for each TE annotation, across all *Microbotryum* genomes. Each color corresponds to a specific annotation. The dashed line indicates the 5 kb expected mean length of *Copia* and *Ty3* retroelements. Similar annotations representing a small proportion of the *Microbotryum* genomes were pooled in all the other figures; e.g., *ClassII:TIR* with two inverted repeats corresponds to all the *TIR* elements, i.e., *CACTA*, *Harbinger*, *hAT*, *MuDR*, *MuLE* and *Tc1-Mariner*.

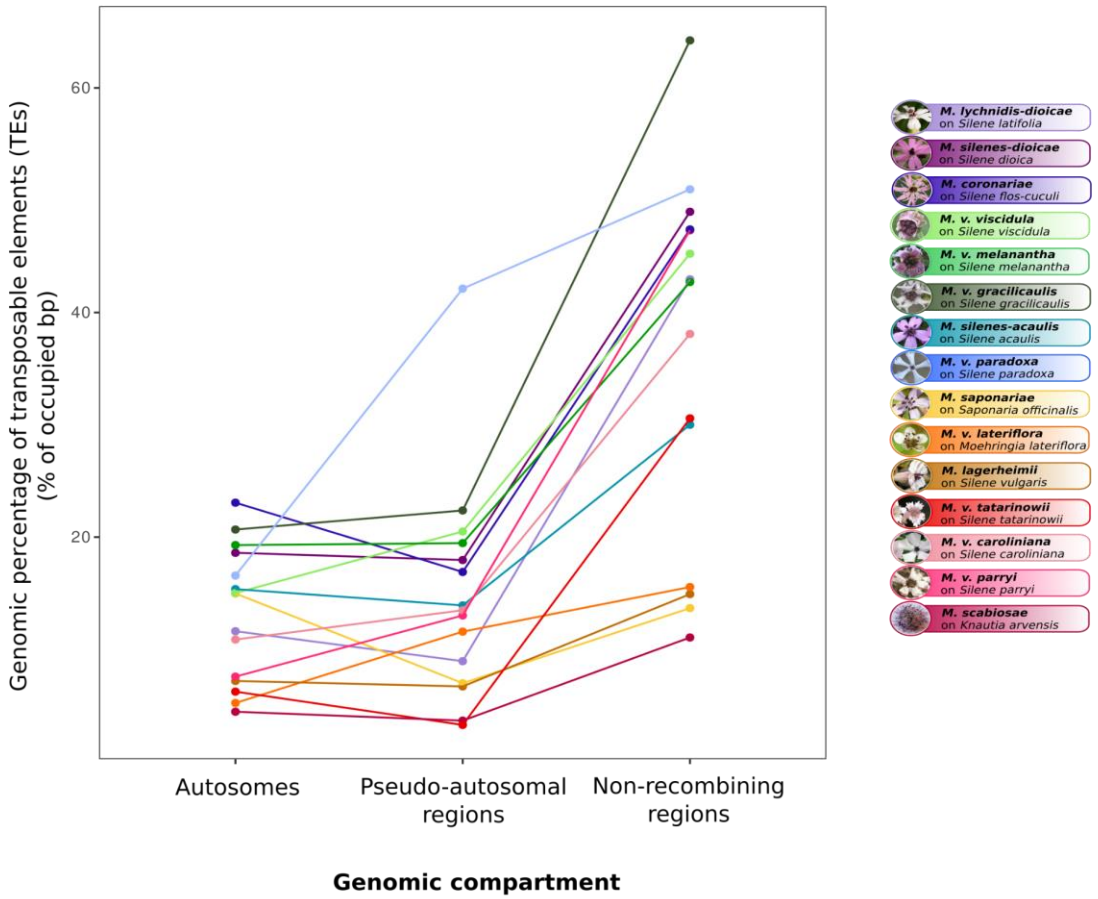


**Supplementary Figure S6: Transposable element (TE) proportions in the different genomic compartments of *Microbotryum* fungi.** Total TE load per genomic compartment, i.e., autosomes (without the centromeres), pseudo-autosomal regions and non-recombining regions. The lines connect the values in the same species to facilitate comparisons. Each color represents a *Microbotryum* species.

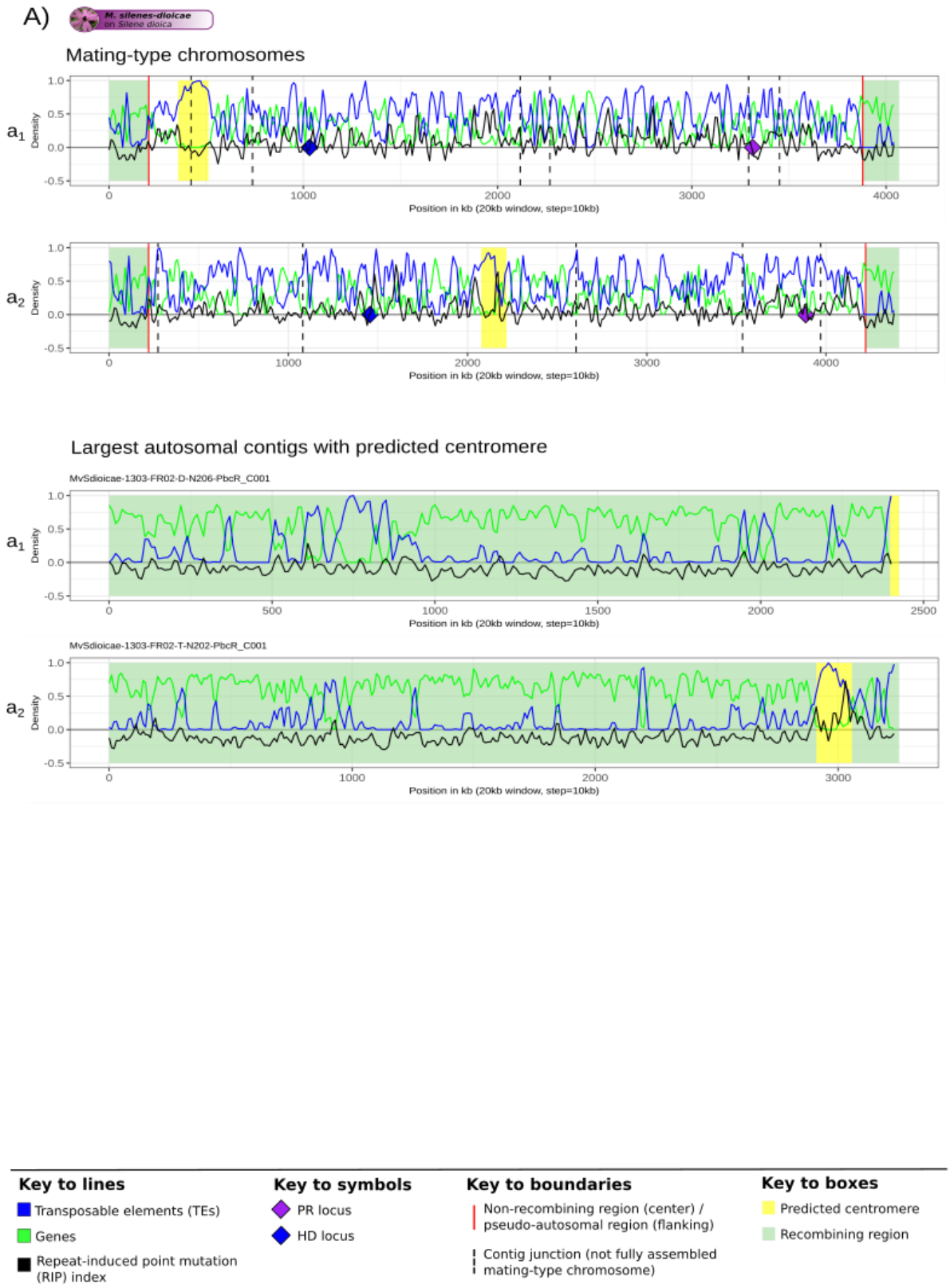
A)
M. silenes-dioicae
on Silene dioica
Mating-type chromosomes
a1
a2
Density
Position in kb (20kb window, step=10kb)
Largest autosomal contigs with predicted centromere
MvSdioicae-1303-FR02-D-N206-PbcR_C001
MvSdioicae-1303-FR02-T-N202-PbcR_C001
Key to lines
Transposable elements (TEs)
Genes
Repeat-induced point mutation (RIP) index
Key to symbols
PR locus
HD locus
Key to boundaries
Non-recombining region (center) / pseudo-autosomal region (flanking)
Contig junction (not fully assembled mating-type chromosome)
Key to boxes
Predicted centromere
Recombining region

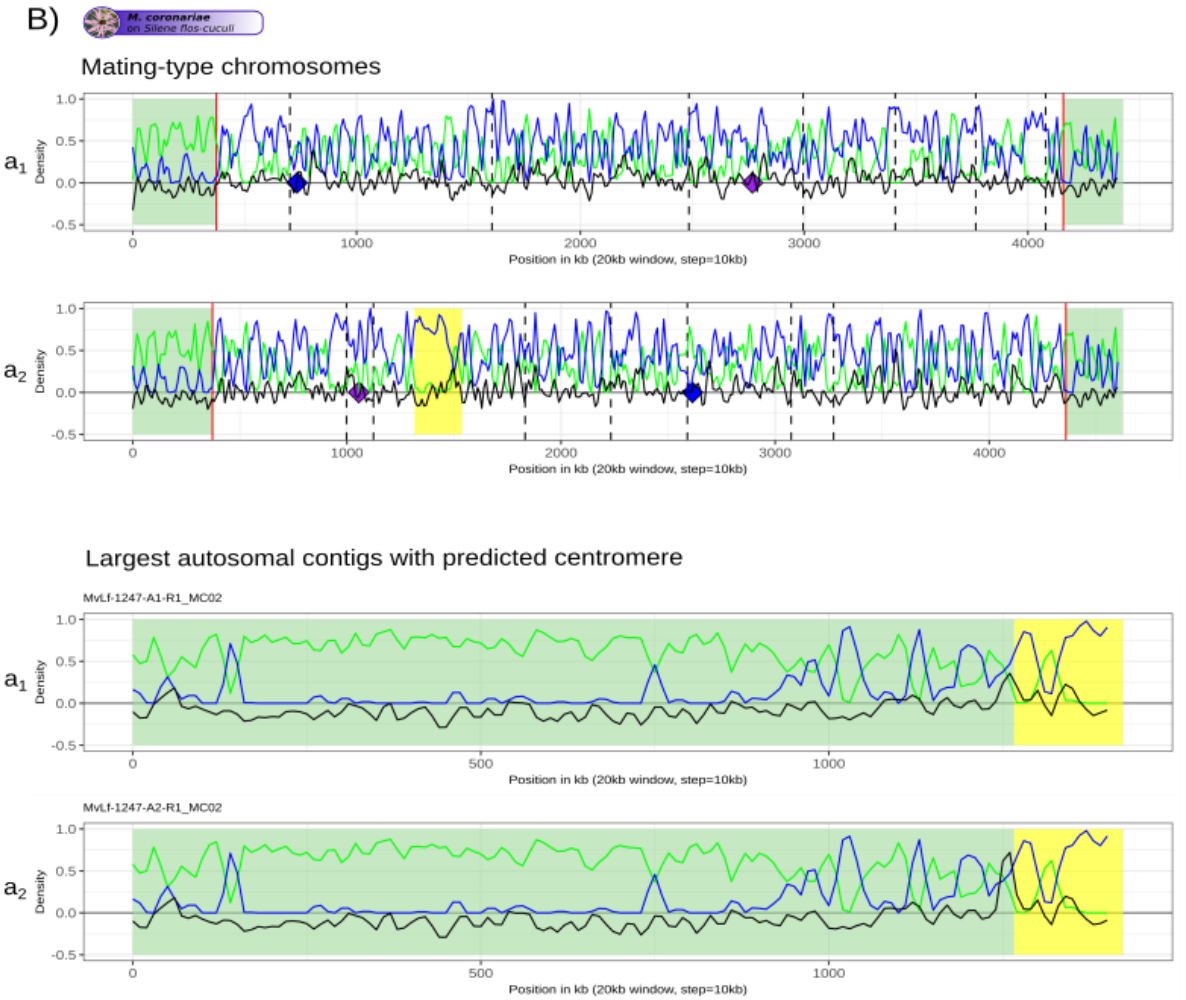


**Key to lines**
- Transposable elements (TEs)
- Genes
- Repeat-induced point mutation (RIP) index

**Key to symbols**
- PR locus
- HD locus

**Key to boundaries**
- Non-recombining region (center) / pseudo-autosomal region (flanking)
- Contig junction (not fully assembled mating-type chromosome)

**Key to boxes**
- Predicted centromere
- Recombining region

1230

C) *M. v. viscidula* * on *Silene viscidula*

Mating-type chromosomes

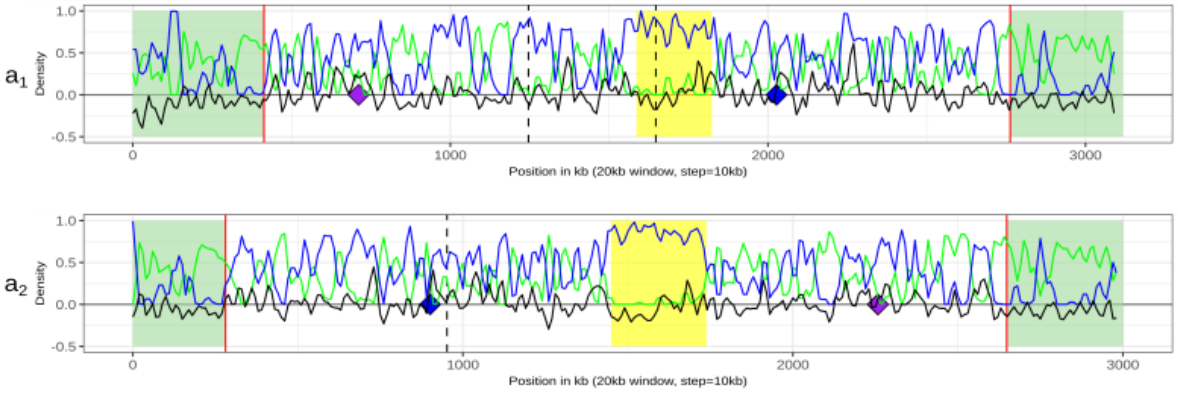


Largest autosomal contigs with predicted centromere

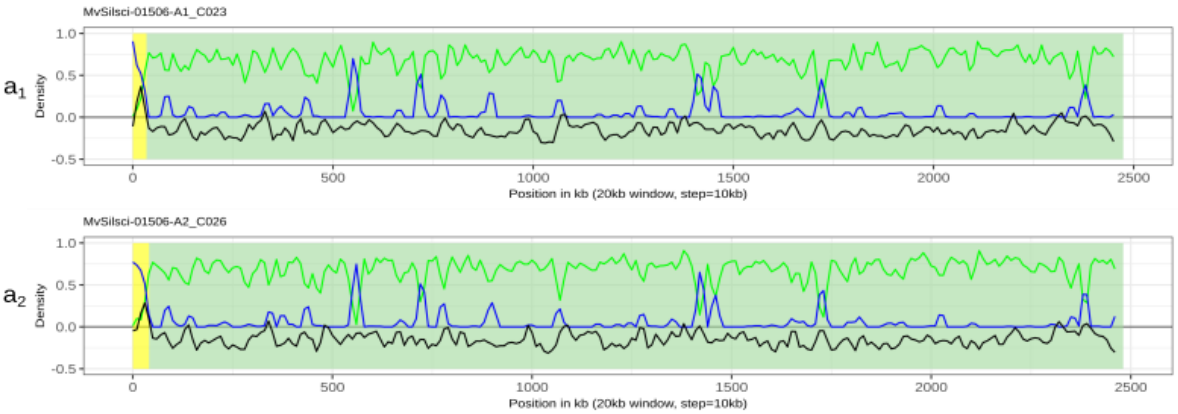


**Key to lines**

- Transposable elements (TEs)
- Genes
- Repeat-induced point mutation (RIP) index

**Key to symbols**

- PR locus
- HD locus

**Key to boundaries**

- Non-recombining region (center) / pseudo-autosomal region (flanking)
- Contig junction (not fully assembled mating-type chromosome)

**Key to boxes**

- Predicted centromere
- Recombining region

D) *M. v. melanantha* on *Silene melanantha*

Mating-type chromosomes

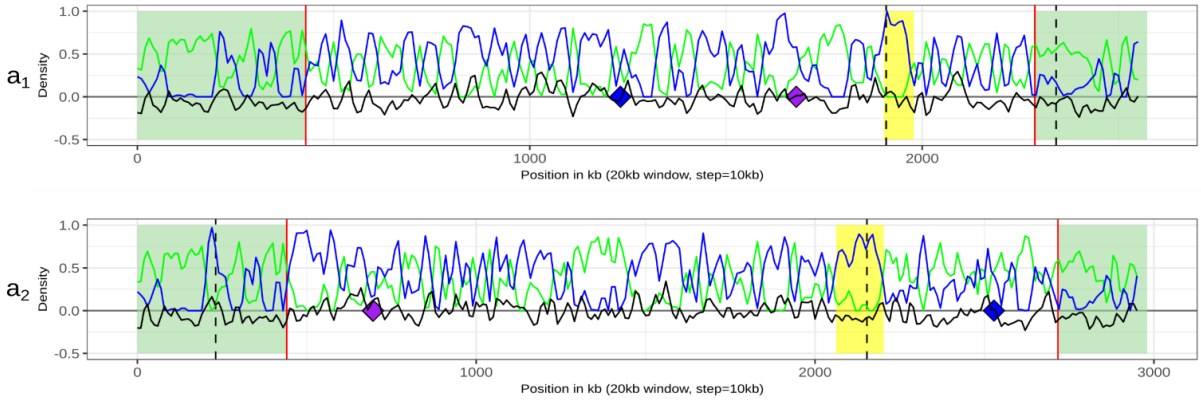


Largest autosomal contigs with predicted centromere

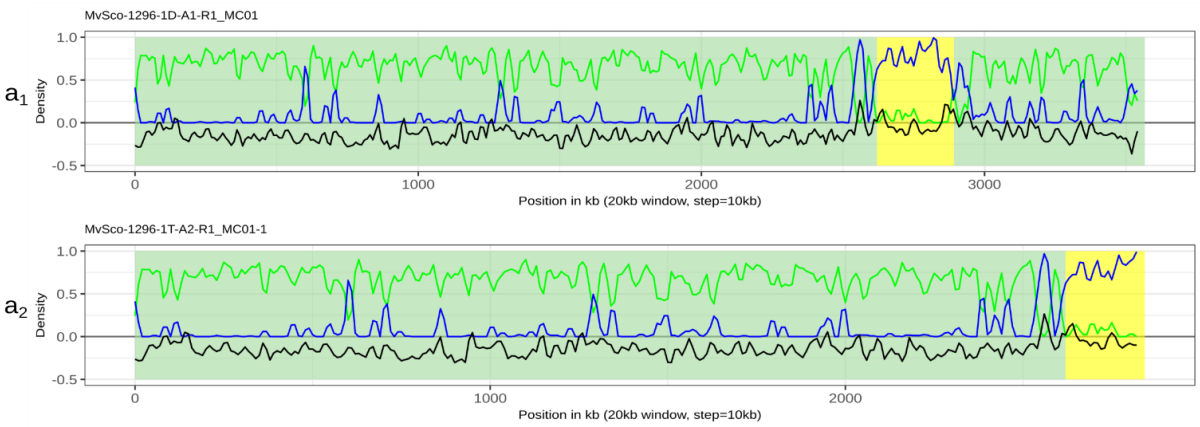


**Key to lines**

- Transposable elements (TEs)
- Genes
- Repeat-induced point mutation (RIP) index

**Key to symbols**

- PR locus
- HD locus

**Key to boundaries**

- Non-recombining region (center) / pseudo-autosomal region (flanking)
- Contig junction (not fully assembled mating-type chromosome)

**Key to boxes**

- Predicted centromere
- Recombining region

E) *M. v. gracilicaulis* * on *Silene gracilicaulis*

Mating-type chromosomes

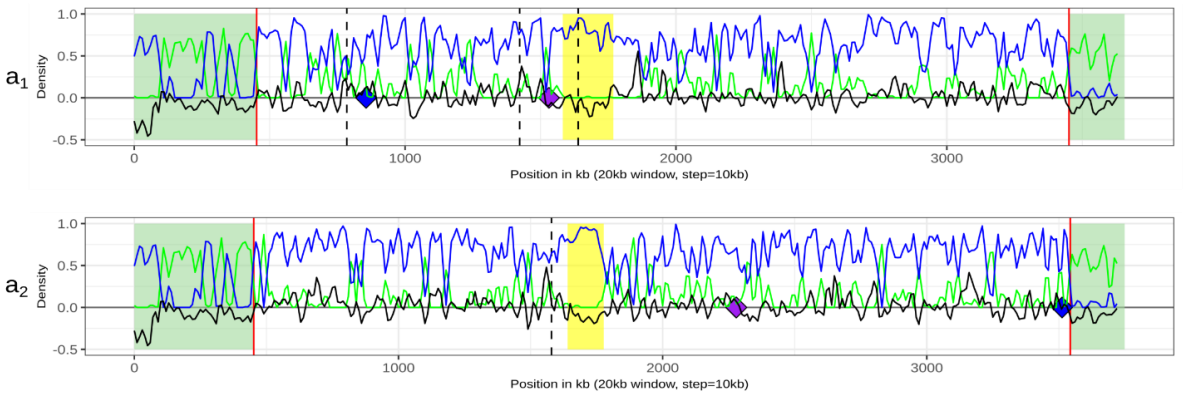


Largest autosomal contigs with predicted centromere

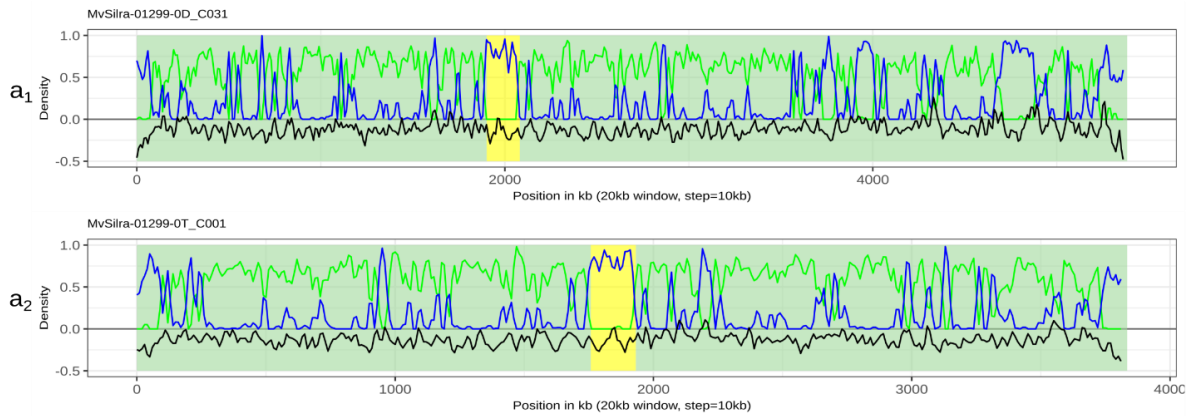


**Key to lines**

- Transposable elements (TEs)
- Genes
- Repeat-induced point mutation (RIP) index

**Key to symbols**

- PR locus
- HD locus

**Key to boundaries**

- Non-recombining region (center) / pseudo-autosomal region (flanking)
- Contig junction (not fully assembled mating-type chromosome)

**Key to boxes**

- Predicted centromere
- Recombining region

F) *M. silenes-acaulis* on *Silene acaulis*

Mating-type chromosomes

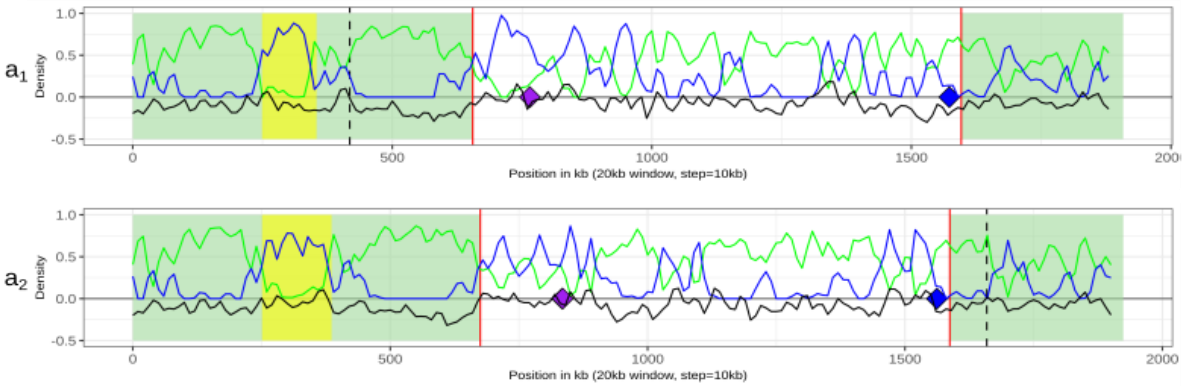


Largest autosomal contigs with predicted centromere

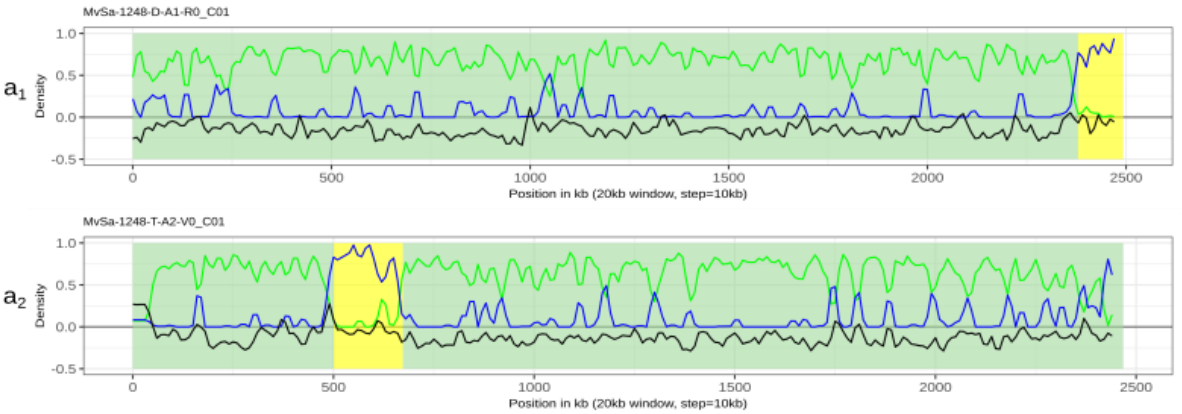


**Key to lines**

- Transposable elements (TEs)
- Genes
- Repeat-induced point mutation (RIP) index

**Key to symbols**

- PR locus
- HD locus

**Key to boundaries**

- Non-recombining region (center) / pseudo-autosomal region (flanking)
- Contig junction (not fully assembled mating-type chromosome)

**Key to boxes**

- Predicted centromere
- Recombining region

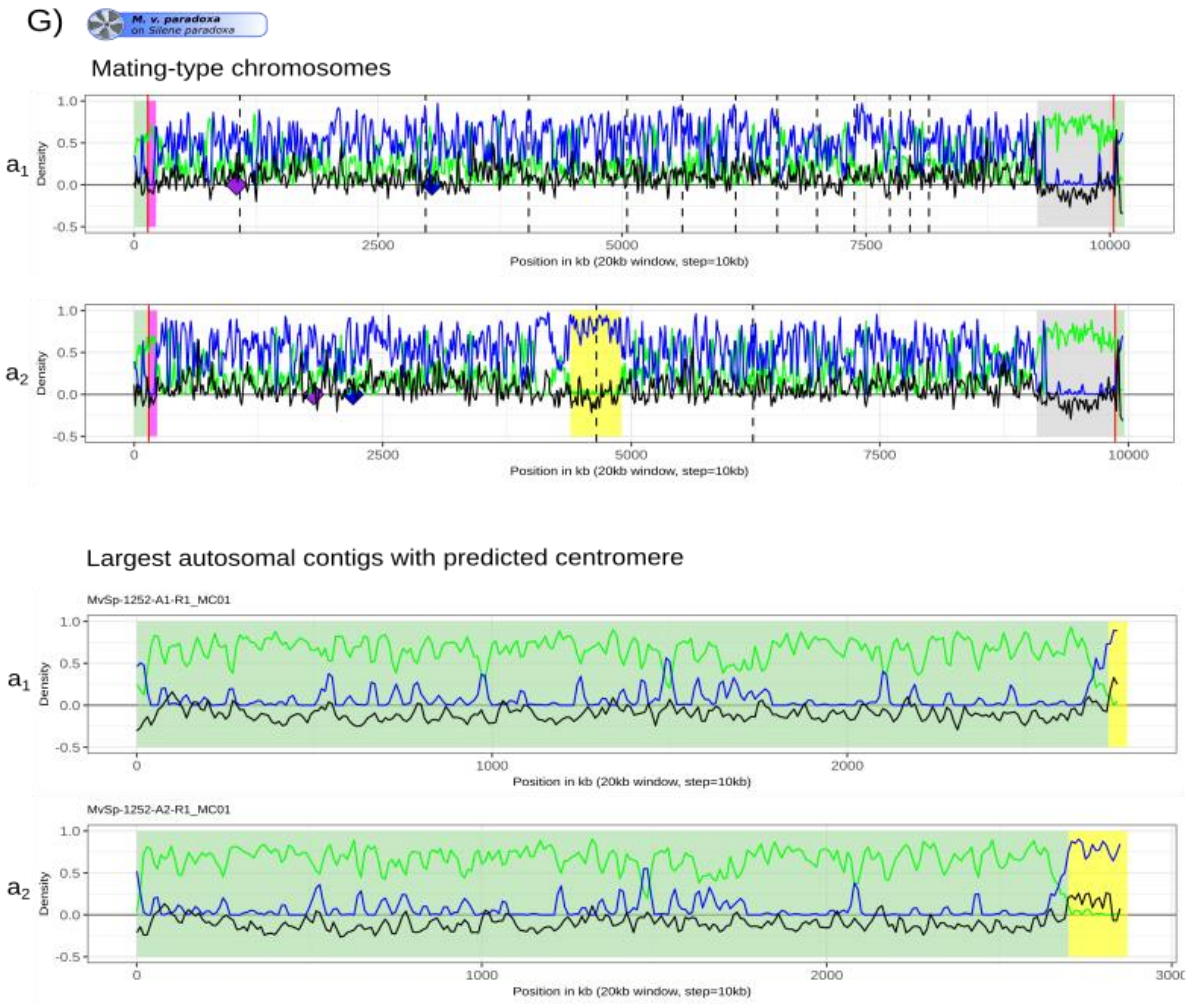


**Key to lines**
- Transposable elements (TEs)
- Genes
- Repeat-induced point mutation (RIP) index

**Key to symbols**
- PR locus
- HD locus

**Key to boundaries**
- Non-recombining region (center) / pseudo-autosomal region (flanking)
- Contig junction (not fully assembled mating-type chromosome)

**Key to boxes**
- Predicted centromere
- Recombining region
- Young pink stratum
- Young white stratum

1235

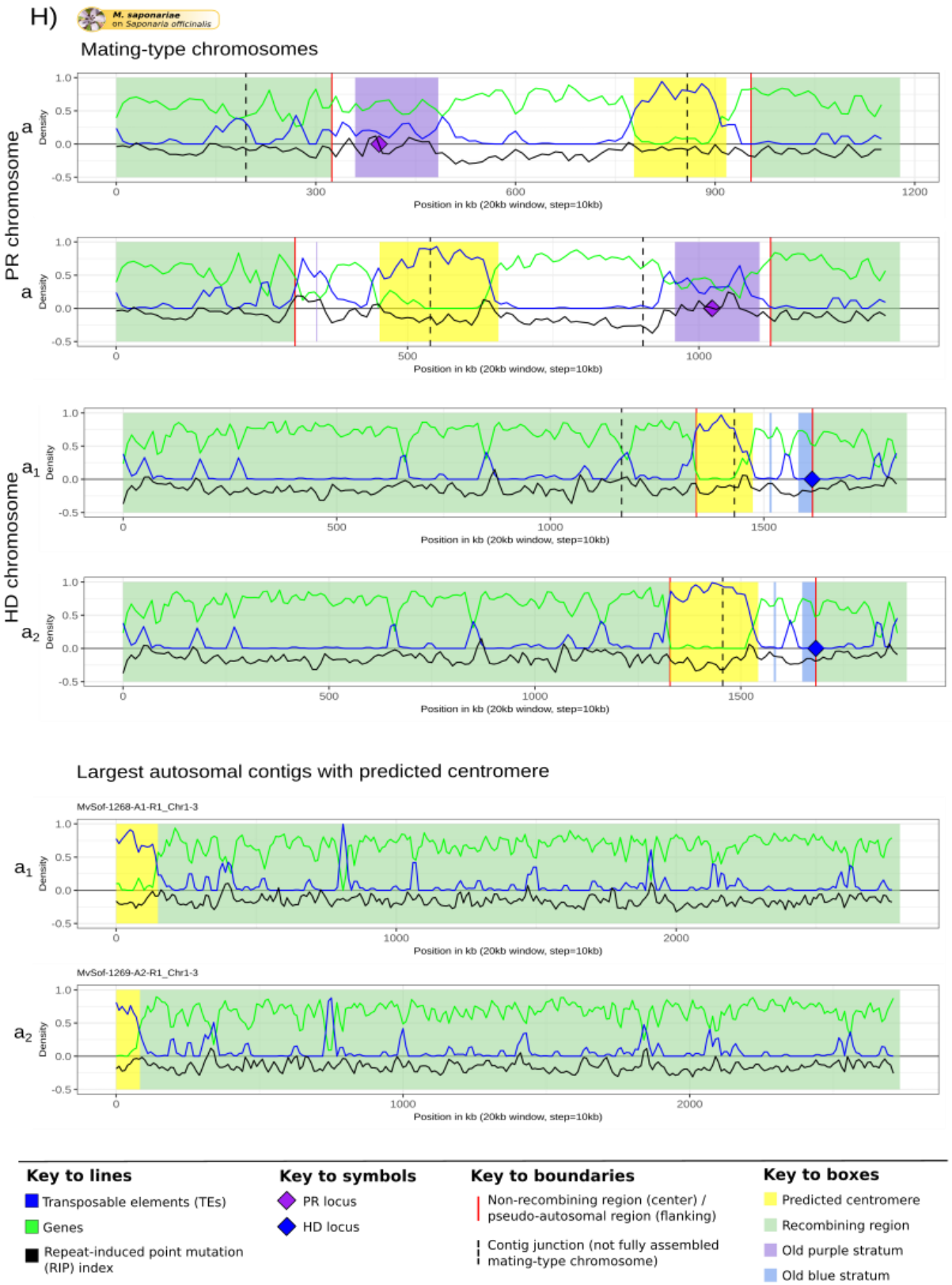
H)
M. saponariae on Saponaria officinalis
Mating-type chromosomes
PR chromosome
HD chromosome
a
a
a1
a2
Density
Position in kb (20kb window, step=10kb)
Largest autosomal contigs with predicted centromere
MvSof-1268-A1-R1_Chr1-3
MvSof-1269-A2-R1_Chr1-3
Key to lines
Transposable elements (TEs)
Genes
Repeat-induced point mutation (RIP) index
Key to symbols
PR locus
HD locus
Key to boundaries
Non-recombining region (center) / pseudo-autosomal region (flanking)
Contig junction (not fully assembled mating-type chromosome)
Key to boxes
Predicted centromere
Recombining region
Old purple stratum
Old blue stratum

I)

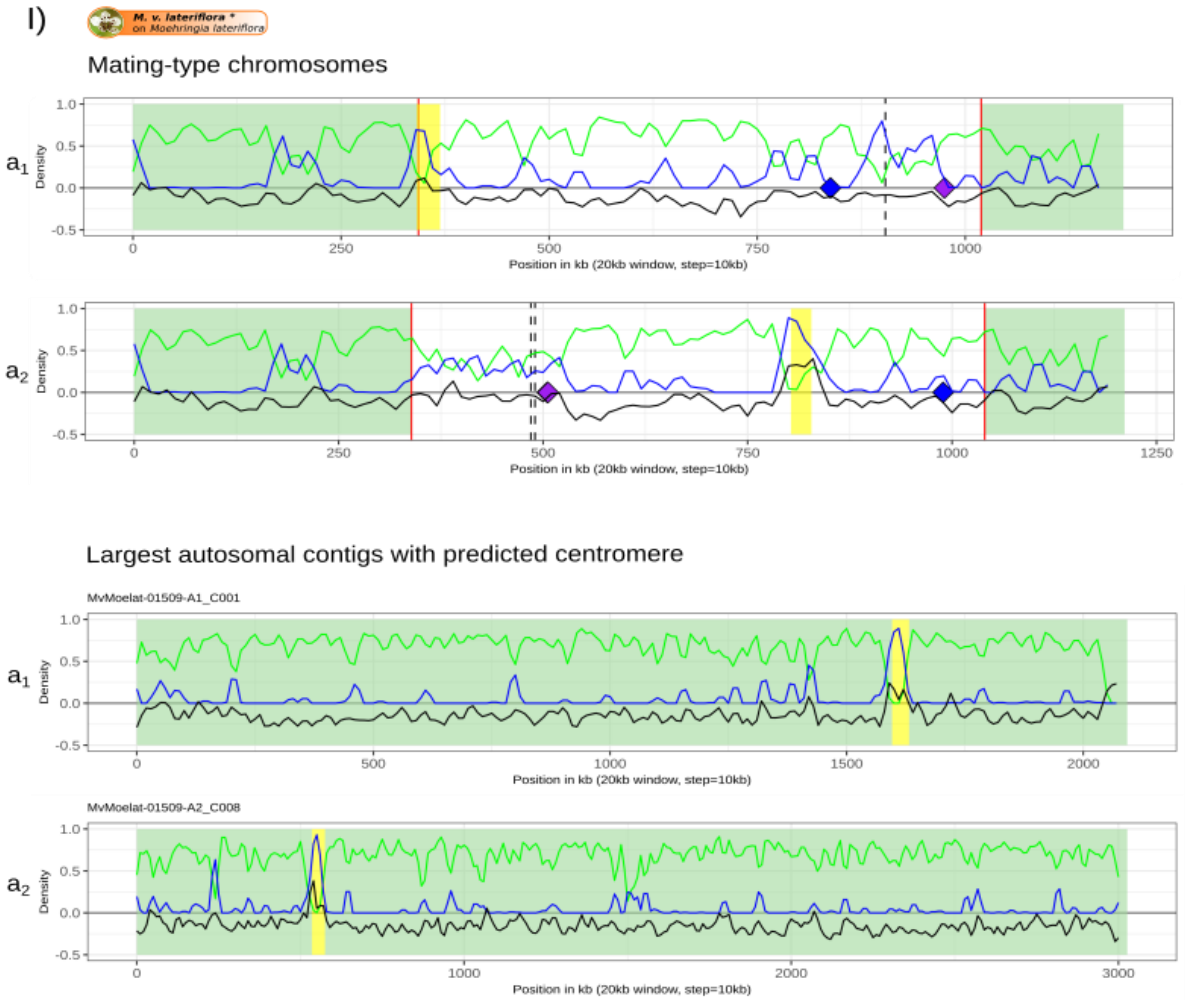


**Key to lines**

- Transposable elements (TEs)
- Genes
- Repeat-induced point mutation (RIP) index

**Key to symbols**

- PR locus
- HD locus

**Key to boundaries**

- Non-recombining region (center) / pseudo-autosomal region (flanking)
- Contig junction (not fully assembled mating-type chromosome)

**Key to boxes**

- Predicted centromere
- Recombining region
- Old purple stratum
- Old blue stratum

J) *M. lagerheimii* on *Silene vulgaris*

Mating-type chromosomes

Largest autosomal contigs with predicted centromere

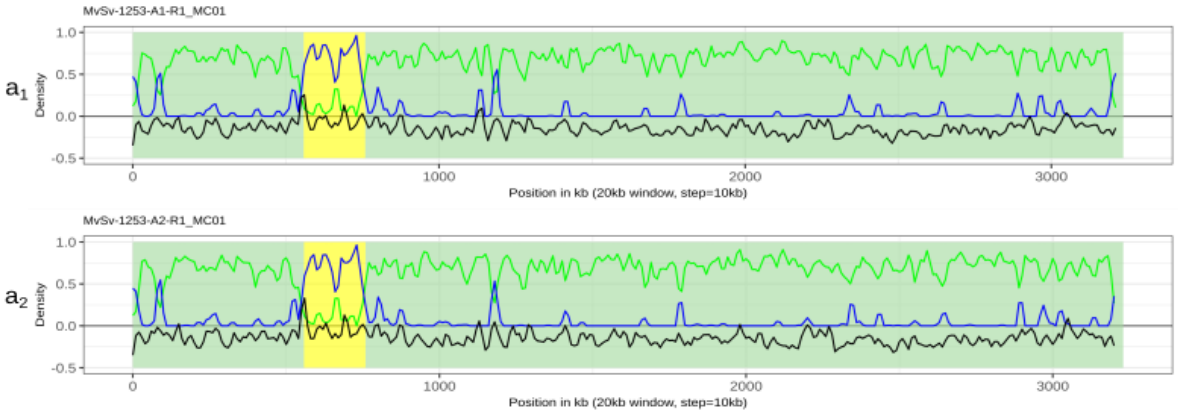


**Key to lines**
- Transposable elements (TEs)
- Genes
- Repeat-induced point mutation (RIP) index

**Key to symbols**
- PR locus
- HD locus

**Key to boundaries**
- Non-recombining region (center) / pseudo-autosomal region (flanking)
- Contig junction (not fully assembled mating-type chromosome)

**Key to boxes**
- Predicted centromere
- Recombining region
- Old purple stratum
- Old blue stratum

K)

Mating-type chromosomes

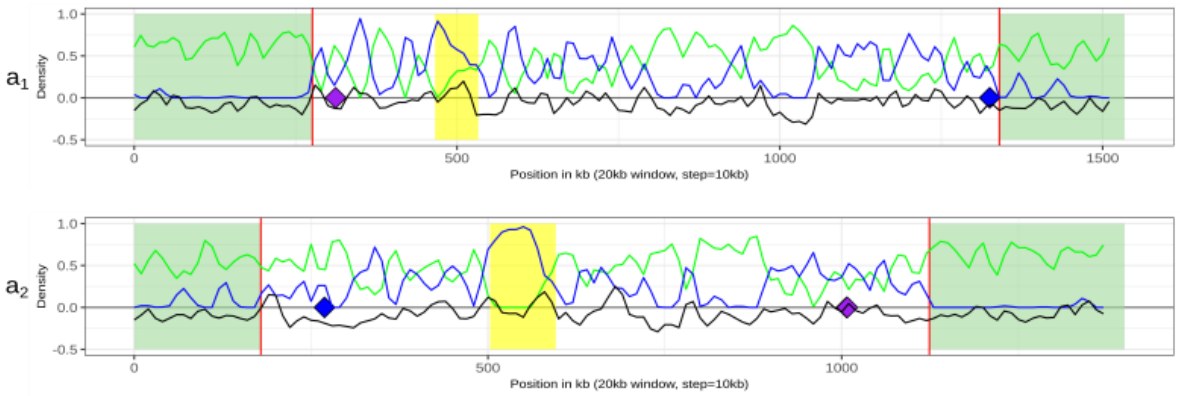


Largest autosomal contigs with predicted centromere

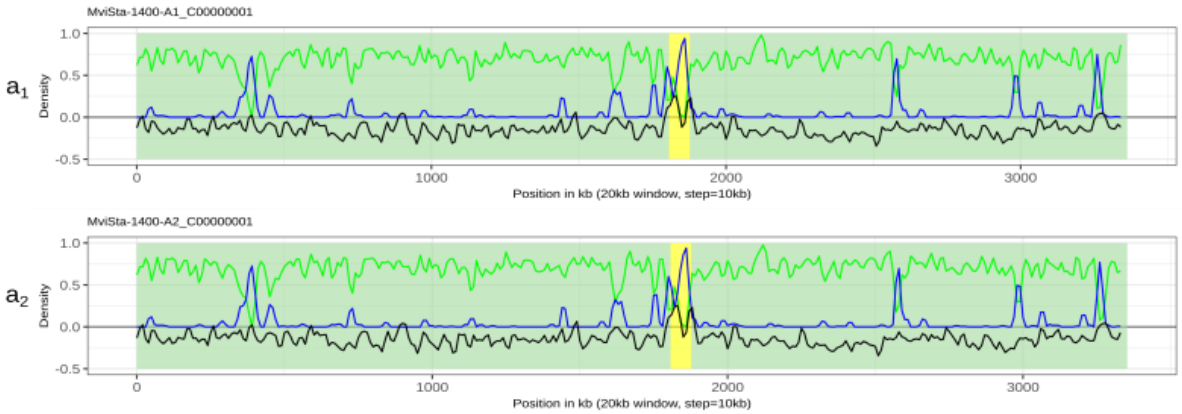


**Key to lines**

- Transposable elements (TEs)
- Genes
- Repeat-induced point mutation (RIP) index

**Key to symbols**

- PR locus
- HD locus

**Key to boundaries**

- Non-recombining region (center) / pseudo-autosomal region (flanking)

**Key to boxes**

- Predicted centromere
- Recombining region
- Old purple stratum
- Old blue stratum

L)

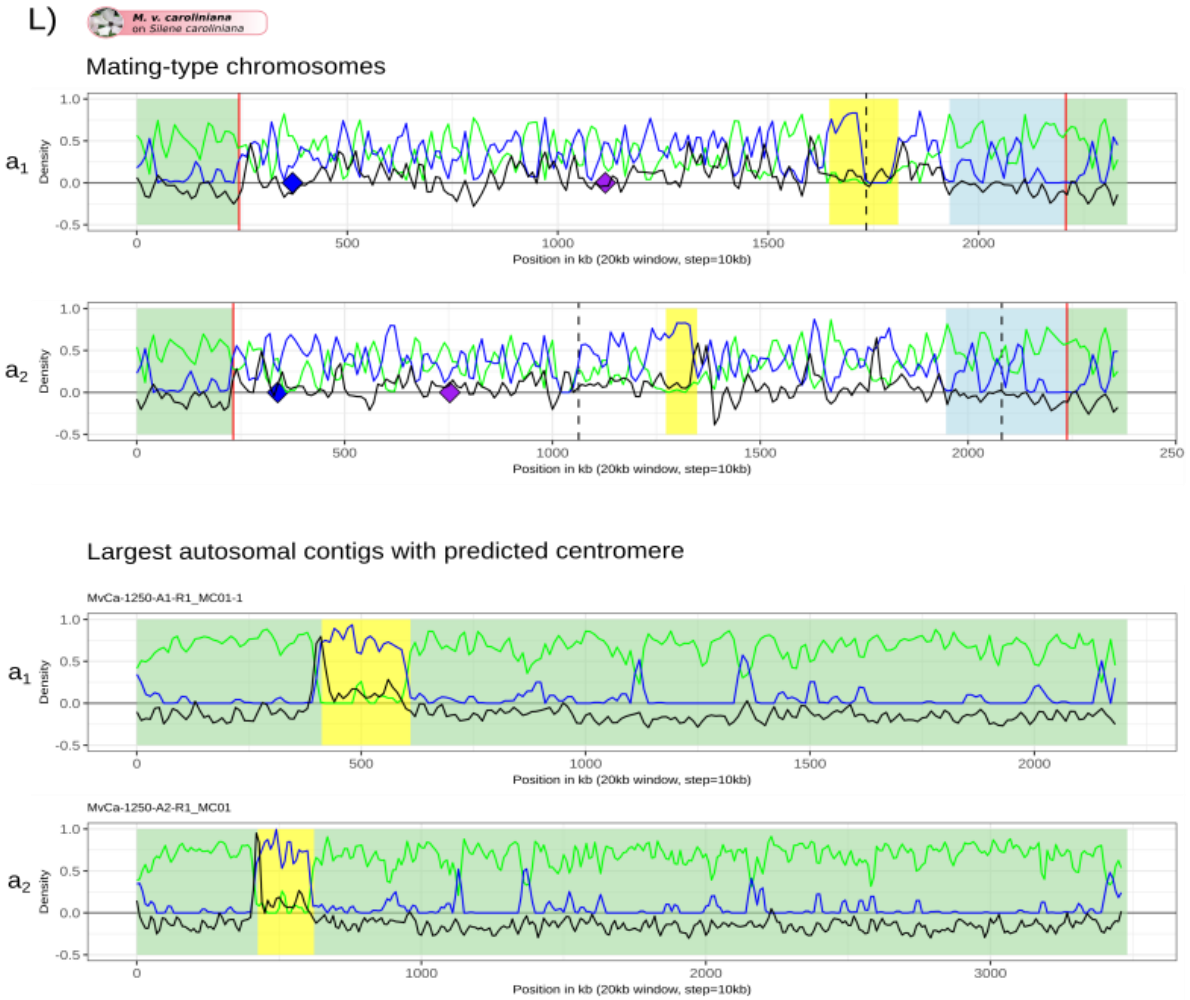


**Key to lines**
- Transposable elements (TEs)
- Genes
- Repeat-induced point mutation (RIP) index

**Key to symbols**
- PR locus
- HD locus

**Key to boundaries**
- Non-recombining region (center) / pseudo-autosomal region (flanking)
- Contig junction (not fully assembled mating-type chromosome)

**Key to boxes**
- Predicted centromere
- Recombining region
- Young light blue stratum

1240

M) *M. v. parryi* * on *Silene parryi*

Mating-type chromosomes

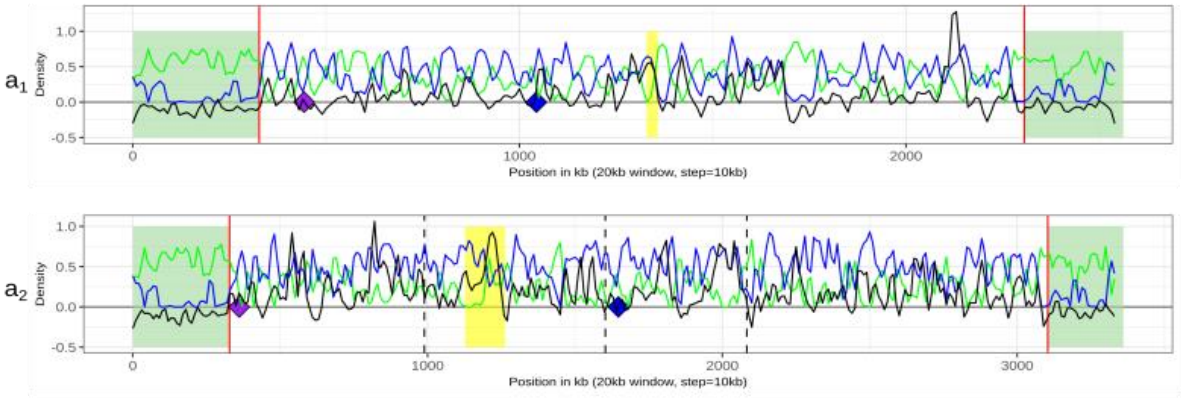


Largest autosomal contigs with predicted centromere

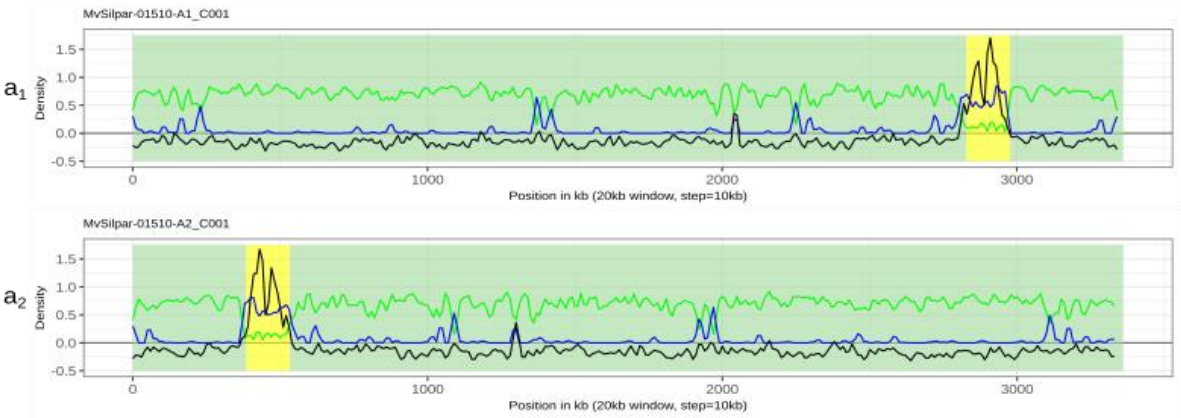


**Key to lines**
- Transposable elements (TEs)
- Genes
- Repeat-induced point mutation (RIP) index

**Key to symbols**
- PR locus
- HD locus

**Key to boundaries**
- Non-recombining region (center) / pseudo-autosomal region (flanking)
- Contig junction (not fully assembled mating-type chromosome)

**Key to boxes**
- Predicted centromere
- Recombining region

N) *M. scabiosae* on *Knautia arvensis*

Mating-type chromosomes

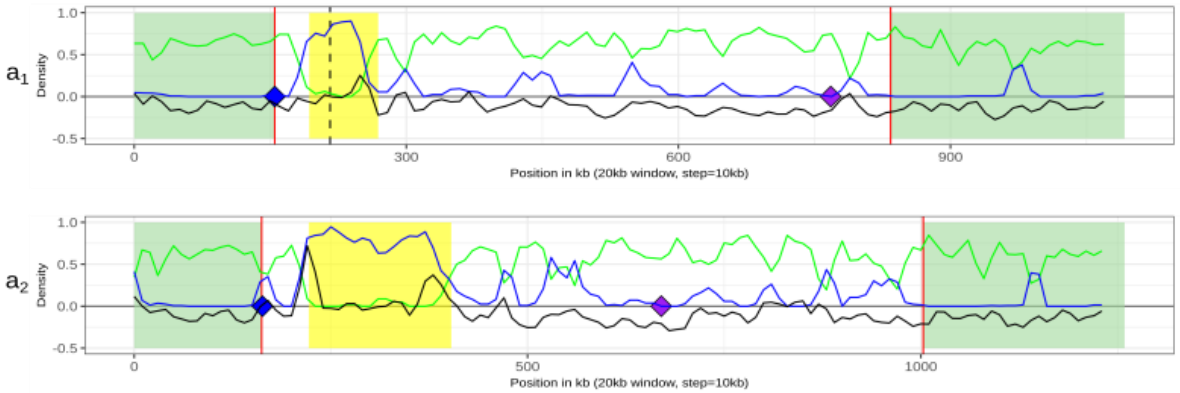


Largest autosomal contigs with predicted centromere

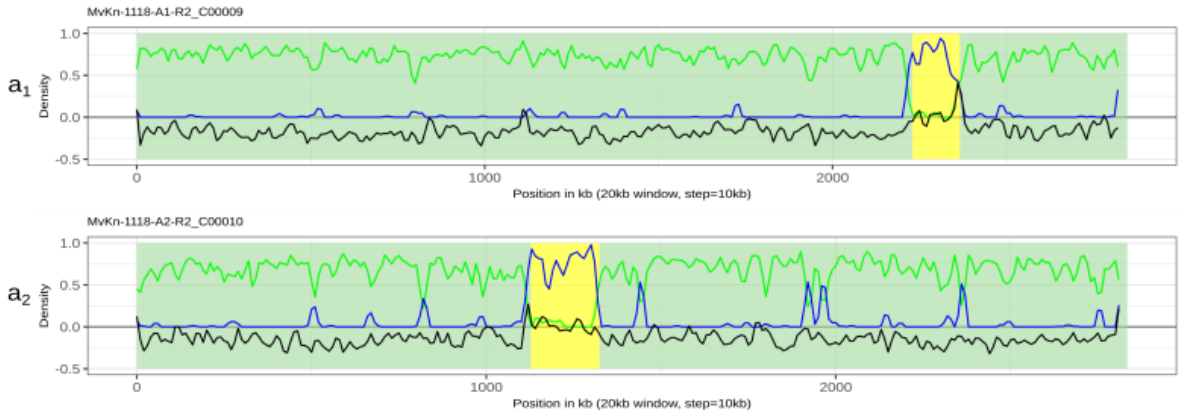


**Key to lines**

- Transposable elements (TEs)
- Genes
- Repeat-induced point mutation (RIP) index

**Key to symbols**

- PR locus
- HD locus

**Key to boundaries**

- Non-recombining region (center) / pseudo-autosomal region (flanking)
- Contig junction (not fully assembled mating-type chromosome)

**Key to boxes**

- Predicted centromere
- Recombining region

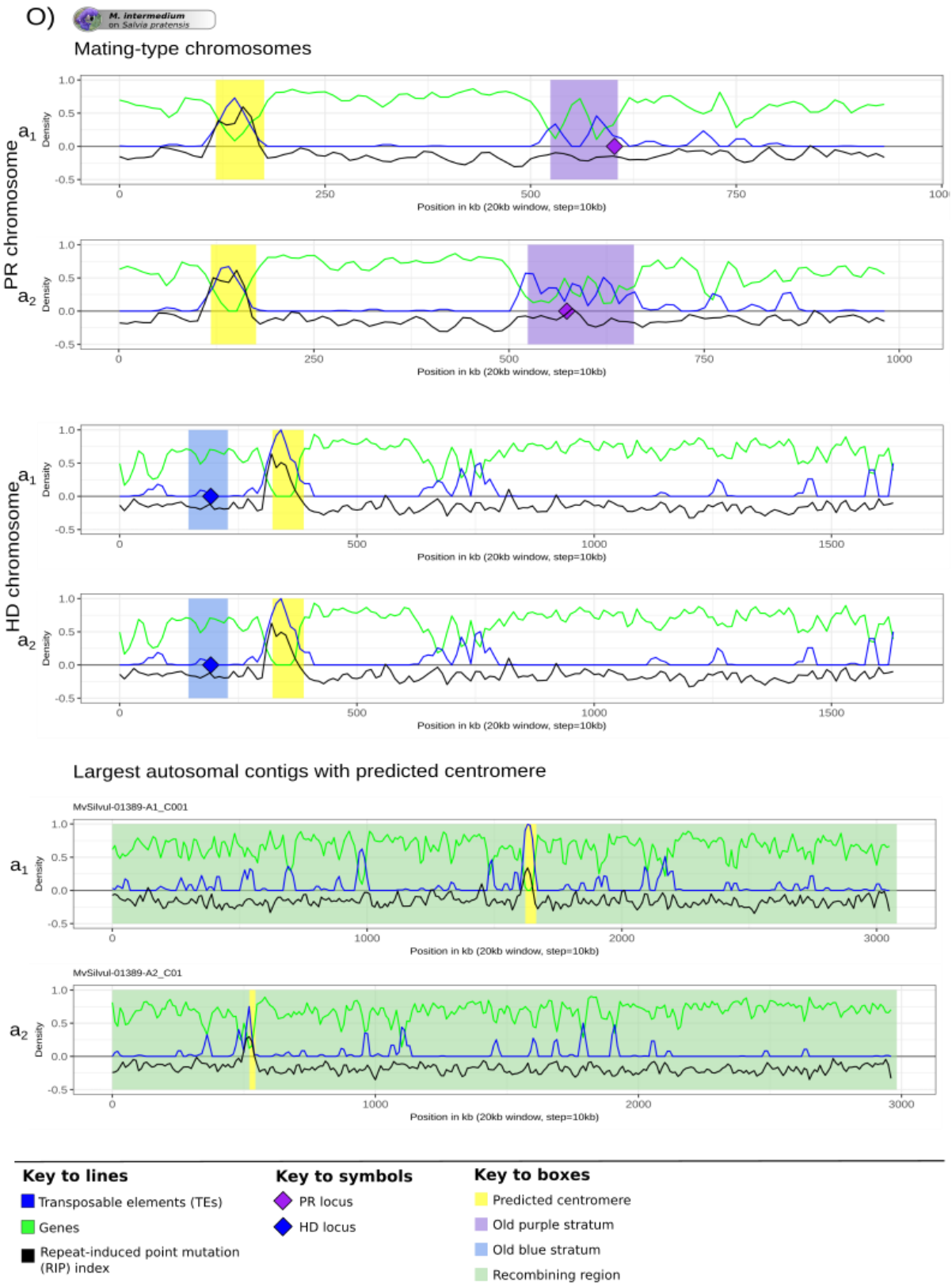


**Supplementary Figure S7: Density of transposable elements (TEs), genes and repeat-**

**induced point mutations (RIP) along the mating-type chromosomes and the autosomes of *Microbotryum* genomes.** Density of TEs, genes and RIP index were calculated in 20 kb non-overlapping windows. A RIP index greater than one indicates that the region is RIP-affected. Predicted centromeres are indicated in yellow. Recombining regions of the mating-type chromosomes (pseudo-autosomal regions) and the autosomes (largest autosomal contig harboring a predicted centromere in each genome) are highlighted in pale green. Non-recombining regions are delimited by red lines. Non-rearranged evolutionary strata are displayed in their corresponding color (see legend). Non-fully assembled mating-type chromosomes have been joined and the junctions are indicated by black dashed lines. Pheromone-receptor (PR) and homeodomain (HD) loci are indicated by purple and blue diamonds, respectively.

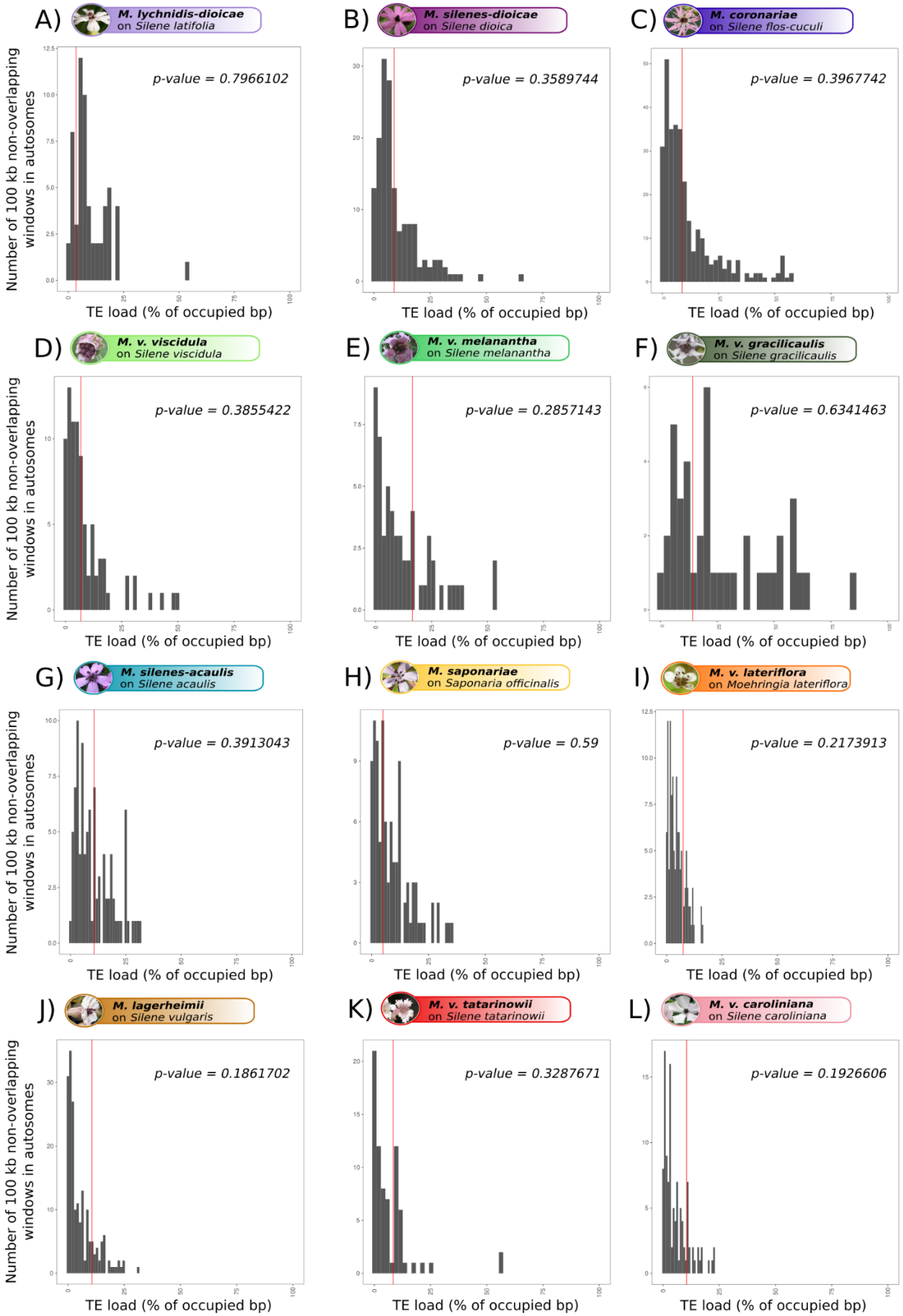
A)
M. lychnidis-dioicae
on Silene latifolia
p-value = 0.7966102
B)
M. silenes-dioicae
on Silene dioica
p-value = 0.3589744
C)
M. coronariae
on Silene flos-cuculi
p-value = 0.3967742
D)
M. v. viscidula
on Silene viscidula
p-value = 0.3855422
E)
M. v. melanantha
on Silene melanantha
p-value = 0.2857143
F)
M. v. gracilicaulis
on Silene gracilicaulis
p-value = 0.6341463
G)
M. silenes-acaulis
on Silene acaulis
p-value = 0.3913043
H)
M. saponariae
on Saponaria officinalis
p-value = 0.59
I)
M. v. lateriflora
on Moehringia lateriflora
p-value = 0.2173913
J)
M. lagerheimii
on Silene vulgaris
p-value = 0.1861702
K)
M. v. tatarinowii
on Silene tatarinowii
p-value = 0.3287671
L)
M. v. caroliniana
on Silene caroliniana
p-value = 0.1926606
Number of 100 kb non-overlapping windows in autosomes
TE load (% of occupied bp)

**Supplementary Figure S8: Transposable element (TE) load at the margin of the non-recombining regions compared to the distribution in recombining autosomal regions.** The average value of TE content in the region flanking the non-recombining region is indicated by a red line and the ones in autosomal windows constitute the grey distribution. The *p-value* corresponds to the percentage of windows in autosomes with higher TE load than in the region flanking the non-recombining regions.

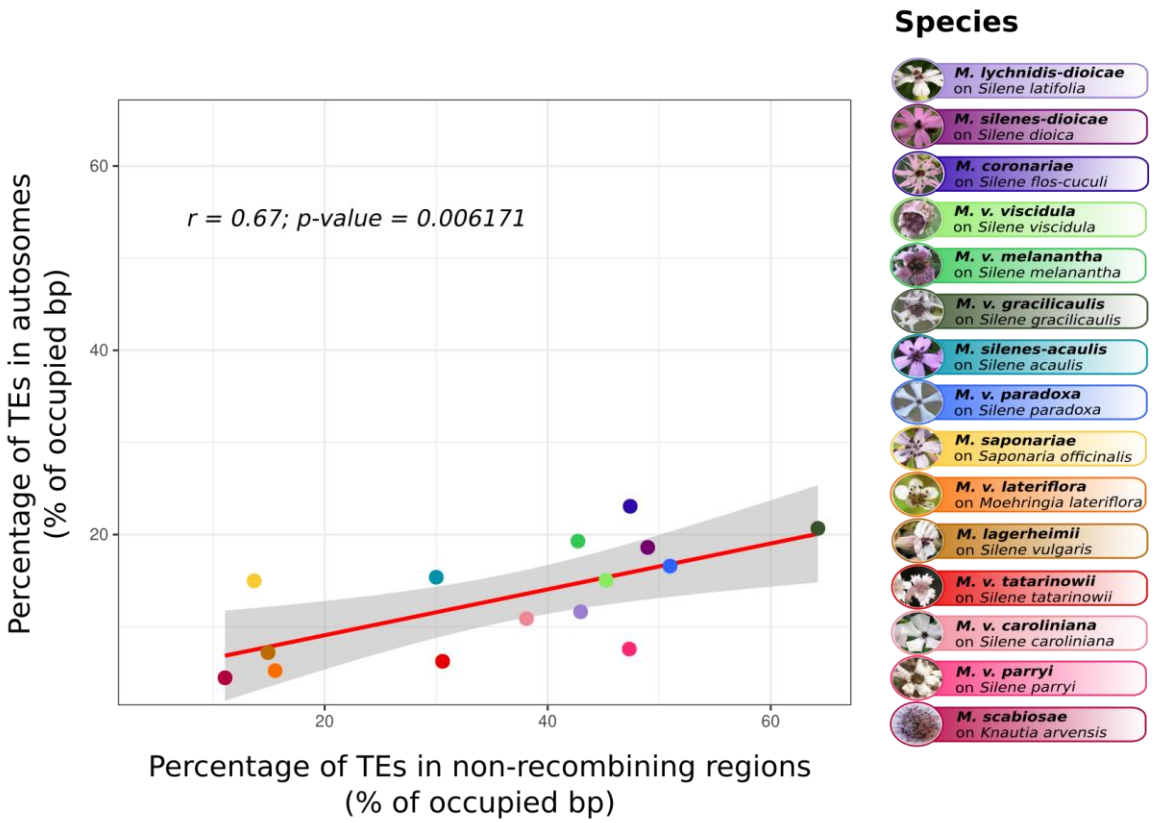


**Supplementary Figure S9: Correlation between the proportion of base pairs occupied by transposable elements (TEs) in the non-recombining regions and the autosomes.**

A) ***M. silenes-dioicae*** on *Silene dioica*

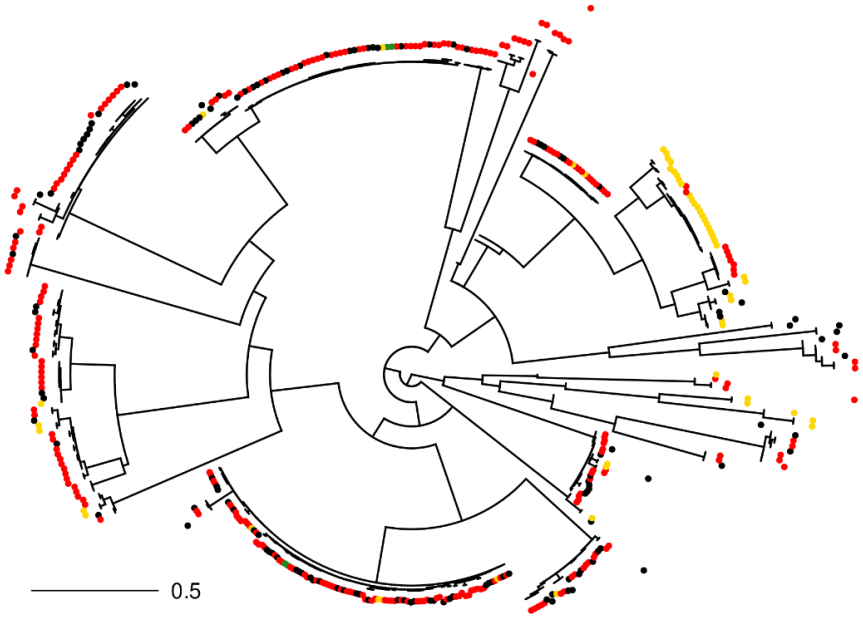


B) ***M. coronariae*** on *Silene flos-cuculi*

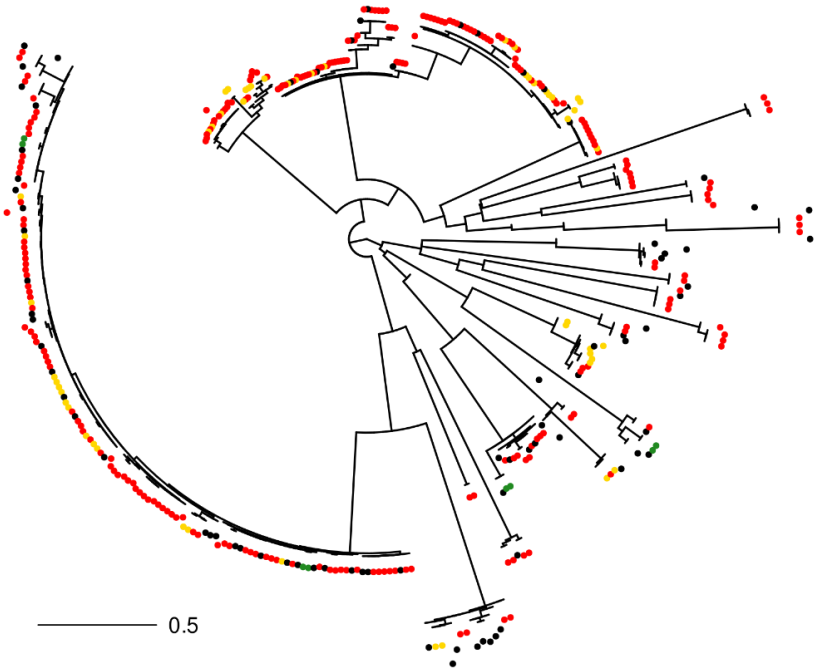


**Genomic location**

- Non-recombining regions of the mating-type chromosomes
- Pseudo-autosomal regions
- Autosomes
- Centromeres

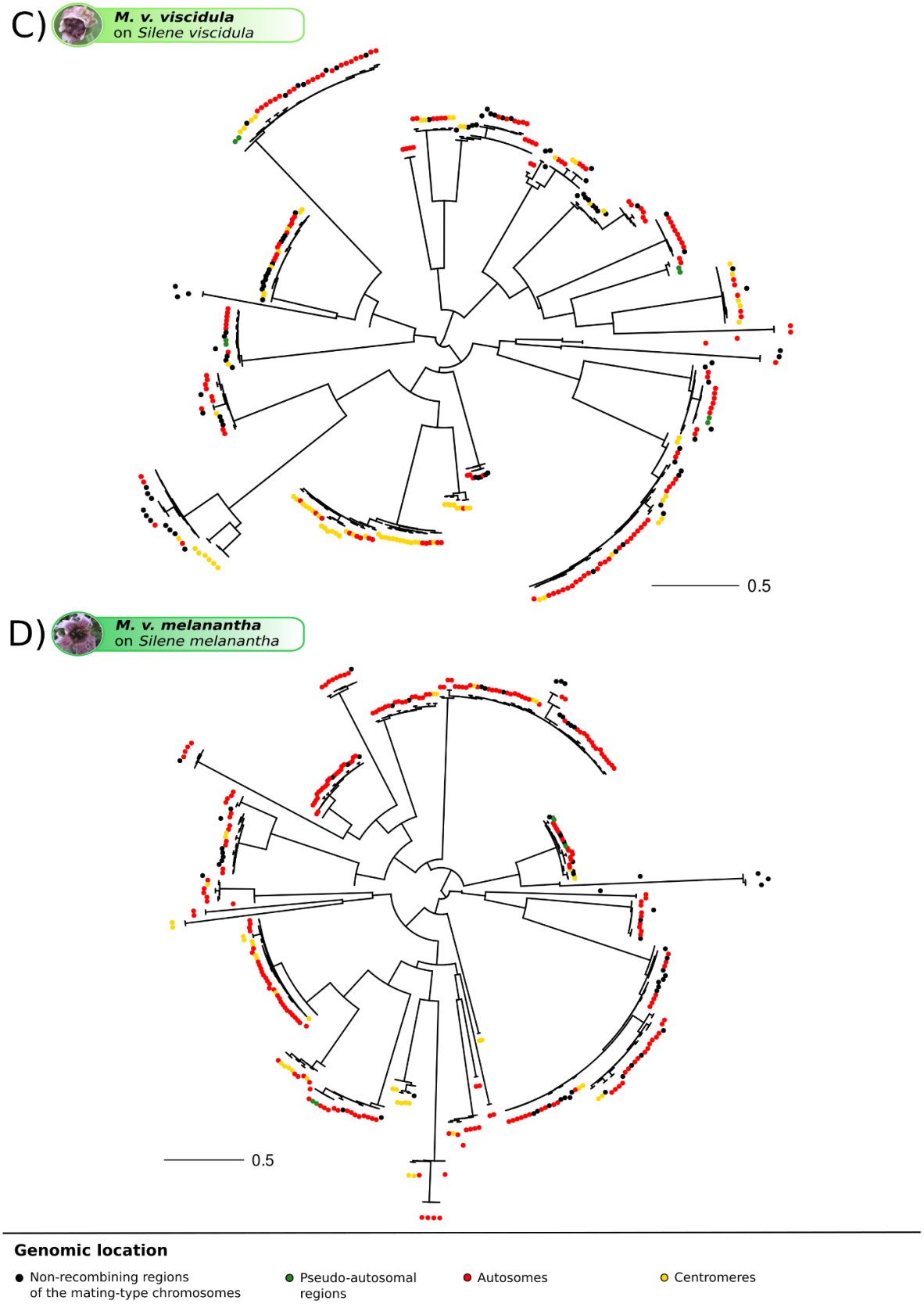
C)
M. v. viscidula
on Silene viscidula
0.5
D)
M. v. melanantha
on Silene melanantha
0.5
Genomic location
Non-recombining regions of the mating-type chromosomes
Pseudo-autosomal regions
Autosomes
Centromeres

1270

E) ***M. v. gracilicaulis*** on *Silene gracilicaulis*

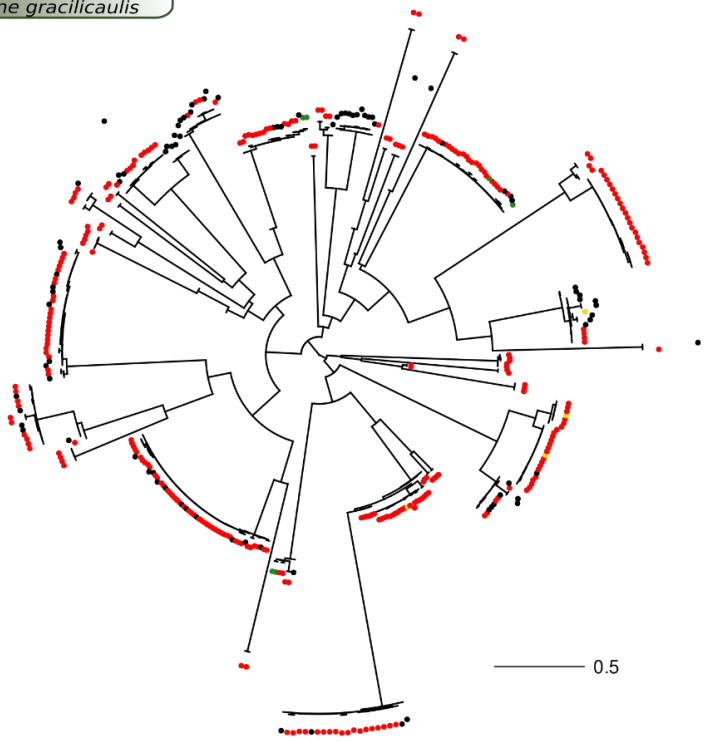


F) ***M. silenes-acaulis*** on *Silene acaulis*

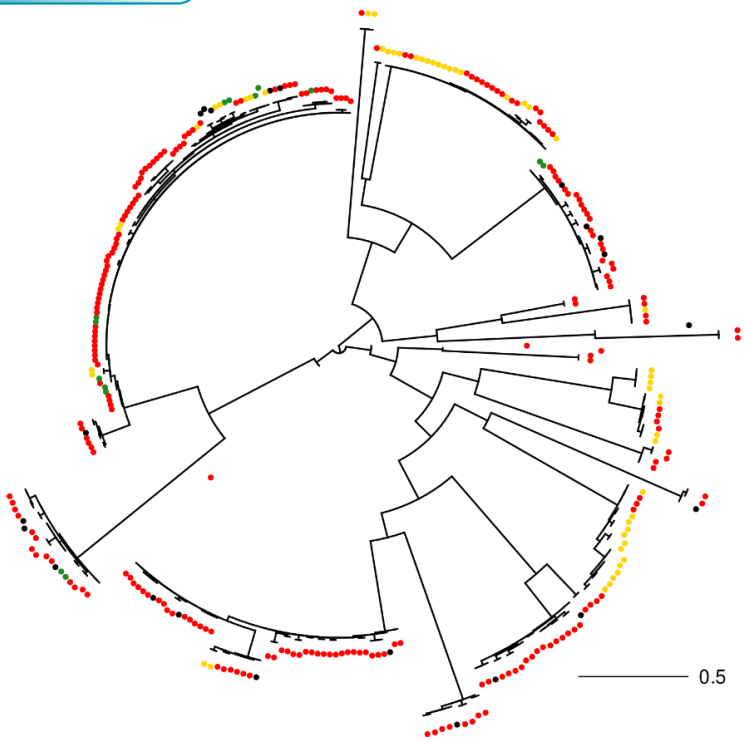


**Genomic location**

- Non-recombining regions of the mating-type chromosomes
- Pseudo-autosomal regions
- Autosomes
- Centromeres

G) ***M. saponariae*** on *Saponaria officinalis*

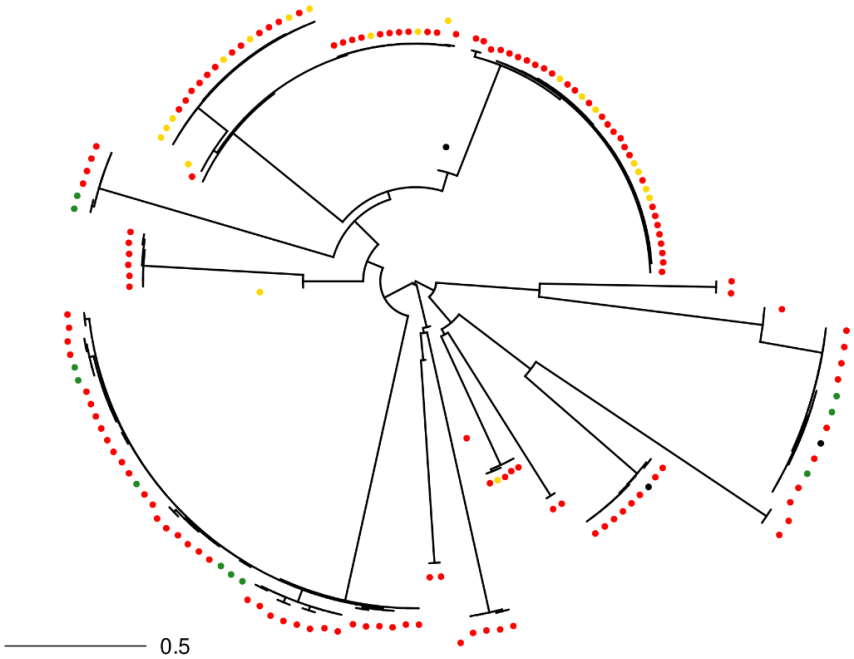


H) ***M. lagerheimii*** on *Silene vulgaris*

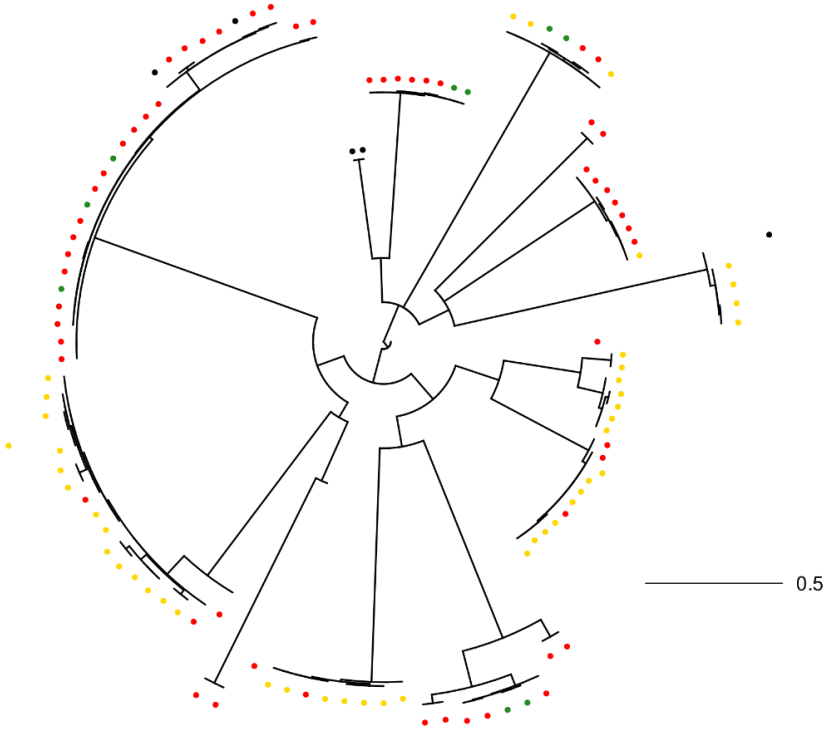


**Genomic location**

- Non-recombining regions of the mating-type chromosomes
- Pseudo-autosomal regions
- Autosomes
- Centromeres

I) ***M. v. tatarinowii*** on *Silene tatarinowii*

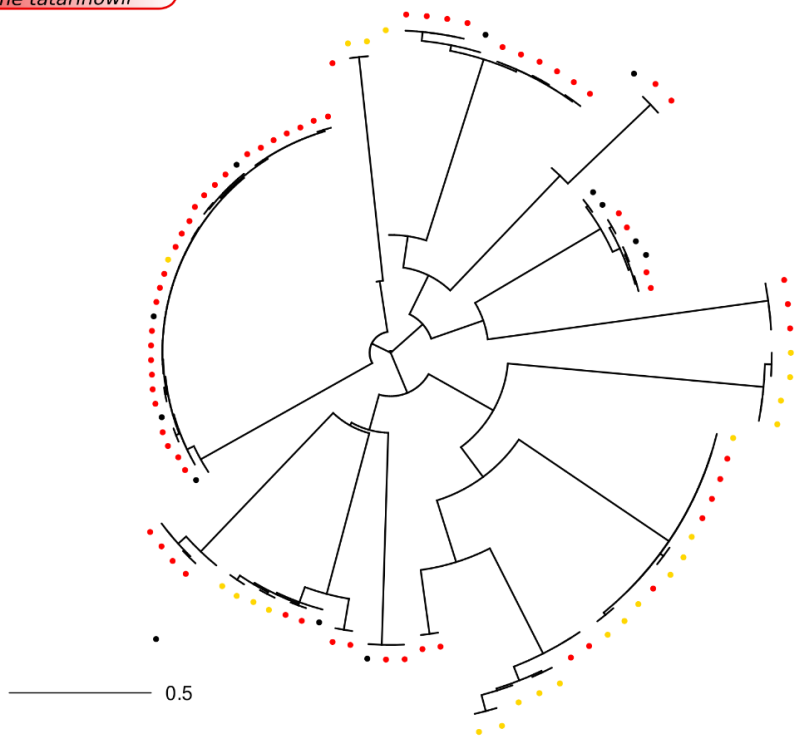


J) ***M. v. caroliniana*** on *Silene caroliniana*

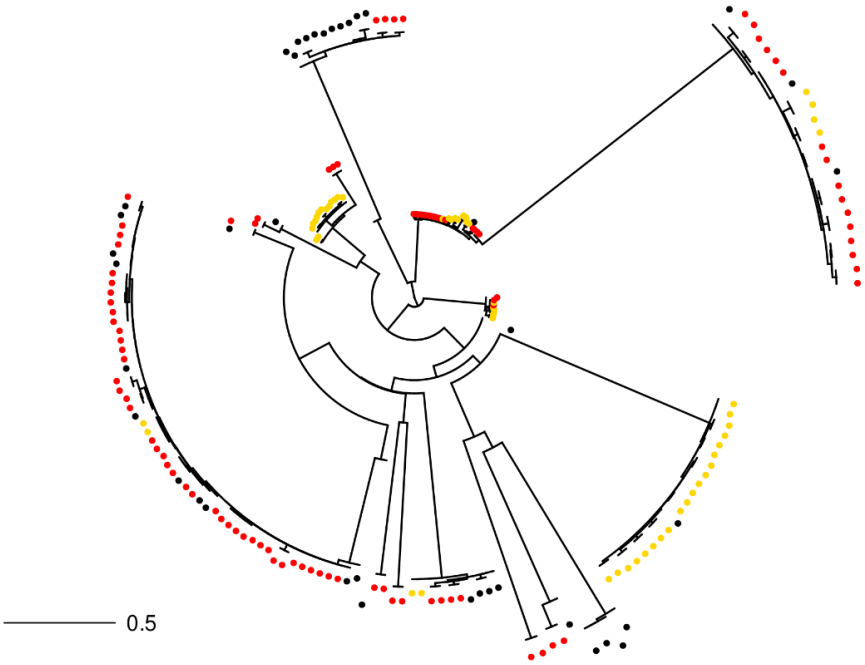


**Genomic location**

- Non-recombining regions of the mating-type chromosomes
- Pseudo-autosomal regions
- Autosomes
- Centromeres

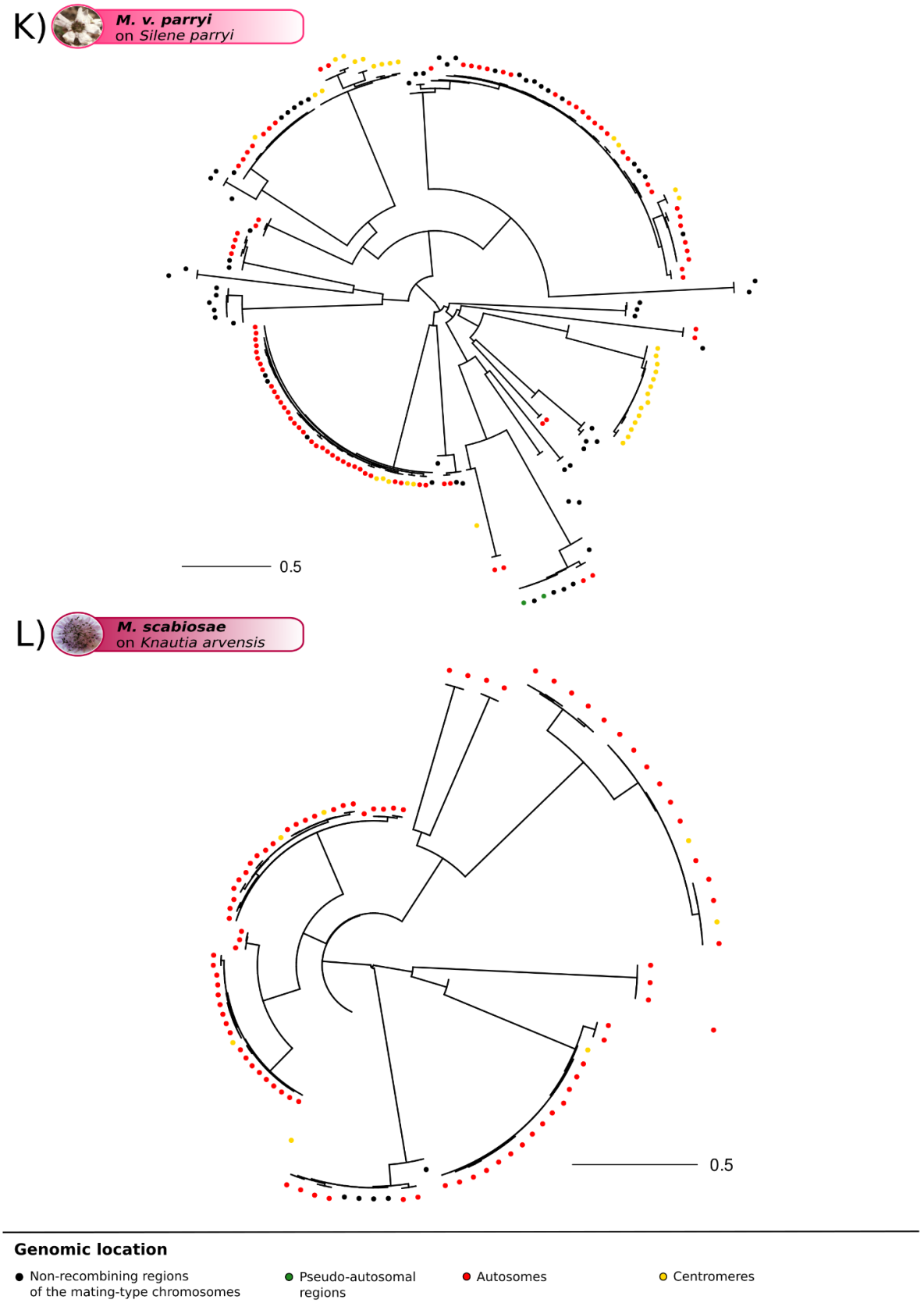


1275 **Supplementary Figure S10: Single-species genealogies of *Copia* retroelement copies in**

***Microbotryum* genomes.** Single-species genealogies of *Copia* copies in *Microbotryum silenes-dioicae* **(A)**, *M. coronariae* **(B)**, *M. violaceum viscidula* **(C)**, *M. v. melanantha* **(D)**, *M. v. gracilicaulis* **(E)**, *M. silenes-acaulis* **(F)**, *M. saponariae* **(G)**, *M. lagerheimii* **(H)**, *M. v. tatarinowii* **(I)**, *M. v. caroliniana* **(J)**, *M. v. parryi* **(K)** and *M. scabiosae* **(L)**. The color of the dots at the tip of the branches corresponds to the genomic location of the transposable element (TE) copies.

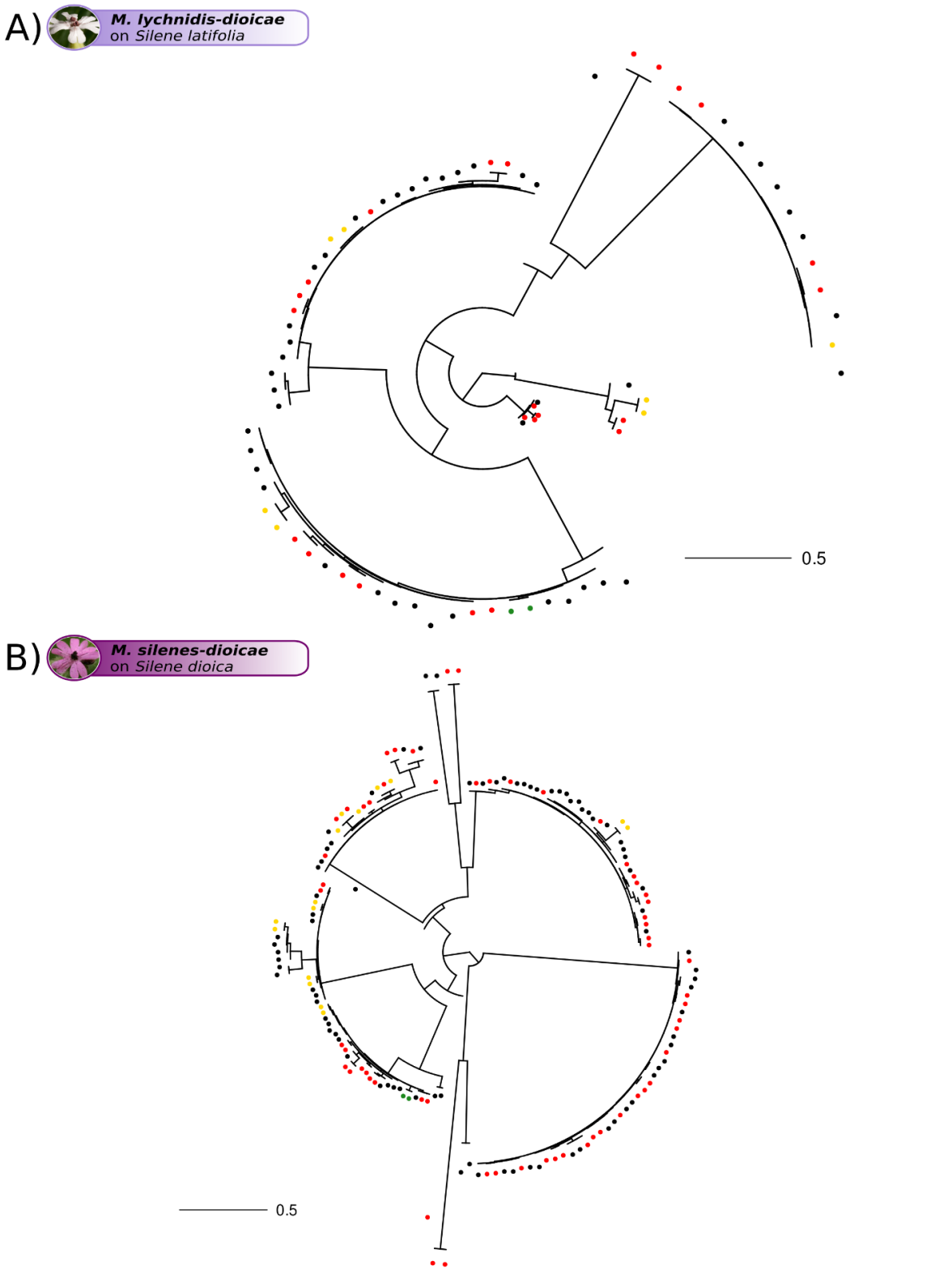
A)
M. lychnidis-dioicae
on Silene latifolia
0.5
B)
M. silenes-dioicae
on Silene dioica
0.5
Genomic location
Non-recombining regions of the mating-type chromosomes
Pseudo-autosomal regions
Autosomes
Centromeres

C) ***M. coronariae***
on *Silene flos-cuculi*

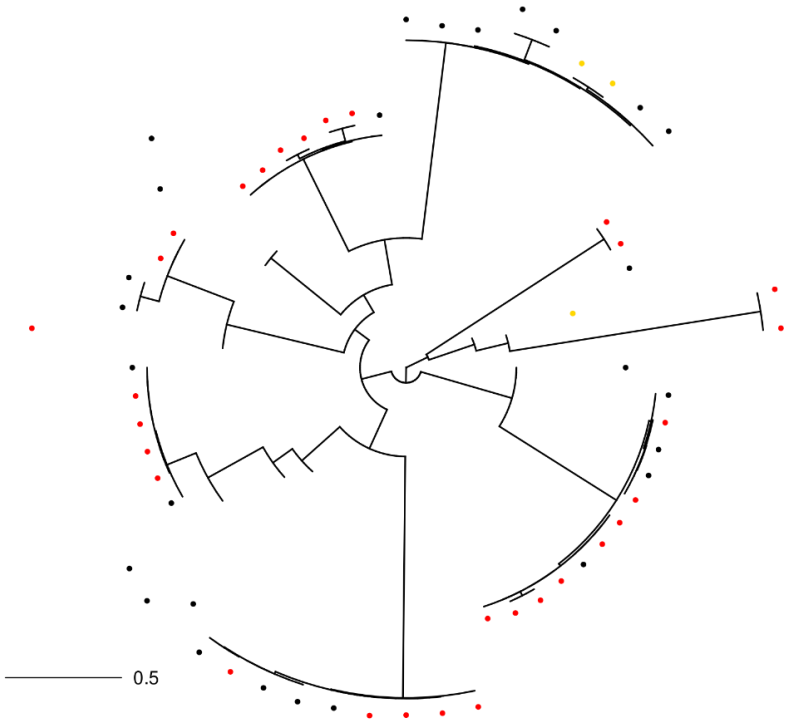


D) ***M. v. viscidula***
on *Silene viscidula*

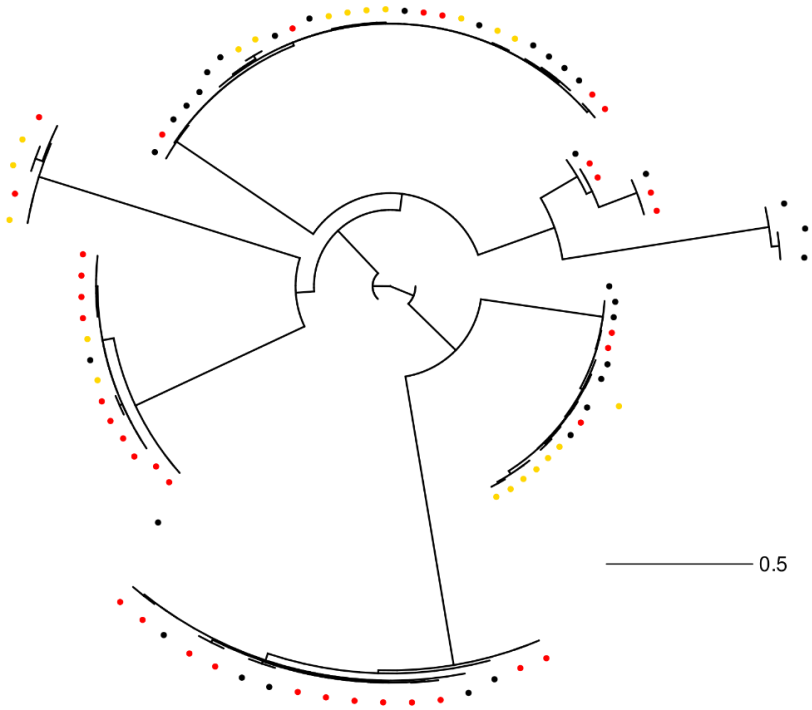


**Genomic location**

- Non-recombining regions of the mating-type chromosomes
- Autosomes
- Centromeres

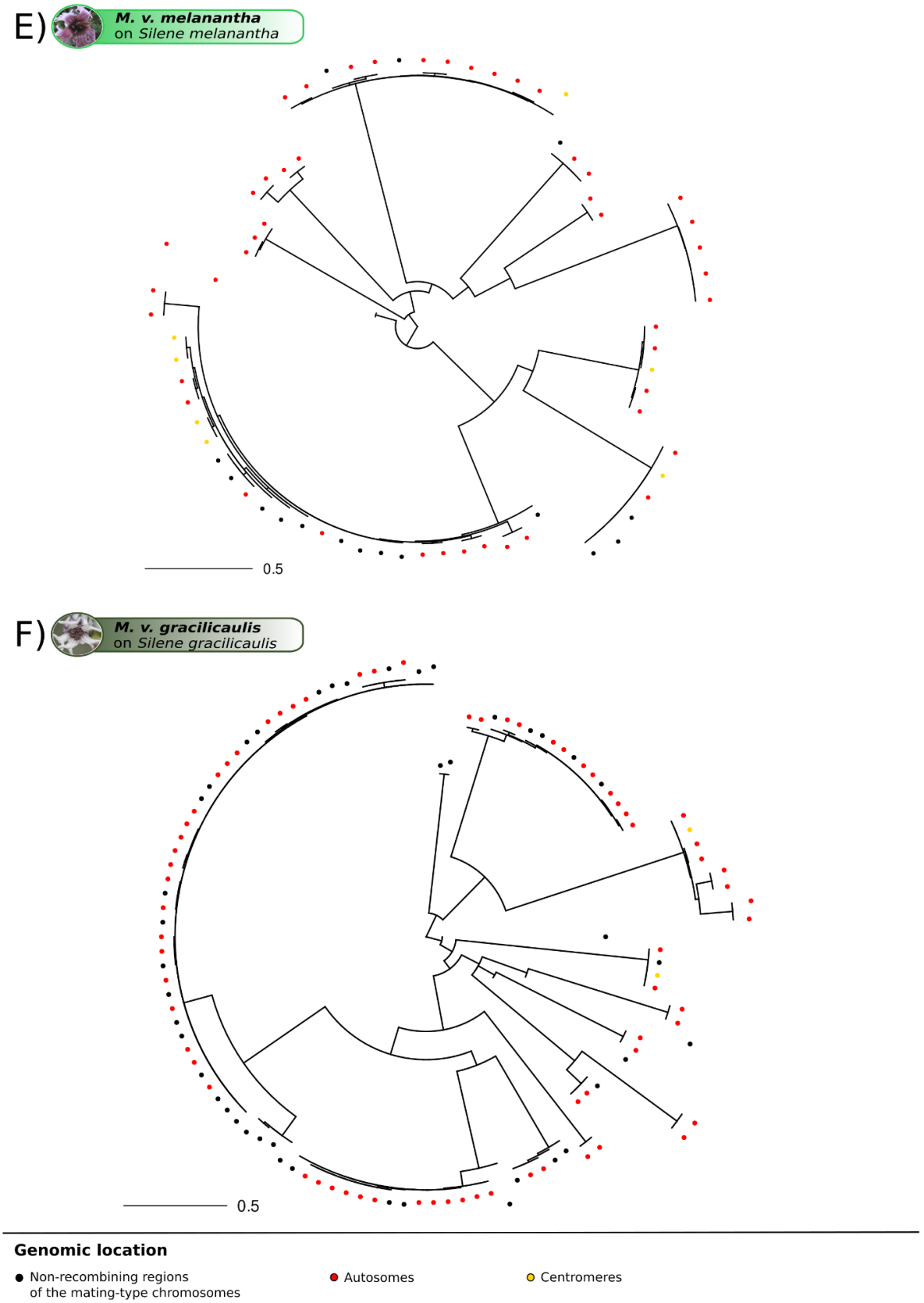
E)
M. v. melanantha
on Silene melanantha
0.5
F)
M. v. gracilicaulis
on Silene gracilicaulis
0.5
Genomic location
Non-recombining regions
of the mating-type chromosomes
Autosomes
Centromeres

1285

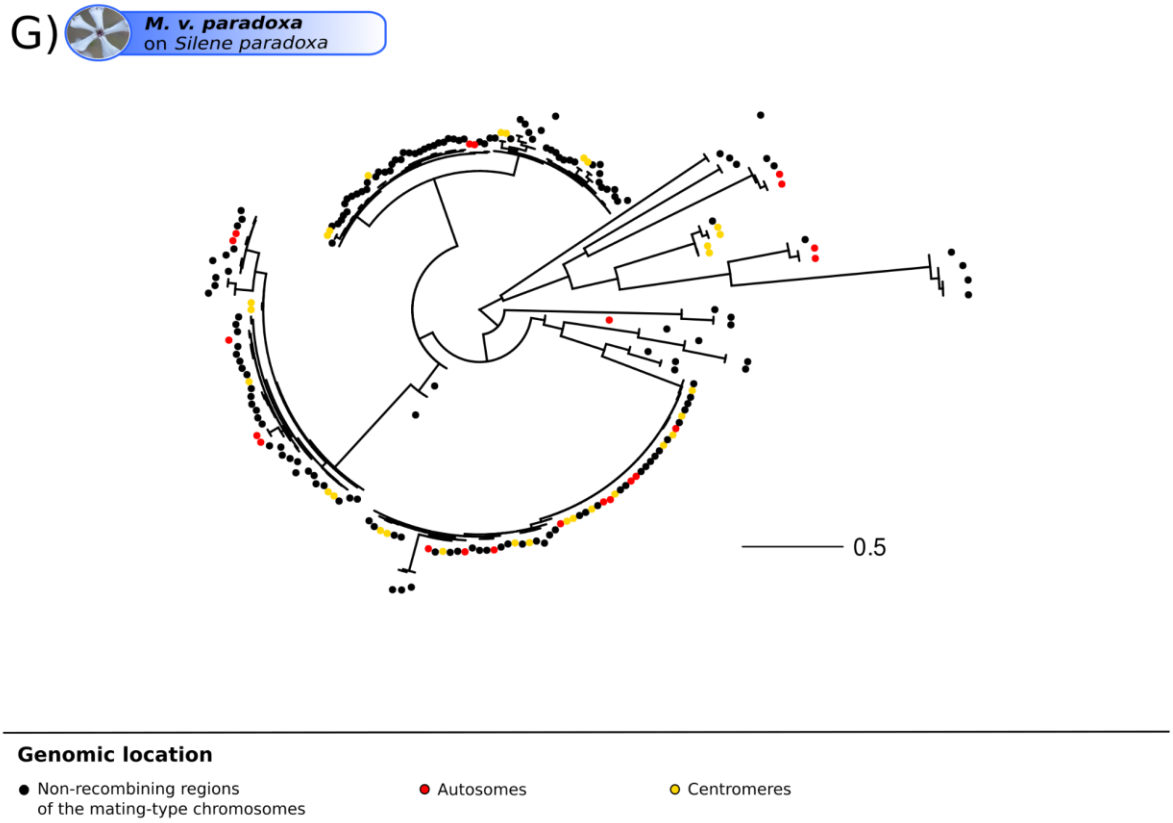


**Supplementary Figure S11: Single-species genealogies of *Ty3* retroelement copies in *Microbotryum* genomes.** Single-species genealogies of *Ty3* copies in *Microbotryum lychnidis-dioicae* **(A)**, *M. silenes-dioicae* **(B)**, *M. coronariae* **(C)**, *Microbotryum violaceum viscidula* **(D)**, *M. v. melanantha* **(E)**, *M. v. gracilicaulis* **(F)** and *M. v. paradoxa* **(G)**. The color of the dots at the tip of the branches corresponds to the genomic location of the transposable element (TE) copies.

A)

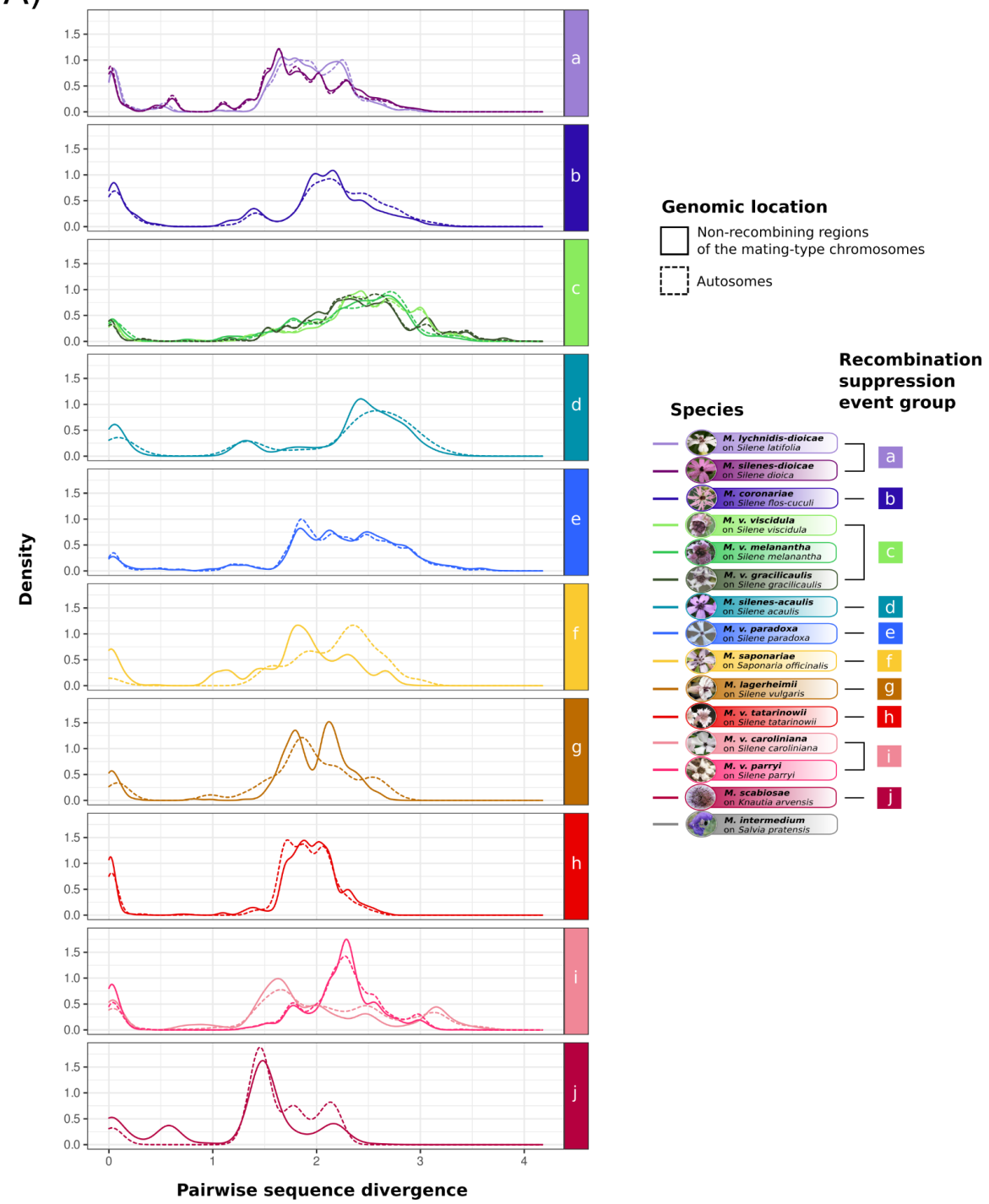
Density
Pairwise sequence divergence
a
b
c
d
e
f
g
h
i
j
Genomic location
Non-recombining regions of the mating-type chromosomes
Autosomes
Species
Recombination suppression event group
M. lychnidis-dioicae on Silene latifolia
M. silenes-dioicae on Silene dioica
M. coronariae on Silene flos-cuculi
M. v. viscidula on Silene viscidula
M. v. melanantha on Silene melanantha
M. v. gracilicaulis on Silene gracilicaulis
M. silenes-acaulis on Silene acaulis
M. v. paradoxa on Silene paradoxa
M. saponariae on Saponaria officinalis
M. lagerheimii on Silene vulgaris
M. v. tatarinowii on Silene tatarinowii
M. v. caroliniana on Silene caroliniana
M. v. parryi on Silene parryi
M. scabiosae on Knautia arvensis
M. intermedium on Salvia pratensis

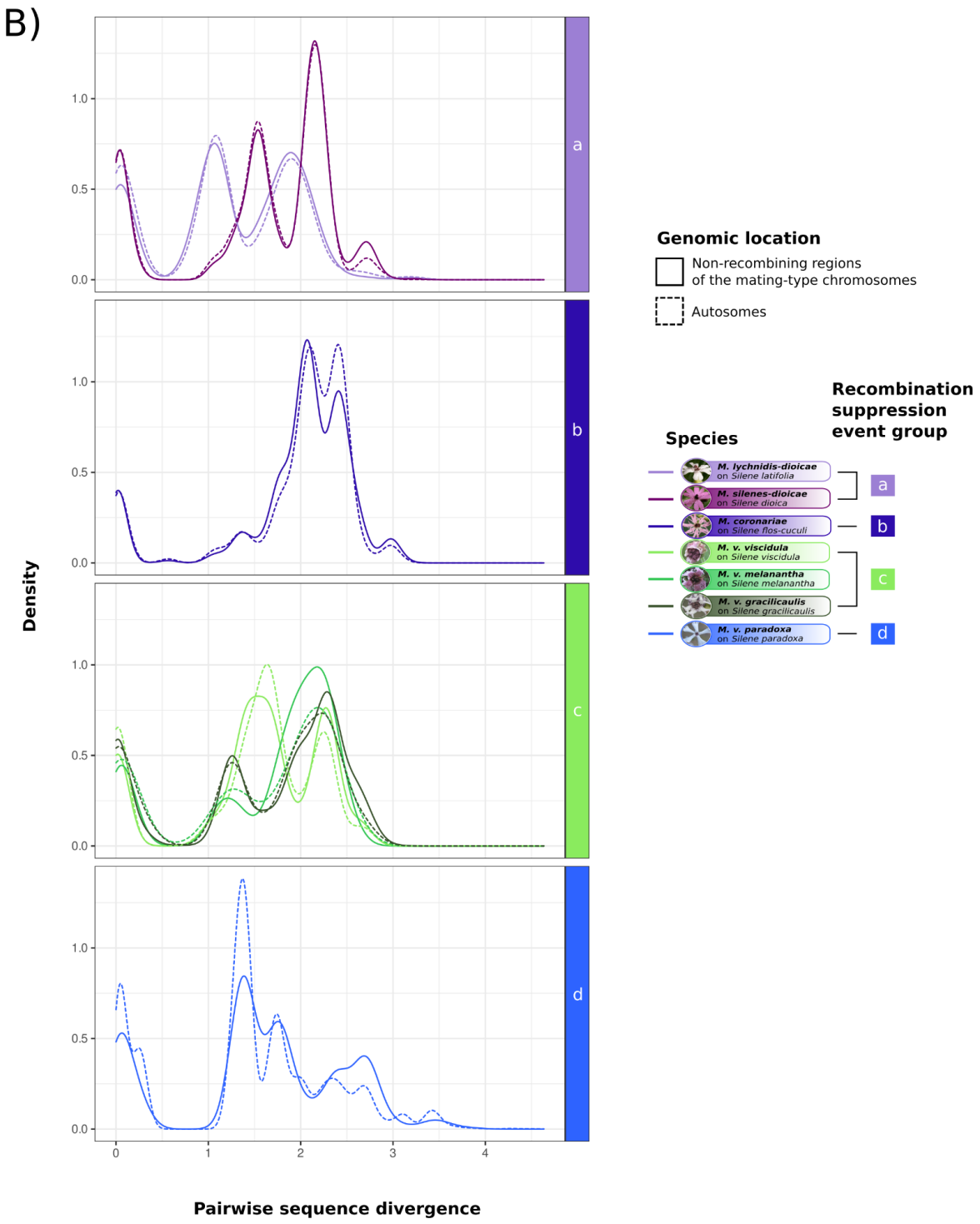


**Supplementary Figure S12: Distribution of pairwise divergence for retroelements in the non-recombining regions of the mating-type chromosomes and the autosomes in each**

**species**, plotted separately for the different independent events of recombination suppression. **(A)** *Copia* retrotransposons, **(B)** *Ty3* retrotransposons.

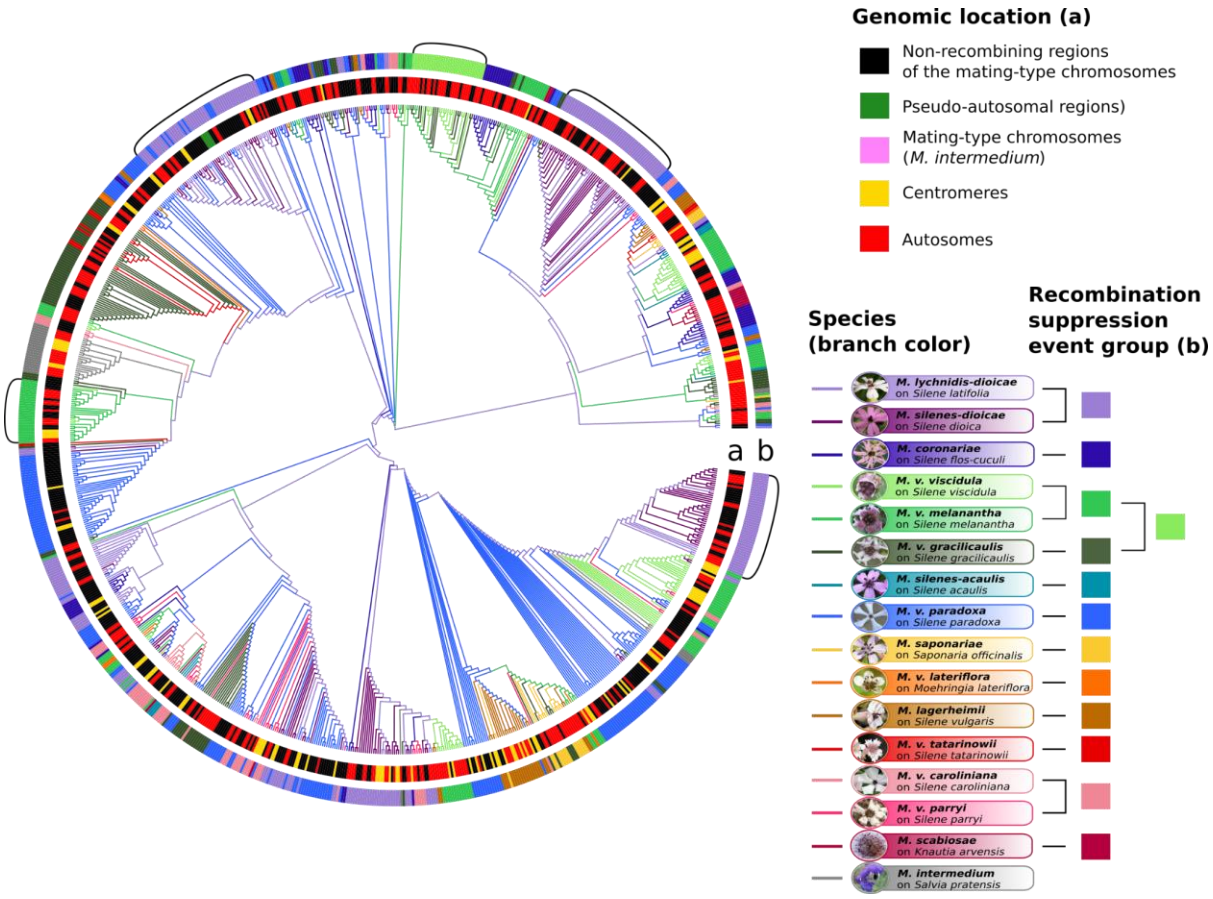


**Supplementary Figure S13: Multi-species genealogies of *Ty3* retroelement copies in *Microbotryum* genomes.** Multi-species *Ty3* trees of all *Microbotryum* species analysed in this study. The branch color corresponds to the species, the first inner track (a) corresponds to the genomic location of the transposable element (TE) copies, the second outer track (b) corresponds to the linkage event group of the species carrying the TE copy. Brackets highlight bursts of TEs.

A)

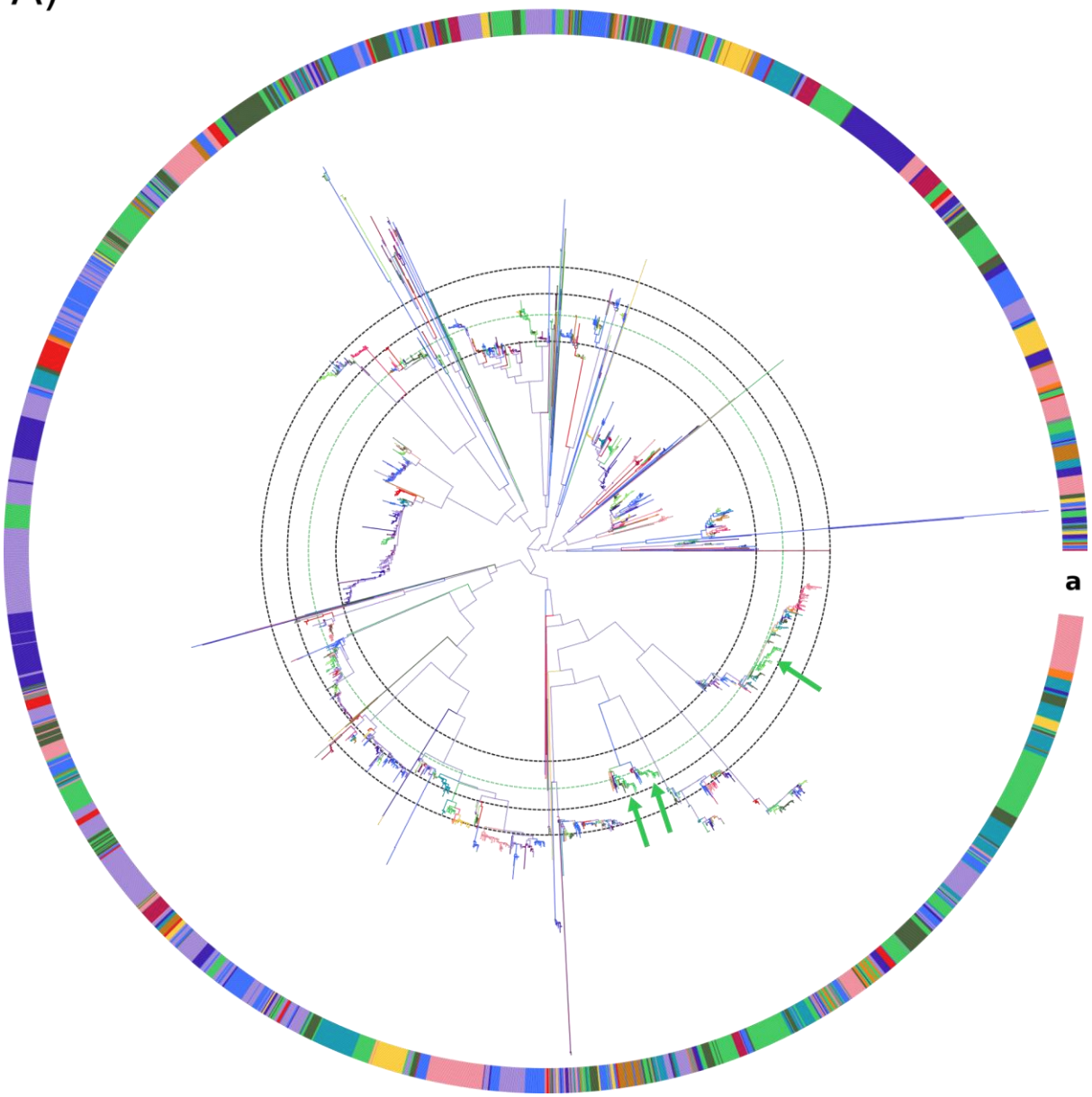

B)

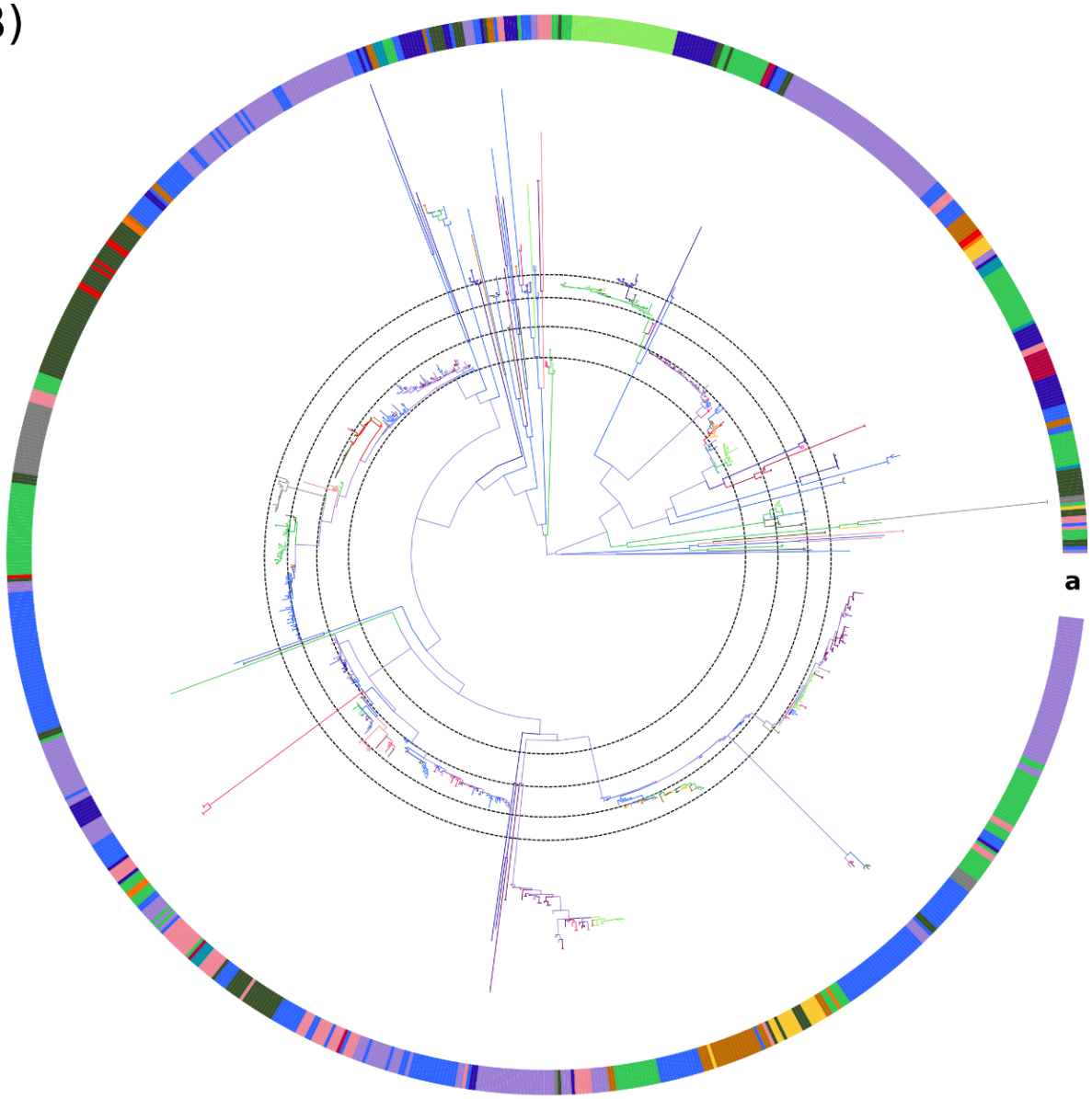


**Species (branch color)**

**Recombination suppression event group (a)**

- *M. lychnidis-dioicae* on *Silene latifolia*
- *M. silenes-dioicae* on *Silene dioica*
- *M. coronariae* on *Silene flos-cuculi*
- *M. v. viscidula* on *Silene viscidula*
- *M. v. melanantha* on *Silene melanantha*
- *M. v. gracilicaulis* on *Silene gracilicaulis*
- *M. silenes-acaulis* on *Silene acaulis*
- *M. v. paradoxa* on *Silene paradoxa*
- *M. saponariae* on *Saponaria officinalis*
- *M. v. lateriflora* on *Moehringia lateriflora*
- *M. lagerheimii* on *Silene vulgaris*
- *M. v. tatarinowii* on *Silene tatarinowii*
- *M. v. caroliniana* on *Silene caroliniana*
- *M. v. parryi* on *Silene parryi*
- *M. scabiosae* on *Knautia arvensis*
- *M. intermedium* on *Salvia pratensis*

**Supplementary Figure S14: Multi-species genealogies of retroelement copies in *Microbotryum* genomes.** The phylogenies of *Copia* **(A)** and *Ty3* **(B)** are the same as those displayed on Figure 5 and Supplementary Figure S14, respectively, but here plotted with branch lengths. The branch color corresponds to the species, the track (a) corresponds to the linkage event group of the species carrying the TE copy. The dashed circles are a help to visualize the timing of the bursts. The green dashed circle highlights the *Copia* bursts which are almost synchronized in the clade of *M. v. gracilicaulis*, pointed by green arrows.

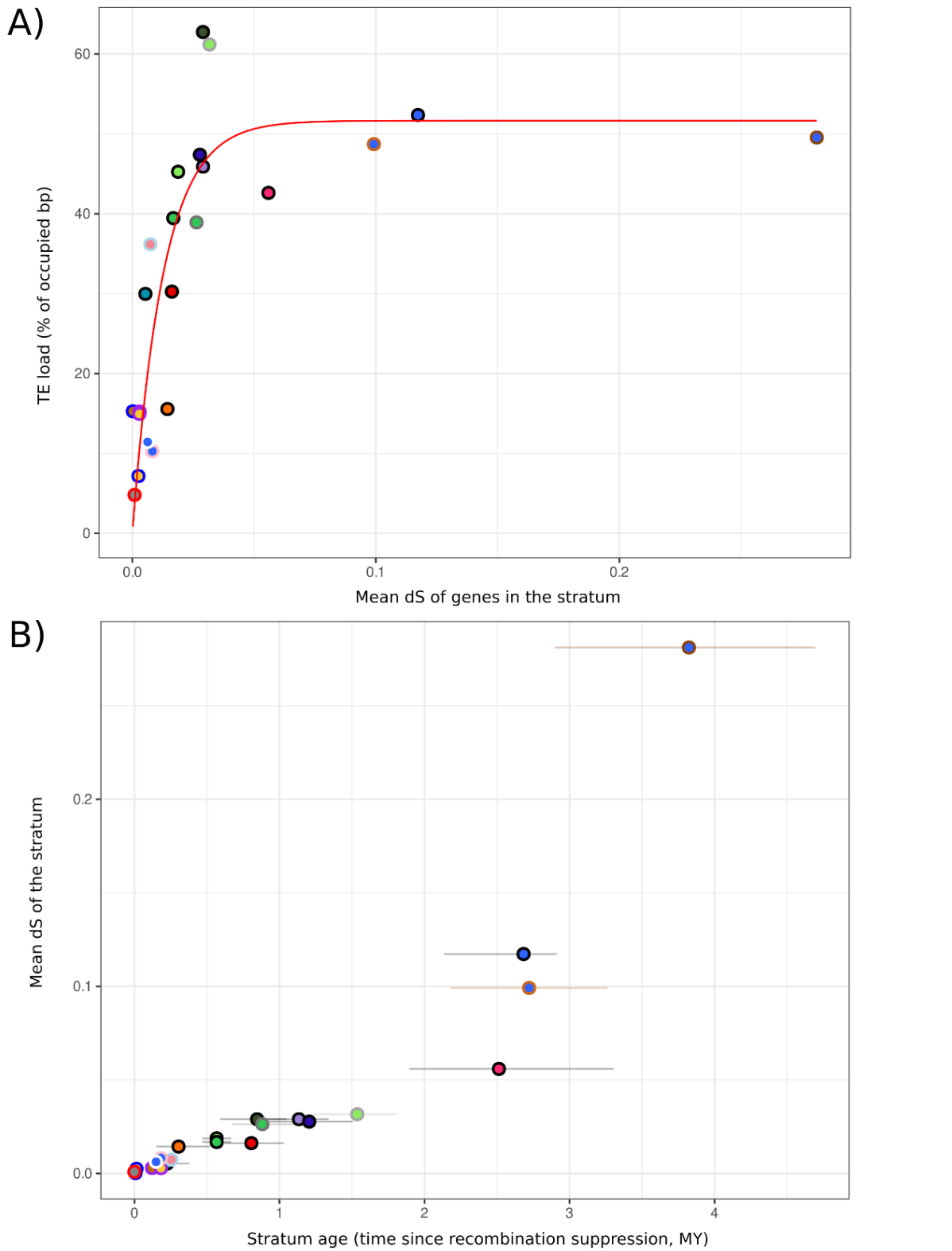
A)
TE load (% of occupied bp)
Mean dS of genes in the stratum
B)
Mean dS of the stratum
Stratum age (time since recombination suppression, MY)
Key to points
M. lychnidis-dioicae on Silene latifolia
M. silenes-dioicae on Silene dioica
Black stratum
M. coronariae on Silene flos-cuculi
Black stratum
M. v. viscidula on Silene viscidula
Black stratum
M. v. melanantha on Silene melanantha
Black stratum
Dark grey stratum
Light grey stratum
M. v. gracilicaulis on Silene gracilicaulis
Black stratum
M. silenes-acaulis on Silene acaulis
Black stratum
M. v. paradoxa on Silene paradoxa
White stratum
Pink stratum
Black stratum
Light brown stratum
Brown stratum
M. saponariae on Saponaria officinalis
Blue-to-centromere stratum
Purple-to-centromere stratum
M. v. lateriflora on Moehringia lateriflora
Black stratum
M. lagerheimii on Silene vulgaris
Blue-to-centromere stratum
Purple-to-centromere stratum
M. v. tatarinowii on Silene tatarinowii
Black stratum
M. v. caroliniana on Silene caroliniana
Light blue stratum
M. v. parryi on Silene parryi
Black stratum
M. intermedium on Salvia pratensis
Autosomes

**Supplementary Figure S15: Relationship between synonymous divergence ($d_S$), transposable element (TE) load and stratum age in *Microbotryum* mating-type chromosomes. A)** Percentage of base pairs occupied by TEs in non-recombining regions (means in $a_1$ and $a_2$ genomes and means across species sharing the same strata) as a function of the mean $d_S$ of the genes present in the stratum. The red curve shows the prediction of the best model corresponding to a negative exponential model. **B)** Relationship between the stratum age in million years (MY) and the mean $d_S$ of the genes contained in this stratum. Each dot corresponds to an independent evolutionary stratum in A) and B).

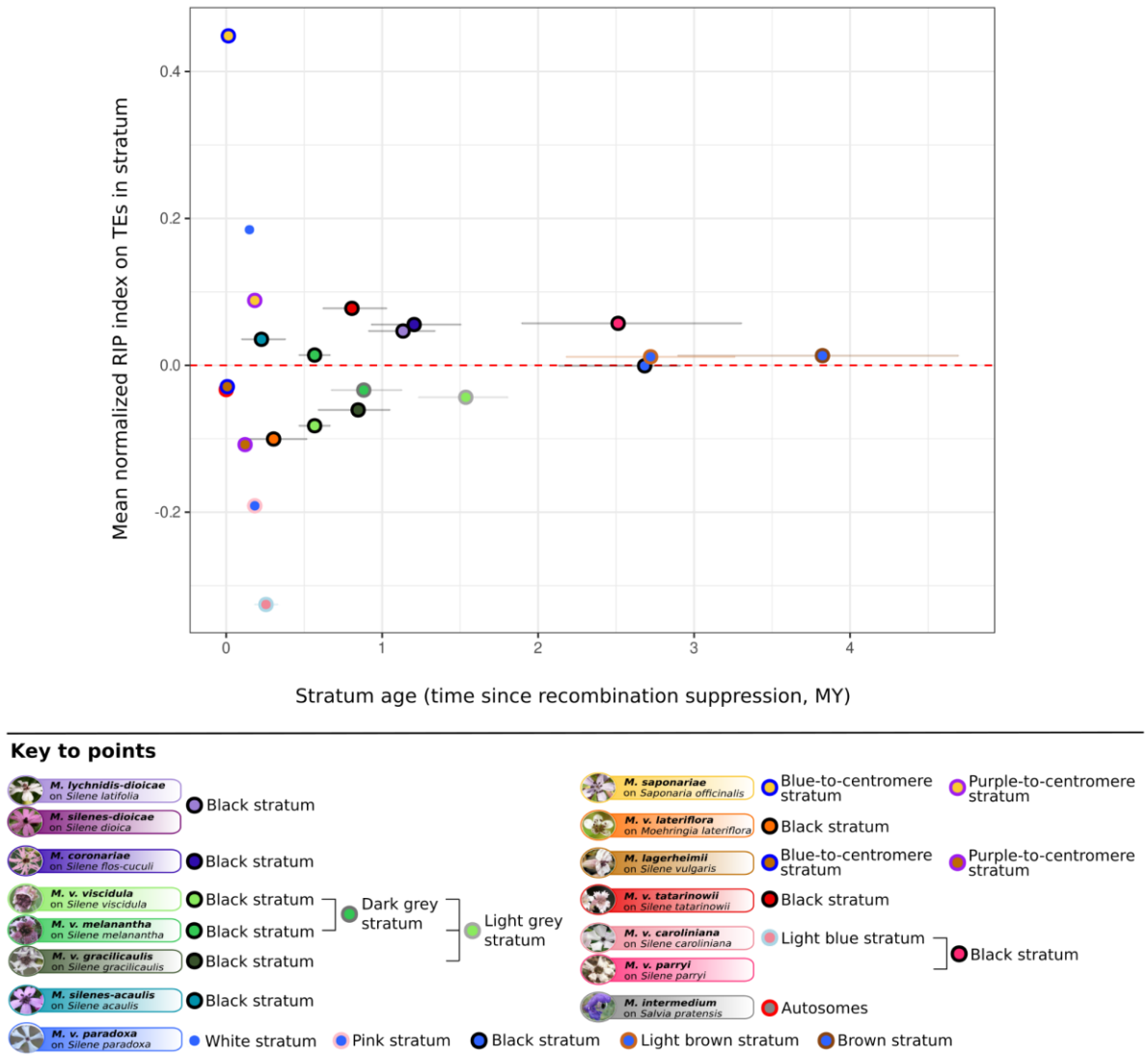


**Supplementary Figure S16: Relationship between the abundance of transposable element (TE) inactivation footprints by repeat-induced point mutation (RIP) in the non-recombining regions of the *Microbotryum* mating-type chromosomes and time since recombination suppression in million years (MY).** Mean normalized RIP index on TEs in non-recombining regions as a function of their age with confidence intervals. The red dashed line separates the RIP index values suggesting RIP mutations (> 0) or no RIP activity (≤ 0). The two-sided Pearson correlation test was not significant (*p-value* = 0.9003).

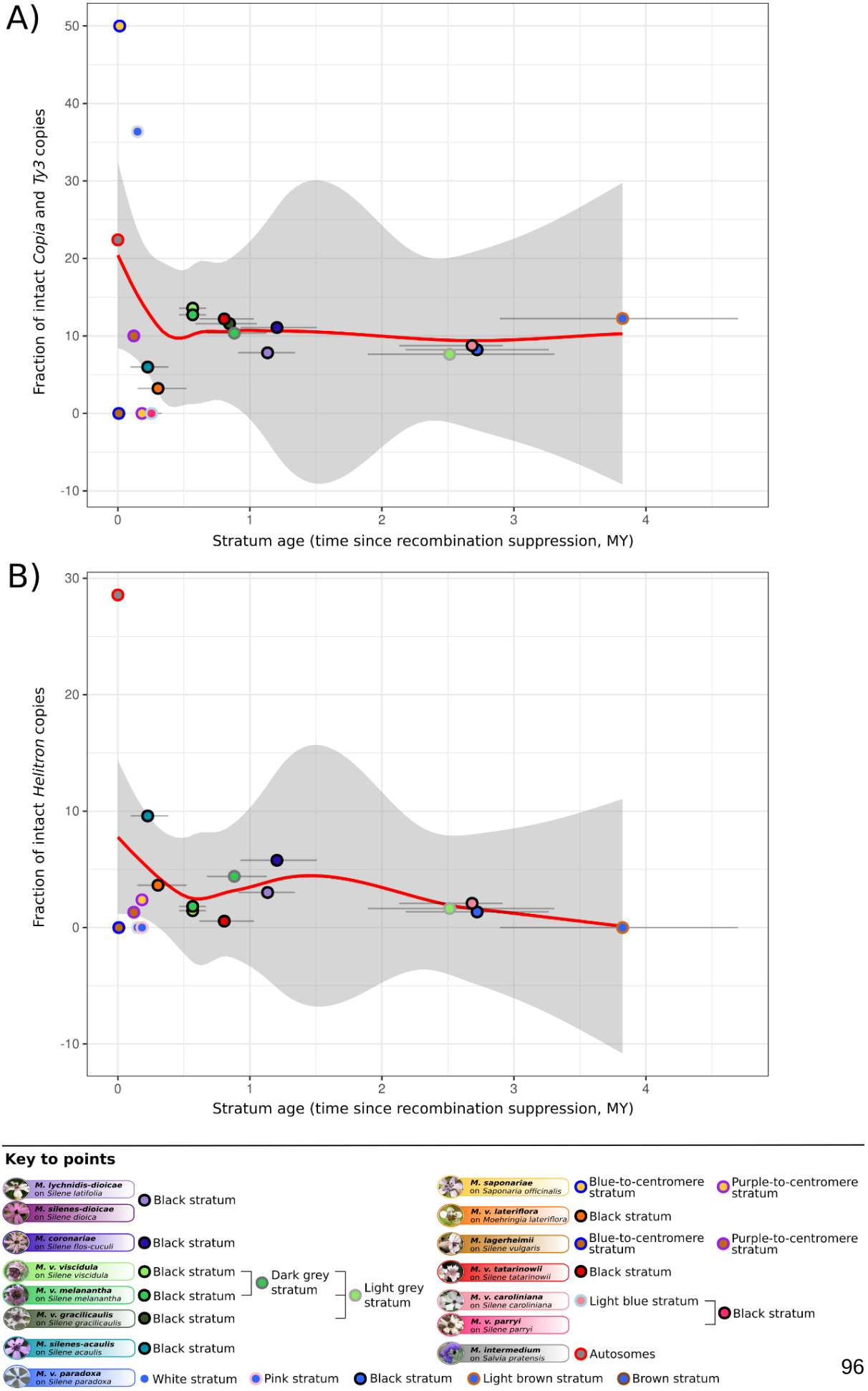
A)
Fraction of intact Copia and Ty3 copies
Stratum age (time since recombination suppression, MY)
B)
Fraction of intact Helitron copies
Stratum age (time since recombination suppression, MY)
Key to points
M. lychnidis-dioicae on Silene latifolia
M. silenes-dioicae on Silene dioica
Black stratum
M. coronariae on Silene flos-cuculi
Black stratum
M. v. viscidula on Silene viscidula
Black stratum
M. v. melanantha on Silene melanantha
Black stratum
Dark grey stratum
Light grey stratum
M. v. gracilicaulis on Silene gracilicaulis
Black stratum
M. silenes-acaulis on Silene acaulis
Black stratum
M. v. paradoxa on Silene paradoxa
White stratum
Pink stratum
Black stratum
Light brown stratum
Brown stratum
M. saponariae on Saponaria officinalis
Blue-to-centromere stratum
Purple-to-centromere stratum
M. v. lateriflora on Moehringia lateriflora
Black stratum
M. lagerheimii on Silene vulgaris
Blue-to-centromere stratum
Purple-to-centromere stratum
M. v. tatarinowii on Silene tatarinowii
Black stratum
M. v. caroliniana on Silene caroliniana
Light blue stratum
M. v. parryi on Silene parryi
Black stratum
M. intermedium on Salvia pratensis
Autosomes

**Supplementary Figure S17: Relationship between the fraction of intact *Copia, Ty3* and *Helitron* copies and stratum age in *Microbotryum* mating-type chromosomes.** Fraction of intact *Copia* and *Ty3* copies (5-7.5 kb for intact copies) **(A)** and *Helitron* copies (5-11 kb for intact copies) **(B)** in non-recombining regions (means in $a_1$ and $a_2$ genomes and means across species sharing the same strata) as a function of the time since recombination suppression in million years (MY). Each dot corresponds to an independent evolutionary stratum in A) and B). The red curve shows the smooth curve obtained by local regression.